Turbulência

Atila P. Silva Freire
Programa de Engenharia Mecânica
COPPE/UFRJ

Anderson Ilha
Divisão de Metrologia Científica
Inmetro

Robert Breidenthal
Department of Aeronautics
University of Washington

Editores

ABCM – Associação Brasileira de Ciências e Engenharia Mecânica
COPPE/UFRJ – Instituto Alberto Luiz Coimbra de
Pós-Graduação e Pesquisa de Engenharia
IME – Instituto Militar de Engenharia

Coleção Cadernos de Turbulência
Turbulência, Volume 5, Tomo 2.

5^a Escola de Primavera em Transição e Turbulência
Instituto Militar de Engenharia, Rio de Janeiro
25 a 29 de setembro de 2006

Editores

Atila P. Silva Freire, *Programa de Engenharia Mecânica*, COPPE/UFRJ
Anderson Ilha, *Divisão de Metrologia Científica*, Inmetro
Robert Breidenthal, *Department of Aeronautics*, University of Washington

Ficha catalográfica preparada pela Seção de Processos Técnicos da
Biblioteca do Centro de Tecnologia da Universidade Federal do Rio de Janeiro

Escola de Primavera em Transição e Turbulência (5. : 2006: Rio de Janeiro, RJ)
Turbulência: Anais da V Escola de Primavera em Transição e Turbulência,
Rio de Janeiro, 25 a 29 de setembro de 2006 /editores Atila P. Silva Freire,
Anderson Ilha e Robert Breidenthal. Rio de Janeiro: ABCM, 2006.
V, 292 p.; 23 cm – Coleção Cadernos de Turbulência. Turbulência, V. 5)
Inclui bibliografias
1. Turbulência. 2. Mecânica dos fluidos. 3. Fenômenos de transporte.
I. Freire, Atila P. Silva II. II. V EPTT (5. : 2006: Rio de Janeiro, RJ).
III. Associação Brasileira de Ciências e Engenharia Mecânica. IV. Título. II.
Série
629.1332
E74T
ISBN

Documento preparado pelos Editores em LaTeX.
Impresso no Brasil pela Gráfica Graffito.

Contents

Preface

A I Escola de Primavera em Transição e Turbulência (ETT) foi uma iniciativa do Comitê de Ciências Térmicas da Associação Brasileira de Ciências Mecânicas (ABCM). Sonho antigo da comunidade de mecânica dos fluidos, ela se tornou realidade graças ao entusiasmo de alguns pesquisadores e ao apoio generoso de várias instituições.

O grande interesse no assunto, aliado à sua importância tecnológica, foram fatores que sempre conspiraram a favor de sua realização. De fato, por ser a turbulência de interesse geral para vários ramos do conhecimento, o atual formato da conferência sempre foi anseio natural da comunidade. Um forum onde métodos e praticas pudessem ser discutidos de modo livre se constituia em demanda legítima.

A Escola supriu essa demanda, adicionando, além disso, ao seu escopo, sessões técnicas de alto nível. Fruto principal da Escola, as notas dos mini-cursos dão origem a este livro. Preparadas com enorme dedicação por excelentes pesquisadores e professores em turbulência, elas certamente deverão servir de material didático para um grande número de cursos de pós-graduação em ciências e engenharias afins.

Este volume, portanto, reproduz praticamente na íntegra os textos apresentados na I ETT. No futuro, novas publicações semelhantes a esta serão editadas pela ABCM.

A.P.S.F.

Acknowledgments

Author Listing

Chapter 1 **page 1**

B. C. Khoo
Dept. of Mechanical Engineering
National University of Singapore
Kent Ridge
Singapore 119260

Y. T. Chew
Singapore-MIT Alliance (SMA)
4 Engineering Drive 3
Singapore 117576

Chapter 2 **page 115**

Dana Dabiri
Dept. of Aeronautics & Astronautics
University of Washington
Seattle, WA 98195
USA

Chapter 3 **page 205**

Robert Breidenthal
University of Washington
Seattle, WA 98195-2400
USA

Chapter 4 **page 223**

Aline Cotel
Dept. of Civil and Environmental Engineering
University of Michigan
Ann Arbor, MI 48109-2125
USA

Chapter 1

Dynamic response of the near-wall hot-wire/hot-film system and near-wall velocity measurements

1.1 Introduction and Contents of Study

Despite the recent progress made in the technique of PIV (Particle Image Velocimetry) for use in velocity measurements and the availability of LDA (Laser Doppler Anemometer) as another alternative since the 1970's, hot-wire anemometry remains the preferred choice for many researchers in turbulence measurements. The smallness in size of the active hot-wire element measuring in microns not only enables good spatial resolution of the velocity field, the correspondingly low thermal inertia of the said wire promises fast response, thus permitting the high frequency fluctuations of a turbulent flow to be followed faithfully.

Earlier, Perry & Morrison (1971) had shown that both their hot-wire and DANTEC-made system yielded a frequency response of at least over 5 kHz when subjected to direct velocity perturbation in a wall remote flow. The velocity perturbation test was carried out using the Karman vortex shed from one side of the cylinder; the frequency response being obtained from the shedding frequency of the vortex expressed in Strouhal number as a known function of flow Reynolds number, Re_d (based on freestream velocity and diameter of cylinder), while the amplitude response was deduced from comparisons of the intensity of streamwise velocity fluctuations across the wakes of cylinders with different sizes at corresponding downstream positions for a given $\mathrm{Re}_d = 140$. Such a fast response for the conventional hot-wire, as measured in terms of frequency without any amplitude attenuation, is of prime consideration for many workers in turbulence research,

where accurate time resolution of the flow field is of utmost importance.

Researchers, however, are only too aware that the performance of the same hot-wire changes as it approaches the wall. The hot-wire, when operating under wall remote conditions, is principally only subjected to convective heat loss whence the latter can be made related to the prevailing convective velocity via the calibration curve. In the presence of a nearby wall, there is additional heat loss from the wire to the wall substrate. Of equal importance is the accentuation of the aerodynamic interference effect due to the presence of the hot-wire prongs, which may alter the flow field thereby resulting in larger convective heat loss.

The subject of increased aerodynamic interference effects in near-wall hot-wire operations is discussed in Comte Bellot *et al.* (1971), Azad (1983) and in the recent work of Chew *et al.* (1998a). Chew *et al.* (1998a) also systematically investigated the other effects of wall substrate with different thermal conductivity, wire length to diameter (L/d) ratio and the overheat ratio imposed. On the other hand, the hot-wire having been calibrated under the usual free stream conditions must be subjected to some form of wall corrections for near-wall applications (e.g. see Bhatia *et al.*, 1982). Alternatively, the hot-wire may be calibrated directly in a known flow near to the wall with the wall effect being calibrated away. Khoo *et al.* (1996) suggested two methods to account for the wall effect on near-wall hot-wire measurements such that an accurate time-resolved streamwise velocity measurement is still feasible.

Despite the recent spate of works in near-wall hot-wire operations, including investigations of the effects of l^+ (wire length in wall units) on turbulence measurements in the viscous sub-layer (Khoo *et al.*, 1997), and other numerous earlier studies as found in Polyakov & Shindin (1978, 1979) and Zemskaya *et al.* (1979), to name a few, there is still a dearth in the literature on the dynamic response of a hot-wire operating in the vicinity of the wall. This is, to a very large extent, due to the difficulties in implementing a suitable mode of generating a known fluctuating flow field at a relatively high frequency near the wall. The hot wire, in the presence of a nearby wall, may present itself as a system with a vastly different thermal capacity and dynamic response, as compared to a wall-remote situation.

Khoo *et al.* (1995), in their attempt to determine the dynamic response of a marginally-elevated hot-wire anemometer probe for near-wall velocity and wall shear stress measurements, have for the first time, developed a viable means of generating a known high frequency fluctuating velocity field for purposes of quantifying both the frequency and amplitude response of the said hot-wire anemometer. Khoo *et al.* (1995) found that a 5 μm diameter wire mounted at 50 μm above the thermally less conducting epoxy-based wall substrate responded fully to imposed fluctuations of up to 1600 Hz without any amplitude attenuation, so was observed for another similar-sized wire but mounted at 12μm above the wall substrate. Their attempts to impose an increasingly higher fluctuation so as to determine the dynamic response in terms of the so-called "upper frequency limit" (henceforth termed f_D), when amplitude attenuation of imposed velocity change begins or when the said wire cannot respond fast enough to the imposed frequency, whichever occurs first, was thwarted by limitations due to excessive vibration ex-

perienced in their the experimental setup. That being so, Khoo *et al.* were unable to ascertain if there was any difference in the dynamic response of the hot-wire mounted at different heights from the wall, and it may be noted too that their successful tests of up to 1600 Hz were still way below the dynamic response of a wall-remote hot-wire of at least O(5 kHz) as recorded by Perry & Morrison (1971). The work of Khoo *et al.*, however, has definitely indicated the feasibility of imposing a known fluctuating flow very near to the wall for quantification of the near-wall hot-wire response.

In a similar way, despite the importance of quantifying the dynamic response of a hot element mounted very close or flushed with the wall as a wall shear stress gauge for suitability in the study of turbulent wall shear stress fluctuations, no attempt has been made thus far. Already, the hot-element wall shear stress gauge is preferred over the traditional force balance surface gauge with its complex mechanical linkages partly because of the perceived faster response characteristics of the former to reflect faithfully the changing quantities expected in a turbulent flow field although there is hardly any quantitative evidence to substantiate it. Still if interest is primarily confined to measuring the mean quantity in a stationary turbulent flow, the response characteristics of the wall shear stress probe may not be a major issue unless the turbulence statistics of the wall shear stress fluctuations are required or measurements are being made in a non-stationary turbulence field where the mean value is a function of time.

There are, however, only some fairly *qualitative* works carried out in the investigation of the response characteristic of a flush-mounted hot-element wall shear stress gauge. Cook & Giddings (1988) found that the buried flush-wire and Platinum-film gauges placed in a laminar oscillating flow produced on a flat plate by a freestream velocity comprising a mean component and a superimposed sinusoidal variation indicate a wall shear stress variation that lags the true (numerically obtained) variation even in the relatively low frequency range of between 3 to 20 Hz used in their experiments. They attributed the observed lag to "unsteady heat conduction effects in the gauge substrate". Since no attempt was made to calibrate the gauges for determination of the mean and oscillating components of the wall shear stress, there is no comparison concerning the magnitude of wall shear stress to ascertain the possibility of amplitude attenuation. In a subsequent follow up work, Cook (1994) subjected different types of hot-element wall shear stress gauges to unsteady turbulent flow; one of which a step-like flow was generated by rapidly opening the valve between the evacuated vacuum tank and the test facility hence producing a steady downstream velocity. What is most interesting was the observation of a wall remote hot-wire probe requiring only O(0.1) seconds to attain the steady freestream velocity value whereas it took about O(0.3) seconds for the cavity gauge to reach the steady wall shear stress quantity and up to O(40) seconds for the quartz substrate and glue-on gauges to assume the steady state value of the wall shear stress.

The results have two important implications. Firstly, even if the imposed perturbation is not a true step-like flow, the output from the hot-wire in the freestream would have indicated the nature of the flow and its response is clearly a

few factors faster than the hot-element cavity gauge mounted on the wall. Secondly and even more significant is the response indicated by the hot-element quartz substrate gauge or the glue-on gauge coming close to two orders of magnitude slower relative to the cavity gauge. Comparison among the hot-element gauges suggests that the type of thermally conducting/insulating material on which the hot element is mounted on may have far reaching consequences on its response. Other works like Houdeville *et al.* (1984) have also carried out limited testing of the various gauges and their results seem to support the use of the cavity gauge (where the surface level hot element presides above a small cavity beneath presumably to reduce substrate heat transfer) with better response characteristics as compared to other substrate-type gauges. Despite all these efforts carried out to determine a responsive wall shear stress gauge, no study, analytical or experimental, has been made to provide the quantitative information pertaining to the associated response characteristics.

The desire to fill the void in the literature on the quantification of the dynamic response of a marginally-elevated hot-wire as a velocity probe and flush-mounted hot-element wall shear stress gauge provides the motivation for the series of present work. Comparisons are made between the dynamic response frequency and the cut-off frequency according to the usual electronic perturbation test. Consequent to the establishing of a viable near-wall hot-wire velocity probe, near-wall measurements in the turbulent shear flow for both the channel and boundary layer flows are then carried out to elucidate the flow physics.

1.2 Experimental set for determination of the dynamic response (f_D) of hot-wire

1.2.1 Rotating disk

The basic design and construction of the rotating disk apparatus for the generation of a known velocity near to a surface is given previously in great detail in Khoo *et al.* (1995). Here, only the salient features are described with the improvements made such that a much higher frequency of imposed fluctuations is possible without excessive vibration which plagued the original set-up. The improved experimental rig is shown systematically in Fig.(1.1).

A heavy flywheel is placed concentrically over the top rotating disk of 150 mm radius and the said disk is made to rotate via a spring loaded central shaft enclosed within an external housing linked by a timer belt to a heavy duty DC motor mounted firmly on a structural column for purpose of rigidity. The timer belt and spring loaded shaft seek to minimize vibration from the motor, and the latter, with its larger lateral extent, as compared to the previous setup which used a relatively much smaller diameter shaft, also serve the function of reducing possible inaccuracy when mounted perpendicularly to the flywheel. The top rotating disk attached to the flywheel can be changed; in the first instance, a flat top disk was set with different gap sizes (δ) in the range from below 200μm to over 400 μm

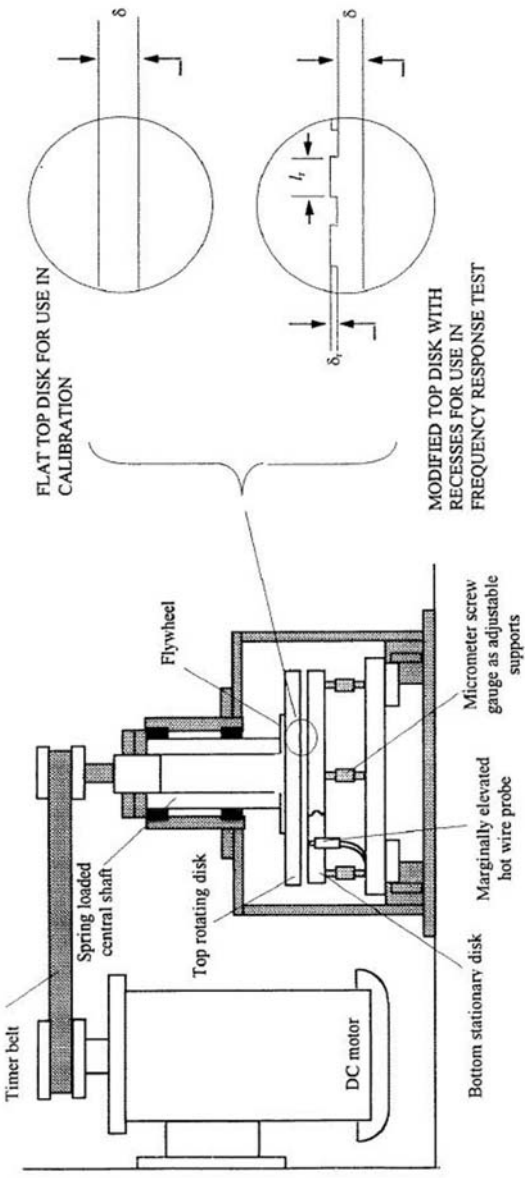

Figure 1.1: Layout of the apparatus for the generation of a known flow field between disks.

for purpose of calibrating the hot-wire. According to Stewartson (1953), the flow generated is given as

$$v = \omega r \left[\varepsilon - (Re_s^2/6300)(8\varepsilon + 35\varepsilon^4 - 63\varepsilon^5 + 20\varepsilon^7) + O(Re_s^4)\right] \quad (1.1)$$

$$u = -\omega r (Re_s^2/60)(4\varepsilon - 9\varepsilon^2 + 5\varepsilon^4) + O(Re_s^3) \quad (1.2)$$

where ω is the angular velocity of the top rotating disk, $\mathrm{Re}_s \equiv \omega\delta^2/\nu$ is the Reynolds number based on the gap size δ. u and v are the radial and azimuthal velocity components, respectively, and $\varepsilon \equiv z/\delta$ is the non-dimensional vertical coordinate with r as the radial coordinate.

During calibration, with the hot-wire mounted at a fixed height above the bottom stationary disk, a known Couette-like flow in the azimuthal direction is present since Re_s was made very small ($\mathrm{Re}_s << 1$) as deduced from Eq.(1**XXX**). In order to generate a known fluctuating flow, the top disk is replaced by a similar sized modified perspex disk whose surface has 100 recesses of 45μm (δ_r) depth machined radially from the outer edge to half the disk radius (see Figure 1.1), similar to that carried out in Khoo *et al.* (1995).

The rectangular shaped recesses are distributed evenly on the disk. As discussed in Khoo *et al.*, the placement of the hot wire at r_m= 115 mm where the local azimuthal extent of each recess l_r (at $\mathrm{r} = \mathrm{r}_m$) is 3.6 mm, hence giving a ratio of $l_r/\delta_r = 80$, coupled with previous known works of flow over a backward facing step which indicates flow separation at the step with reattachment occurring within 10 step heights thereafter (see Isomoto & Honami, 1989 and Shu *et al.*, 1994), strongly suggest the presence of two different Couette-like flows imposed by the modified top disk with two effective surfaces separated by distances of δ and $(\delta + \delta_r)$ from the bottom stationary disk. It is reckoned that the disturbances caused by the sudden change in gap size is largely contained within the reattachment region; this scenario is further supported by the hot-wire output which shows fairly clear 'square-wave' like signals (see Figure 1.4) (Some discussions on the generation of near Couette-like flow can also be found in Khoo *et al.*, 1995). In this work, the hot-wire is also mounted at r_s = 95 mm and r_l = 130 mm, equivalent to l_r/δ_r of 53 and 102, respectively. In this way, the period of the fluctuating waveform as deduced from the hot-wire output can be compared to the imposed fluctuation, and the magnitude of the hot wire signal interpreted as velocity via the calibration curve can be compared quantitatively to the amplitude of the fluctuating velocity field. The presence of any amplitude attenuation of imposed velocity change or the detection of the inability of the hot-wire to follow the imposed fluctuations, whichever comes first, can be construed as the dynamic response frequency (f_D) of the hot-wire system.

To provide for a known fluctuating wall shear stress as dictated by the corresponding fluctuating flow field, the top flat disk is replaced by a modified disk with 100 evenly distributed recesses of 45 μm (δ_r) depth machined on its surface stretching from the disk edge at r = 150 mm to half the disk radius at r = 75 mm. At the respective radial position of $\mathrm{r}_i = \mathrm{r}_s$ (95 mm), r_m (115 mm) and r_l (140 mm) where the hot-element wall shear stress gauge is mounted, the presence of

two Couette-like flows imposed by the modified top disk rotating at a tangential velocity of $\omega \mathrm{r}_i$ separated by two effective gaps of δ and $(\delta + \delta_r)$ necessarily implies the presence of two associated tangential wall shear stresses given as

$$\tau = \mu \frac{\omega r_i}{\delta} \tag{1.3}$$

and

$$\tau = \mu \frac{\omega r_i}{(\delta + \delta_r)}. \tag{1.4}$$

In this way, the frequency of imposed fluctuation (f_{imp}) and the magnitude of the imposed wall shear stresses can be used for comparison to the measured output of the wall shear stress gauge mounted at r_i. With 100 recesses on the modified top disk, the imposed frequency is

$$f_{imp} = \frac{\omega}{2\pi} \times 100 Hz \tag{1.5}$$

The detection of the onset of amplitude attenuation of the imposed wall shear stress change or the inability of the gauge to follow the imposed frequency fluctuation, whichever occurs first, shall be considered as the dynamic response frequency (f_D) of the said gauge.

1.2.2 Marginally elevated hot-wire as a velocity probe

The construction of the hot-wire probe follows closely to that of Chew *et al.* (1994) and Khoo *et al.* (1995), albeit some modifications incorporating a micrometer screw gauge for adjusting the height of the wire from the wall and the use of different wall substrate materials. The probe consists of a KANOMAX-0251 single hot-wire mounted within a cylindrical hollow plug with two small holes at the top section for the protrusion of the said hot-wire prongs above the wall (see Figure 1.2).

Several identical plugs of different thermal conductivities were manufactured such that the placement of the 5 μm diameter DANTEC-made platinum-plated tungsten wire on the tip of the prongs enabled the wire to be exposed to the plugs' top wall substrate made of the respective materials. Because the top section of the plug which measures 7 mm in diameter is considerably bigger in extent compared to the wire length of $\mathrm{l} = 1.2$ mm mounted at the center of the plug (hence giving a wire length to diameter ratio of at least 200 to ensure negligible heat loss through the prongs (see Ligrani & Bradshaw, 1987; Chew *et al.*, 1998a), it is reckoned that the overall active wire element will be subjected to the immediate influence of the particular wall substrate beneath. The whole plug was in turn mounted flush with the wall of the bottom stationary disk during the experiments.

At the other end of the hot-wire probe, a micrometer screw gauge was attached to enable adjustments of the required wire height above the wall. The respective probe was then connected to a DISA 56C01 CTA unit. The CTA unit was linked via the Keithley made DAS-20 data acquisition system to a microcomputer. Data

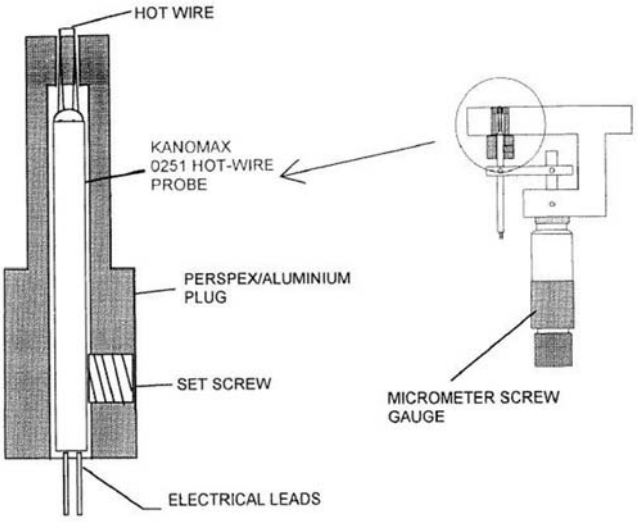

Figure 1.2: Schematic diagram of the marginally elevated hot-wire anemometer.

acquisition was effected at rates between 5 to over 50 kHz, with the higher rates of acquisition used for higher rates of imposed velocity fluctuation via the modified top disk.

1.2.3 Flushed-mounted hot-wire and hot film as wall shear stress probe

Two different types of hot-element wall shear stress gauges are used in the present study. The first type is the commercially available DANTEC-made 55R45 and 55R46 flush-mounted hot-film shear stress probes whose active nickel-based element, deposited on a quartz substrate, measures 0.2 mm by 0.75 mm. For the 55R45 gauge, a 0.5 μm thick quartz coating covers the active element as opposed to a 2 μm thick quartz coating for the 55R46 gauge. The second type is the flush-mounted hot-wire where the 5 μm diameter DANTEC-made platinum plated tungsten wire is placed in contact with the perspex wall substrate. The construction of the latter is similar to that described in Section 1.2.2.

The required hot-wire is soldered onto the prongs and fine adjustment of the wire height above the top surface of the perspex plug till it touches the wall is achieved by means of a micrometer screw gauge which is attached to the probe. A schematic of the probe is given in Fig.(1.3) for ease of reference. The respective wall shear stress gauge was then connected to the DISA 56C01 CTA unit, which in turn was linked to a micrometer via the Keithley-made DAS-20 data acquisition system.

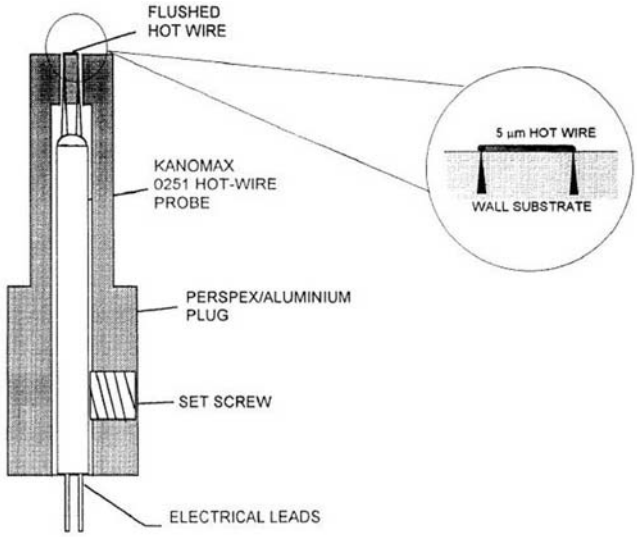

Figure 1.3: Schematic diagram of the flush-mounted hot-wire wall shear stress gauge.

1.3 The dynamic response of the hot-wire anemometer

1.3.1 Near-wall hot-wire for velocity measurement

1.3.1(a) Calibration of the hot-wire probe

Calibration of the marginally-elevated hot-wire probe was carried out in the same manner as in Khoo *et al.* (1995) with the flat rotating disk set at a fixed distance of δ from the bottom stationary disk. By keeping $\mathrm{Re}_s << 1$, for a range of angular speeds, the imposed azimuthal velocity (v) given by Eq.(1.1) at the wire's location (z = h) can be correlated against the output voltage (E) of the hot-wire via King's law

$$E^2 = A + Bv^n \tag{1.6}$$

where A, B and n are calibration constants. As noted in Chew *et al.* (1994) and Khoo *et al.* (1996), calibration of the hot-wire in this manner effectively ensured that the wall influence was accounted for or calibrated away.

To ensure consistency of results, calibration utilizing the flat top disk was carried out before and after each series of experiments. If there was any drift of the calibration constants by more than 2%, the results were discarded. Monitoring of the air temperature was done simultaneously and the data was accepted only

when the temperature variation was less than $\pm 0.2^{\circ}$C.

1.3.1(b) The frequency limit (f_D) of a hot-wire mounted at 50 μm above perspex wall

With the modified top disk set at $\delta = 300$ μm from the stationary bottom disk, typical voltage-time series for selected rotational speeds are shown in Fig.(1.4) for a hot-wire mounted at $r_m = 115$ mm and h = 50 μm above the perspex wall substrate. For each rotational speed of Ω rpm, the imposed fluctuation frequency (f_{imp}) associated with 100 recesses of the modified top disk is evaluated as

$$f_{imp} = 100\Omega/60Hz(4) \tag{1.7}$$

and duly reflected on the same figure.

The typical voltage signals taken w.r.t. time indicate a fairly well-defined and regular "square-wave" series with relatively flat top and trough sections; the respective series yields an average period which coincides with the imposed frequency, hence implying that the hot-wire is responding faithfully to the frequency of the externally imposed fluctuating flow field. As discussed at length in Khoo *et al.* (1995), the presence of the flat top and trough voltage traces provides the possibility that the probe can also respond to the full amplitude change in the imposed velocity fluctuation. Shown in each of the voltage-time traces are the *calculated* maximum and minimum voltages associated with the velocities at the wire's location (via the calibration curve) subjected to near-Couette flows with the top moving surface mounted at δ and $(\delta + \delta_r)$, respectively, from the stationary bottom surface. The top surface is moving at the local tangential velocity given by $\Omega r_m \pi/30$ mm/s.

Figure 1.4 clearly depicts that, with the exception of case (a), the hot wire is able to respond fully to the frequency and amplitude of the imposed fluctuating flow field. For case (a), although the evaluated frequency coincides with f_{imp} at 3000 Hz, there is obvious amplitude attenuation. There is a marked absence of the flat top and trough sections of the periodic waveform and the resulting peak and trough voltages cannot match the *calculated* voltages. This may suggest that amplitude attenuation is the limiting factor in the determination of the dynamic response of the hot-wire rather than just the consideration of the frequency per se. In this respect, the results of Fig.(1.4) are replotted in Figure 1.5(a) with other data showing the maximum and minimum velocities associated with the "saturated" voltage *measured* corresponding to the relatively flat top and trough portions of the voltage-time trace, respectively, via the calibration curve.

As argued in Khoo *et al.* (1995), the fairly sharp rise and fall of the voltage-time trace with small disturbances of higher frequency accompanying the saturated voltage readout are associated with the flow attachment effect following the movement of a recess past the hot-wire. Discounting the rise and fall of the voltage-time trace from the flat top and trough sections, only the voltage readouts in the center half portion of each flat section are evaluated as velocities for computation of the average maximum and minimum velocities. Also shown in Figure 1.5(a) are the

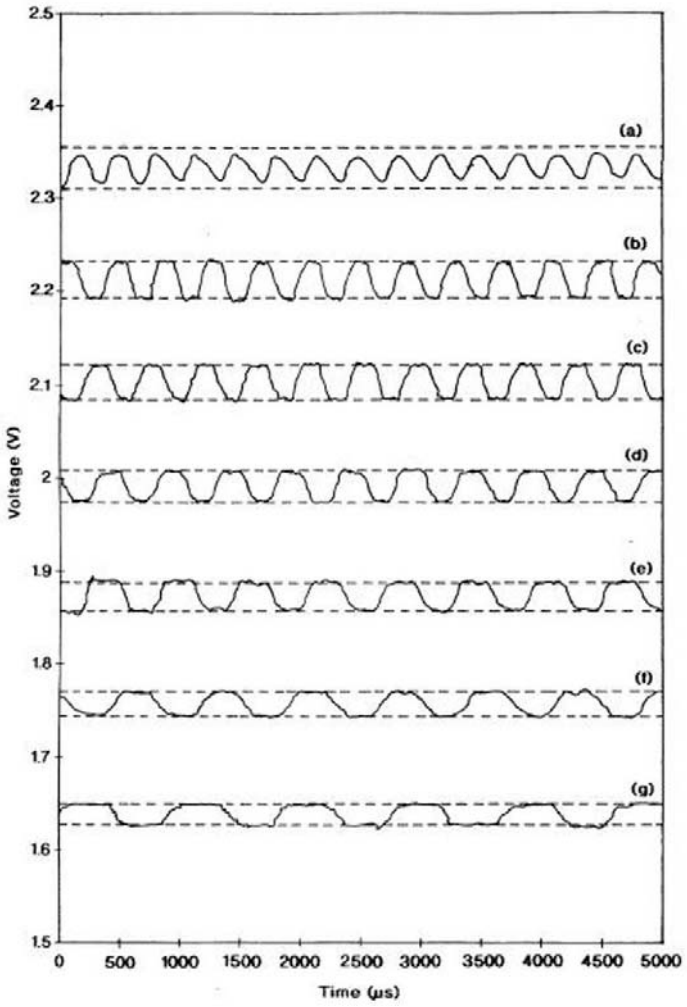

Figure 1.4: The voltage-time trace of the hot-wire mounted at 50 μm above the Perspex wall substrate for different imposed rates of rotation: (a) 3000 Hz, (b) 2490 Hz, (c) 2262 Hz, (d) 1993 Hz, (e) 1625 Hz, (f) 1335 Hz, (g) 1078 Hz. Calculated maximum and minimum voltages for each imposed frequency are shown as broken lines.

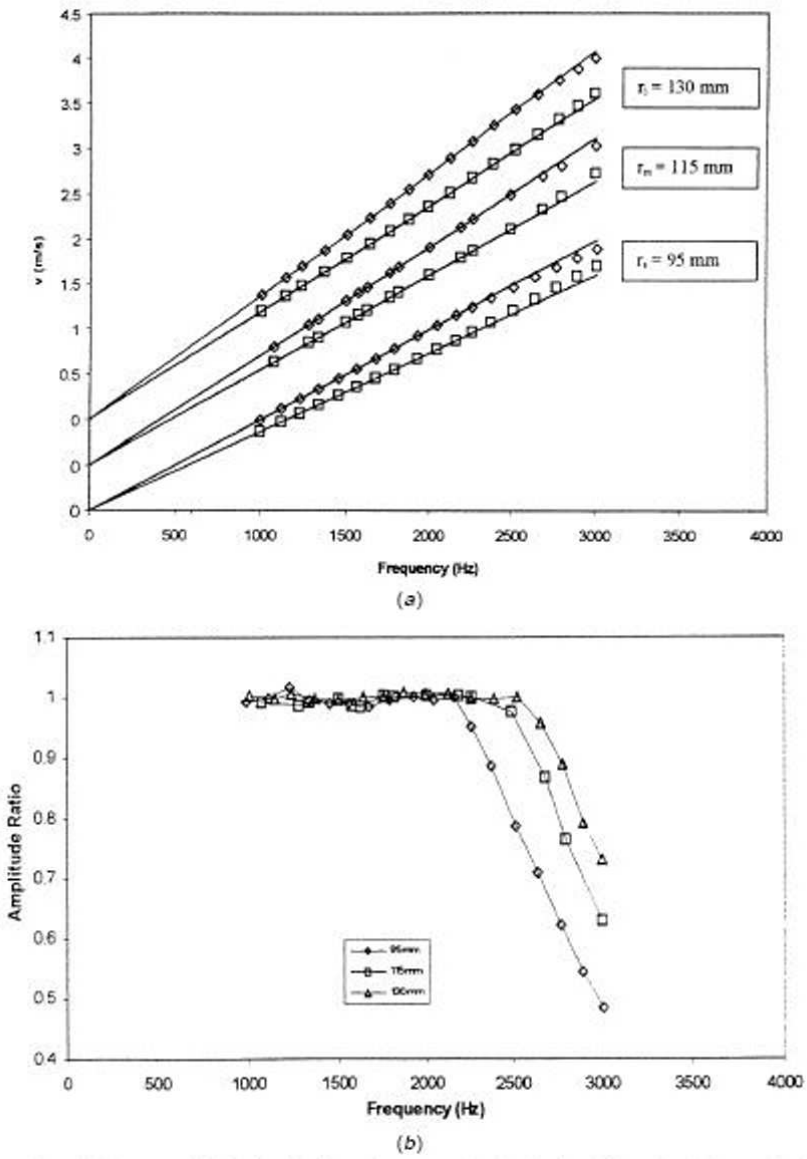

Figure 1.5: Comparison between *calculated* velocity and *measured* velocity for different rotation rates obtained from the hot-wire anemometer mounted 50 μm above the Perspex wall substrate at $r_s = 95$ mm, $r_m = 115$ mm and $r_l = 130$ mm. Calculated velocities are represented as full lines according to equation (1**XXX**). ($\Diamond$) and ($\Box$) represent the maximum and minimum of mean velocity fluctuation respectively. *(b)* Amplitude ratio, defined as a_{mea}/a_{imp}, for the hot-wire anemometer mounted 50 μm above the Perspex wall substrate at $r_s = 95$ mm, $r_m = 115$ mm and $r_l = 130$ mm for different imposed frequencies.

calculated velocities at the wire's position obtained from Eq.(1.1) corresponding to gap sizes of δ and $(\delta + \delta_r)$ which are presented as solid lines passing through the origin.

Figure 1.5(a) shows that the hot-wire mounted at h = 50μm from the perspex wall substrate can respond fully to a fluctuating flow field without any amplitude attenuation up to $f_{imp} \approx 2500$ Hz. Beyond 2500 Hz, the probe shows obvious amplitude attenuation and the measured velocities depart increasingly from the calculated velocities as f_{imp} becomes even larger. Figure 1.5(b) shows the amplitude ratio, defined as a_{mea}/a_{imp} (i.e. ratio of the *measured* amplitude of velocity fluctuation to the amplitude of the imposed velocity fluctuation), versus the imposed frequency. The dynamic response (f_D) is defined as the upper frequency limit where the onset of amplitude attenuation of the imposed velocity change occurs, the threshold of which is set at $a_{mea}/a_{imp} = 0.9$ (which is in line with the experimental uncertainty of about 10% for evaluated a_{mea}/a_{imp}), or when the said wire is no longer able to respond fast enough to the imposed frequency, whichever occurs first. Hence, from Figure 1.5(b), we may conclude that the dynamic response of the said hot-wire mounted at $r_m = 115$ mm and a height of 50 μm above the perspex wall substrate is given as $f_D \approx 2625$ Hz corresponding to a mean imposed convective velocity v_D of 2.94 m/s. It is reasonable to infer that for the same $v_D = 2.94$ m/s, at an imposed frequency of less than $f_D = 2625$ Hz, the hot-wire will not have encountered any amplitude attenuation or at the very most limited to a damping value less than 10%.

Figures 1.5(a) and 1.5(b) also show the results of the *same* hot-wire placed at radial positions $r_s = 95$ mm and $r_l = 130$ mm. The voltage-time traces (not shown) bear similar features to those depicted in Figure 1.4 for $r_m = 115$ mm; at lower imposed frequencies, distinct flat top and trough sections are discernible whilst at much higher imposed frequencies, the resulting periodic peak and trough voltages are not able to match the calculated voltages even though the evaluated frequencies are identical to the respective imposed frequencies. From Figure 1.5(b), it is observed that for h = 50 μm at $r_s = 95$ mm, f_D is found to be 2345 Hz corresponding to a mean imposed convective velocity v_D of 2.17 m/s. On the other hand, the hot-wire placed at r_l indicates a higher f_D of 2750 Hz and the corresponding mean velocity is $v_D = 3.48$ m/s.

It can thus be seen that a hot-wire mounted at a fixed height of 50 μm above the perspex wall substrate exhibits a distinct trend of increasing dynamic response (f_D) as the convective velocity increases. As the streamwise convective velocity is closely related to the forced convective heat transfer from the wire, it may thus be suggested that the dynamic response of a hot-wire system is also positively correlated with larger convective heat loss from the wire-element.

The placement of the modified top disk at $\delta = 300$ μm in the experiments, together with a fixed $\delta_r = 45$ μm, necessarily implied an amplitude of velocity change ($\Delta v/v$) of 13% for the above dynamic response tests. In the present study, we maintained a constant ($\Delta v/v$) of 13% throughout.

1.3.1(c) Wall effect on the dynamic response of a marginally-elevated hot-wire

Further tests were carried out to investigate the influence of wall effect on f_D for a marginally-elevated hot-wire. To discount the influence of convective velocity, it is imperative that the convective velocity at the wire's location be kept constant. However, in the determination of f_D using the present experimental rig, the convecting velocity at the wire's location cannot be preset independently, as both f_D and the corresponding v_D are obtained simultaneously. In this regard, several tests at different r and h were carried out with the aim of achieving similar values of v_D. Shown in Figs.(1.6a) and (b) are the results for wires mounted at h = 65 μm and r_s = 95 mm, for which f_D = 2390 Hz and v_D = 2.9 m/s; for the wire at h = 40 μm and r_l = 130 mm, f_D = 2690 Hz and v_D = 2.7 m/s.

Also plotted on the same figure for comparison is the result previously presented for h = 50 μm at r_m = 115 mm, where f_D = 2625 Hz and v_D = 2.9 m/s. It is evident that with the same nominal convective velocity at the wire's location, hence implying a similar convective heat transfer from the wire, the placement of the wire closer to the wall from h = 65 μm to h = 50 μm and finally down to h = 40 μm has resulted in a monotonically increasing f_D.

Conventionally, the closer the hot-wire is to the wall, the greater is the wall influence. It is therefore appropriate to suggest that the increase in wall effect has led to an improvement in f_D of the said wire. It is also important to mention that the wall effect is closely associated with greater heat transfer from the wire due to the physical presence of the wall. This can be mainly attributed to direct radiation heat transfer to the surrounding wall substrate or to the localized aerodynamic interference of the flow around the wire w.r.t. the nearby wall, thus resulting in an increase in convective heat transfer from the wire to the flow and the surrounding wall substrate.

1.3.1(d) Summary of results of f_D in semi-dimensionless plot

The findings from previous Sections 1.3.1(b) and 1.3.1(c) have shown that an increase in heat transfer from the hot-wire, whether due to convective heat transfer or to increasing wall effect, results in an improvement in f_D. These results obtained for the perspex wall substrate are reiterated in the semi-dimensionless plot of f_D versus h^+ (i.e. height of wire expressed in wall units $\nu/\overline{U_\tau}$) in Fig.(1.7). Besides the data for fixed heights of h = 25 μm and 50 μm, as well as for $v_D \approx 2.9$ m/s as demarcated by the respective loci, other results obtained are also plotted together with the "interpolated" loci indicating possible behaviour of the hot-wire mounted at r_l, r_m and r_s.

Several interesting features can be observed from Fig.(1.7). The hot-wire registers f_D as 2690 Hz with v_D = 2.7 m/s when positioned at r_l = 130 mm and h = 40 μm (equivalent to $h^+ = 2.6$). At about the same value of h^+, corresponding to h = 50 μm and r_s = 95 mm, the hot-wire exhibits f_D as 2345 Hz with a correspondingly smaller v_D of 2.17 m/s. Since a similar value of h^+ implies equivalent influence of wall effect on the hot-wire, it becomes apparent that an increase in the convective velocity on the wire with resulting greater convective heat transfer gives rise to

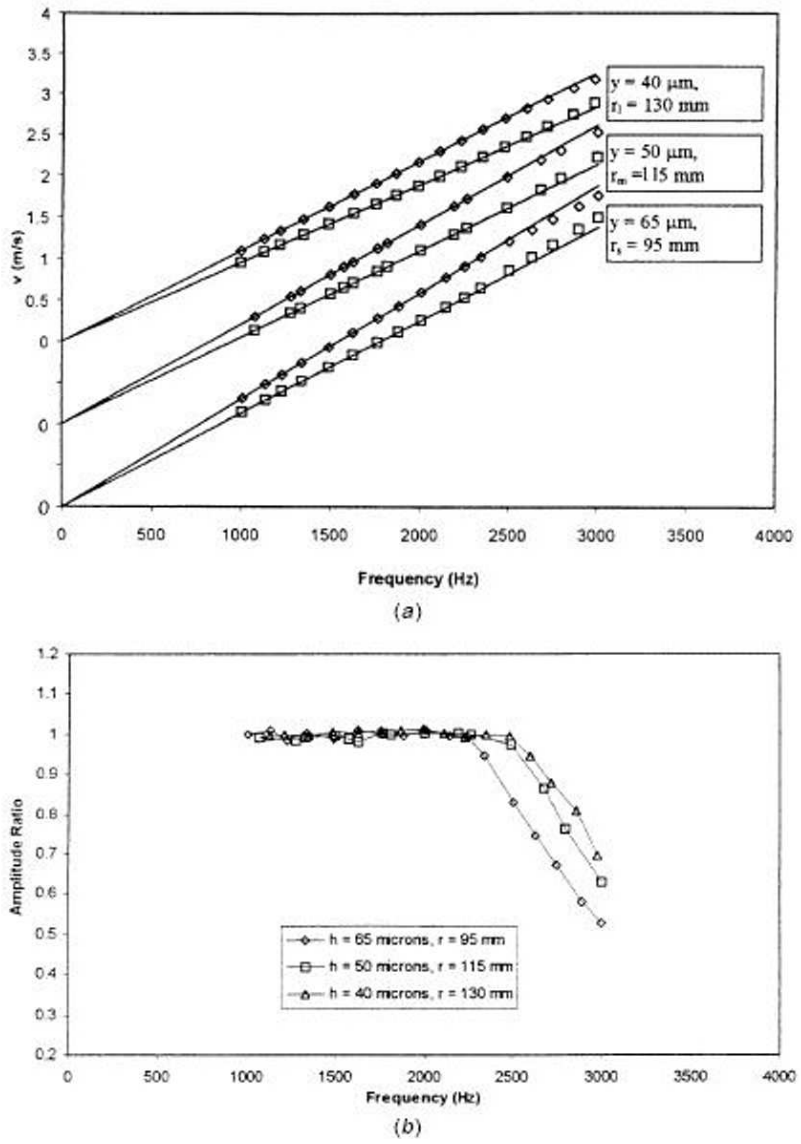

Figure 1.6: Comparison between *calculated* velocity and *measured* velocity for different rotation rates obtained from the hot-wire anemometer mounted 65 μm, 50 μm and 40 μm above the Perspex wall substrate at $r_s = 95$ mm, $r_m = 115$ mm and $r_l = 130$ mm respectively. Calculated velocities are represented as full lines according to equation (1**XXX**). ($\Diamond$) and ($\Box$) represent the maximum and minimum of mean velocity fluctuation respectively. *(b)* Amplitude ratio, defined as a_{mea}/a_{imp}, for the hot-wire anemometer mounted 65 μm, 50 μm and 40 μm above the Perspex wall substrate at $r_s = 95$ mm, $r_m = 115$ mm and $r_l = 130$ mm for different imposed frequencies.

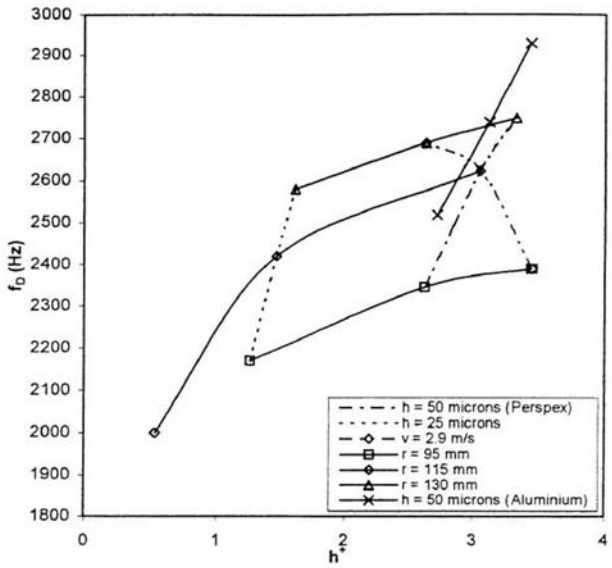

Figure 1.7: Semi-dimensionless plot of f_D for different values of h^+ for marginally elevated hot-wires placed above the Perspex and aluminium wall substrates.

an increase in f_D. Another feature, already discussed in Section 1.3.1(c), which is worth reiterating is that, for the same convective velocity of $v_D \approx 2.9$ m/s, the hot-wire shows the trend of increasing f_D with decreasing h^+, the latter being directly related to decreasing h. Since a smaller h^+ implies larger wall influence on the performance of a hot-wire with accompanying larger heat transfer from the wire, this suggests that a larger wall influence has actually a positive effect on f_D. The above two features clearly support the notion of f_D for a marginally-elevated hot wire increasing with enhanced heat transfer.

Finally, the results obtained for fixed heights of h = 25 μm and 50 μm show that as v_D increases, f_D increases. It is interesting to note that at a fixed elevation, an increase in h^+ is caused by an increase in v_D. As already discussed, a larger h^+ implies smaller wall influence with the tendency to cause a drop in f_D. Therefore, an increase in v_D, with consequential increase in the convective heat transfer from the wire, must have been sufficiently large to offset the effects of decreasing wall influence (corresponding to increasing h^+) such that the overall heat transfer is still larger, as manifested by the corresponding rise in f_D. The converse, i.e. the dominance of decreasing v_D on the convective heat transfer from the wire over the effect of increasing wall influence hence resulting in an overall decrease in f_D, is also true.

1.3.1(e) Effect of wall substrate material on f_D

The findings from Sections 1.3.1(c) and 1.3.1(d) have suggested that an increase in heat transfer from the wire due to increasing influence of wall effect has actually resulted in an increase in f_D. In their investigation of the near-wall corrections for single hot-wire measurements, Chew *et al.* (1995) found that a thermally more conducting wall substrate brings about an overall larger wall effect on the hot-wire resulting in larger heat loss to the wall, thereby necessitating a greater magnitude of wall corrections. In this regard, it is deemed appropriate to perform another series of tests to determine f_D for a wall substrate of different thermal conductivity to evaluate and further substantiate the effect of wall influence on the behaviour of f_D. A thermally more conducting Aluminium wall substrate, as compared to the perspex wall substrate used previously, was selected for this purpose. The hot-wire was mounted at a fixed height of h = 50 μm above the wall of the Aluminium plug, which was in turn mounted at r_s = 95 mm, r_m = 115 mm and r_l = 130 mm on the bottom stationary disk for the determination of the respective f_D.

Figure 1.8 shows the results for the measured maximum and minimum velocities versus imposed frequency for the hot-wire at r_s, r_m and r_l for comparison with the *calculated* velocities which are presented as straight lines passing through the origin. The results of Fig.(1.5) and Fig.(1.8) can then be compared to investigate the effects of wall substrate thermal conductivity on f_D for wires sharing same values of h and r.

For the case of the wire mounted at r_m, with the modified top disc rotating at 1575 rpm (equivalent to an imposed frequency of 2625 Hz), the wire above the perspex wall shows signs of amplitude attenuation first, and f_D is subsequently found to be 2625 Hz (see Figure 1.5). On the other hand, under the same operating conditions, the wire above the Aluminium wall did not show any indication of amplitude attenuation at 2625 Hz; it was only at a higher rotating speed of the top disc (at f_D = 2740 Hz) did the said wire show signs of amplitude attenuation (see Figure 1.8). It is therefore logical to conclude that *relatively*, a wire at a particular height above a perspex wall exhibits a poorer dynamic response (as characterized by f_D) compared to a wire mounted at the same height above a Aluminium wall.

The same behaviour can also be observed for hot wires mounted at r_s and r_l for the two different perspex and Aluminium wall substrates (c.f. Fig.(1.5) and Fig.(1.8)), thereby lending further support to the conclusion that an increase in wall influence on hot-wire performance has correspondingly given rise to an improvement in f_D.

Results for the hot-wire placed next to an Aluminium wall at h = 50 μm are also plotted in a semi-dimensionless form and shown in Fig.(1.7) for further comparison to results for the hot-wire above a perspex wall. A locus is also drawn through the former data points which supposedly should characterize the dynamic response of the said wire at the same height but subjected to different imposed convective velocities. The same argument holds for the locus passing through the data points of the hot-wire mounted at h = 50 μm above the perspex wall. At any given value of h^+, the value of f_D on the interpolated locus of the Aluminium wall

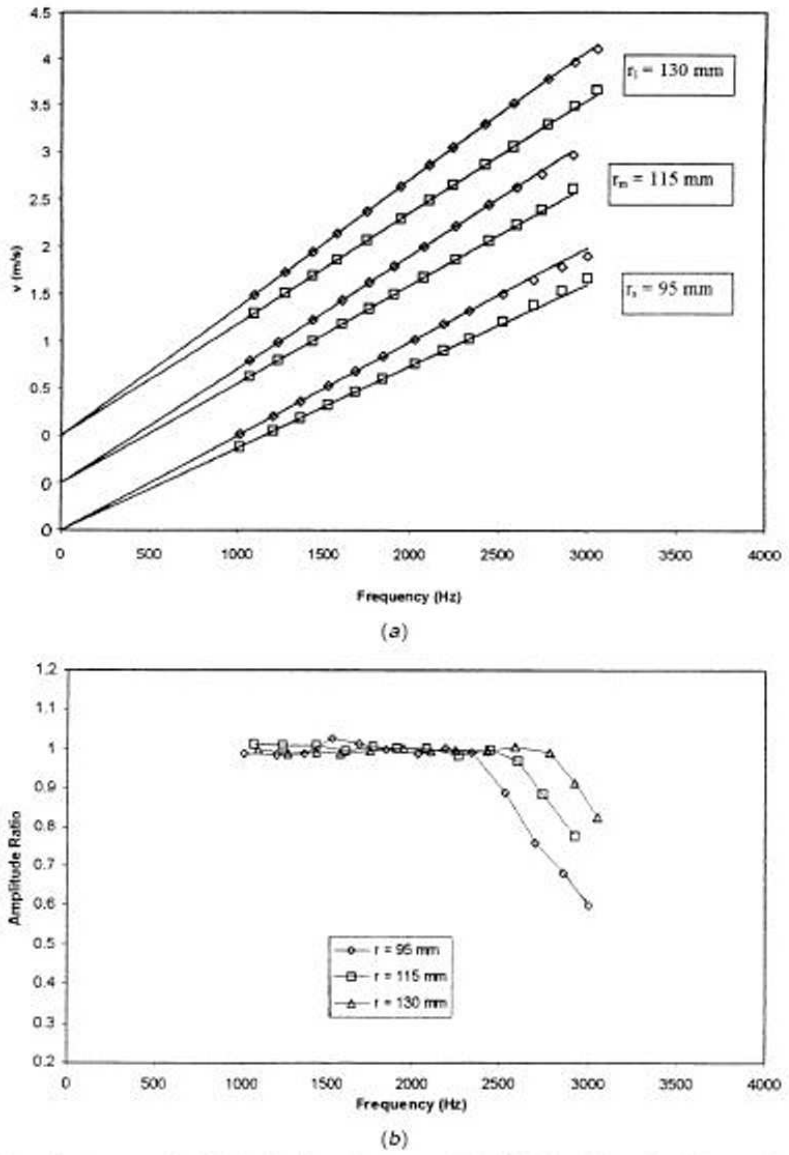

Figure 1.8: Comparison between *calculated* velocity and *measured* velocity for different rotation rates obtained from the hot-wire anemometer mounted 50 μm above the aluminium wall substrate at r_s = 95 mm, r_m = 115 mm and r_l = 130 mm. Calculated velocities are represented as full lines according to equation (1**XXX**). ($\Diamond$) and ($\Box$) represent the maximum and minimum of mean velocity fluctuation respectively. *(b)* Amplitude ratio, defined as a_{mea}/a_{imp}, for the hot-wire anemometer mounted 50 μm above the aluminium wall substrate at r_s = 95 mm, r_m = 115 mm and r_l = 130 mm for different imposed frequencies.

substrate is almost always larger than the corresponding f_D lying on the locus for the perspex wall.

Previous works have shown experimentally (Khoo *et al.* (1996) and Chew *et al.* (1998(a)) and numerically (Chew *et al.* (1995)) that a wire of the same diameter at the same h^+ exhibits a larger heat loss for the case of a thermally more conducting wall as opposed to one with lower thermal conductivity. In other words, at the same h^+, the wall effect due to the Aluminium wall substrate is invariably greater than the perspex wall substrate. It is therefore evident that the presence of a thermally more conducting wall with larger wall effects has resulted in a larger f_D which is in accord with the conclusions arrived at in the earlier sections.

1.3.1(f) Concluding remarks for Section 1.3.1

Experiments were carried out using a specially designed apparatus consisting of a modified top rotating disk with recesses cut on its surface and a bottom stationary disk to generate a known near-wall fluctuating flow field for purpose of quantifying the dynamic response of marginally-elevated hot-wire probes. Results have shown that while the hot-wire may be able to respond to the imposed frequency, it is the amplitude of velocity change ($\Delta v/v$) which serves as the limiting factor for the hot-wire to follow fully which leads to amplitude attenuation. For a hot-wire mounted at height $h = 50$ μm from the perspex wall substrate , the dynamic response frequency increases monotonically from 2345 Hz to 2750 Hz as the nominal convective velocity (v_D) changes from 2.17 m/s to 3.48 m/s. The same hot-wire mounted at $h = 25$ μm exhibits a similar behaviour for f_D, which improves from 2170 Hz to 2580 Hz, with v_D increasing from 1.00 m/s to 1.63 m/s. These findings suggest that an increase in the convective velocity, which is synonymous with a larger convective heat transfer from the wire, results in an increase in f_D.

When the hot-wire is subjected to a constant convective velocity of $v_D \approx 2.9$ m/s at different heights of 65 μm, 50 μm and 40 μm above the perspex wall, f_D shows an increasing trend with corresponding values of 2390 Hz, 2625 Hz and 2690 Hz, respectively. The decreasing heights, when expressed in wall units, indicate a decreasing h^+ with increasing effect of wall influence. This suggests that f_D improves with larger wall effects. The influence of greater wall effects also invariably implies more heat transfer from the wire due to localized aerodynamic influence of the flow around the wire w.r.t. the nearby wall (Chew *et al.*, 1995). This, together with the above findings, suggest that the dynamic response frequency of a marginally-elevated hot-wire increases with larger heat loss from the said wire irrespective of whether the greater heat loss is due to forced convection or due to wall effects.

Further experiments were also performed on a hot-wire mounted at the same height $h = 50$ μm above a thermally more conducting Aluminium wall substrate. It was found to exhibit a relatively better response characteristic compared to its counterpart above a perspex wall substrate under identical operating conditions. At the same h^+, the hot-wire above the Aluminium wall indicates a con-

sistently higher f_D than that above the perspex wall. As the wall influence on a marginally-elevated hot wire increases for a thermally more conducting wall, the results support the general conclusion that f_D increases with greater heat loss from the wire, in particular the influence of larger wall effect. More importantly, a wall possessing higher thermal conductivity ensures better response characteristics for marginally-elevated hot wires utilized for near-wall velocity measurements.

Further discourse on this Section 1.3.1 can be found in Khoo *et al.* (1998a).

1.3.2 Flushed-mounted hot-wire and hot-film for wall shear stress measurement

1.3.2(a) Calibration of the hot-element wall shear stress probe

The calibration of the respective hot-element wall shear stress probe was carried out with the flat rotating disk set at a distance δ from the bottom stationary disk. With $Re_s << 1$, the tangential wall shear stress (τ) according to Eq.(1.3) is correlated against the output voltage (E) via the equivalent King's law relationship,

$$E^2 = A + B\tau^n \tag{1.8}$$

where A, B and n are calibration constants, for different rotation rates ω and gap sizes δ. The methodology described is similar to that used in Chew *et al.* (1994). It may be noted too that Shah & Antonia (1987) used an identical equation (1.8) for their calibration except they carried out their calibration in a known turbulent channel flow and both the voltage (E) and shear stress (τ) were interpreted as mean quantities. In our experiments, calibration was carried out before and after the tests with the modified top disk. If there was any significant drift of the calibration constants by more than 2%, the results were discarded and repeated. The air temperature was monitored during the experiments to ensure a variation of less than $\pm 0.2^{\circ}$C.

1.3.2(b) The dynamic response (f_D) of a flush-mounted hot-wire wall shear stress gauge

The hot-wire was mounted physically in contact with the perspex wall substrate as a wall shear stress gauge. The modified top disk was placed at a height of $\delta = 300$ μm from the bottom stationary disk where the gauge was mounted throughout the experiments. This implies an amplitude of imposed wall shear stress fluctuations ($\Delta\tau/\tau$) of 13%, similar to the work in Section 1.3.1.

Figure 1.9 shows the various voltage-time traces of the said hot-wire positioned at r_m and subjected to the rotating movement of the modified top disk. At the lower imposed frequency $f_{imp} \leqslant 1250$ Hz (i.e. case (f) - (h)), the typical voltage signal shows a fairly well defined regular series with relatively flat top and trough sections whose average period coincides with the imposed frequency. As similarly

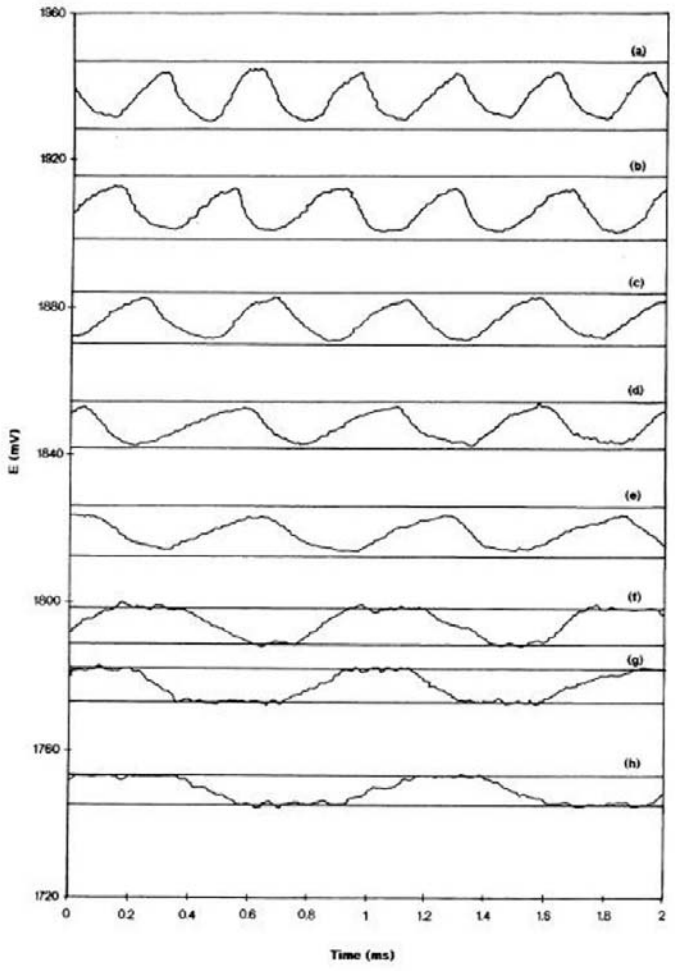

Figure 1.9: The voltage-time trace of the flush-mounted hot-wire wall shear stress gauge for different imposed rates of rotation: (a) 3033 Hz, (b) 2613 Hz, (c) 2250 Hz, (d) 1948 Hz, (e) 1678 Hz, (f) 1250 Hz, (g) 1107 Hz and (h) 925 Hz. *Calculated* maximum and minimum voltages for each imposed frequency are shown as full lines.

carried out in Section 1.3.1, on each voltage-time trace are the *calculated* maximum and minimum voltages associated with the wall shear stress (via the calibration curve) subjected to near-Couette flows with the top surface mounted at δ and $(\delta + \delta_r)$, respectively, from the bottom stationary surface and moving at a local tangential velocity of $\omega \mathrm{r}_m$. The concurrence of the flat top and trough sections of the voltage-time traces with the *calculated* maximum and minimum voltages for case (f) - (h) therefore indicates that the hot-wire can respond fully to the frequency and the amplitude of the imposed fluctuating wall shear stress.

The next higher imposed frequency shown for f_{imp} =1678 Hz (case (e)) shows a marked absence of the flat top and trough sections of the voltage-time trace and whose resulting peak and trough voltages are unable to match the *calculated* voltages, although the average period of the waveform agrees well with the period of the imposed fluctuations. There is clear amplitude attenuation for the above case (e), and the same can be said for the other higher imposed frequencies depicted in Fig.(1.9) from cases (a) to (d). Figure 1.9 therefore suggests that the upper frequency limit whereby the hot-wire can respond fully to the imposed fluctuations is essentially constrained by the occurrence of amplitude attenuation.

Results of Fig.(1.9) are replotted in Fig.(1.10) in terms of the *calculated* and *measured* maximum and minimum wall shear stresses at each imposed frequency. The *measured* maximum and minimum wall shear stresses correspond via the calibration curve to the relatively flat top and trough portions of the voltage-time traces for the lower frequencies in cases (f) - (g), and the peak and trough voltages for the higher frequencies in cases (a) - (e), and others. These measured mean values are ensemble-averaged over many cycles. In the same Figure 1.10(a) are the *calculated* wall shear stress quantities as obtained from Eqns. (1.3) and (1.4) corresponding to the near-Couette flows with gap sizes of δ and $(\delta + \delta_r)$, respectively, and the top surface moving at a velocity of $\omega \mathrm{r}_m$. These are represented as solid lines which pass through the origin.

Shown in Figure 1.10(b) is the amplitude ratio of measured wall shear stress change (a_{mea}) to the imposed wall shear stress change (a_{imp}) for the determination of the dynamic response frequency (f_D), which corresponds to the onset of amplitude attenuation set at $\mathrm{a}_{mea}/\mathrm{a}_{imp} = 0.9$. This is similar to that used in Section 1.3.1 and in line with the experimental uncertainty of about 10% for $\mathrm{a}_{mea}/\mathrm{a}_{imp}$. It is apparent that for the flush-mounted hot-wire, f_D is 1545 Hz and the corresponding mean shear stress value (τ_D) is 0.64 N/m^2. It is logical to infer that at the same $\tau_D = 0.64$ N/m^2, the flush-mounted hot-wire when subjected to a fluctuating wall shear stress with an imposed frequency of less than $f_D = 1545$ Hz will not exhibit any amplitude attenuation or at most limited to a damping value less than 10%.

Figure 1.10 also shows the respective results for the flush-mounted wire positioned at r_s and r_l (the voltage-time traces are not presented). The said figure clearly shows that f_D attains a value of 1240 Hz and a corresponding τ_D of 0.42 N/m^2 for the wire placed at the smaller radial position of r_s. At the larger radial position r_l, the wire registers a higher f_D of 1760 Hz, with a corresponding τ_D of 0.82 N/m^2. The above results therefore suggest a trend of increasing f_D with

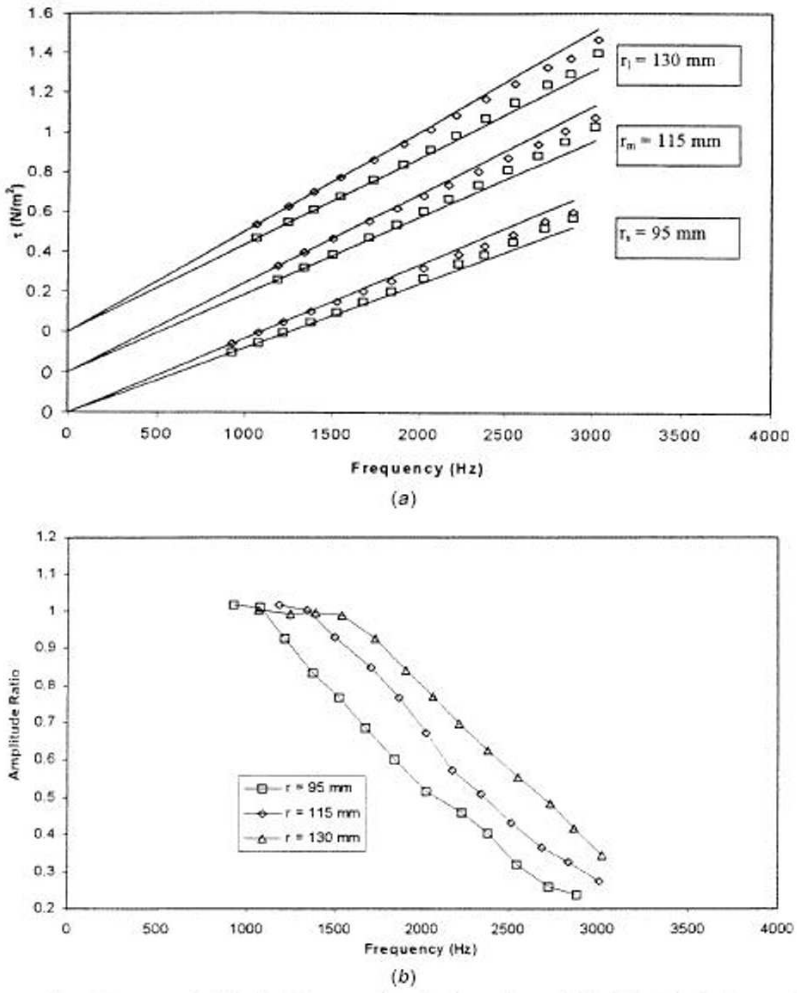

Figure 1.10: Comparison between calculated and measured wall shear stress obtained for the flush-mounted hot-wire gauge mounted at r_s = 95 mm, r_m = 115 mm and r_l = 130 mm for different rotation rates and δ = 300 μm. Calculations are represented as full lines according to equation (4**XXX**) with effective gaps given as δ and $(\delta + \delta_r)$. Experimental data: ($\Diamond$), ($\Box$) represent the maximum and minimum of wall shear stress fluctuations respectively. *(b)* Amplitude ratio, defined as a_{mea}/a_{imp}, for the flush-mounted hot-wire shear stress probe at r_s = 95 mm, r_m = 115 mm and r_l = 130 mm for different imposed frequencies.

greater imposed wall shear stress. Since a larger wall shear stress (and hence a larger velocity gradient) necessarily implies greater convective heat transfer from the hot-wire, the findings suggest a positive correlation between enhanced heat loss from the flush-mounted hot-wire and $f_{D,}$ which is a trend similarly observed for the dynamic response of an elevated hot-wire as discussed at length in Section 1.3.1.

1.3.2(c) The dynamic response (f_D) of the DANTEC-made 55R45 and 55R46

In reality, the above "flush-mounted" hot wires touching the perspex wall substrate are offset by 2.5 μm from the wire center to the wall and it is conceivable that (forced) convection remains the dominant mode of heat transfer as compared to conduction heat loss, since the region of contact with the wall substrate is rather limited. On the other hand, it would be interesting to determine the dynamic response of a flush-mounted hot film with the active element completely buried flush with the surrounding wall substrate. For the latter, it can be reckoned that conduction heat transfer is the dominant mode with secondary contribution from convective heat loss at the surface. In this respect, the commercially available DANTEC-made 55R45 and 55R46 wall shear stress gauges are selected; the former has a 0.5 μm quartz coating as opposed to the latter with a 2.0 μm quartz coating over the identical active hot element.

In the preliminary runs using the modified top disk with 100 recesses mounted at $\delta = 300\mu$m and rotating at only O(10) rpm, the 55R45 and 55R46 wall shear stress gauges placed at r_m exhibited great difficulties in following the amplitude of imposed wall shear stress fluctuations. In direct comparison to the experiments using the flush-mounted hot-wire under similar operating conditions where the hot-wire did not encounter any difficulty pertaining to amplitude attenuation until a much higher imposed frequency of 1545 Hz, it can be suggested that *relatively*, the hot-wire possesses better response characteristics than either the 55R45 or 55R46 shear stress probes. Because the apparatus is not designed for very low rotation rates, another modified top disk with only one recess of $\delta_r = 45$ μm was manufactured and employed to characterize the responsiveness of the hot-film wall shear stress gauge. The same gap size of $\delta = 300$ μm was maintained throughout. The imposed frequency is given as

$$f_{imp} = \frac{\omega}{2\pi} Hz \tag{1.9}$$

where ω is the angular velocity of the top disk in rad/s. With the 55R46 gauge mounted at r_m, the typical output voltage-time traces at different imposed frequencies show similar behaviour and salient features as those depicted for the flush-mounted hot-wire in Fig.(1.9) (except the timescale for the abscissa is several orders greater), and are thus not presented here. The results are expressed in terms of τ versus f_{imp} in Figure 1.11(a). Figure 1.11(b) shows the corresponding ratio of a_{mea} to a_{imp}, and it can be deduced that f_D assumes the value of 0.46 Hz with $\tau_D = 0.02$ N/m^2. The results obtained for the same gauge mounted at radial

positions r_s and r_l are also shown in the same figure. At the larger radial position of r_l, the 55R46 gauge exhibits a better response characteristic of $f_D = 0.59$ Hz, occurring at $\tau_D = 0.028$ N/m^2. On the other hand, the said gauge indicates $f_D = 0.41$ Hz at $\tau_D = 0.014$ N/m^2 when mounted at the smaller radial position r_s. From the above, the trend of f_D increasing with larger τ_D is discernibly similar to that found for the flush-mounted hot-wire. In other words, an increase in the convective heat transfer at the surface of the wall results in an improvement in the response characteristics of the flush-mounted 55R46 hot-film gauge.

The next series of tests is carried out for the 55R45 wall shear stress gauge mounted at r_s, r_m and r_l, and the corresponding results are plotted in Fig.(1.12). Figure 1.12(b) shows that f_D takes on the values of 0.63 Hz, 0.86 Hz and 1.15 Hz corresponding to τ_D of 0.022 N/m^2, 0.036 N/m^2 and 0.054 N/m^2, respectively. In general, the trend of increasing f_D with increasing τ_D is apparent for the 55R45 gauge, which bears resemblance in behaviour to the flush-mounted hot-wire and 55R46 gauges. It may be noted that under the same operating conditions for both the 55R45 and 55R46 gauges mounted at the same radial position, say r_m, when the imposed frequency is increased, the 55R46 gauge experiences amplitude attenuation first with $f_D = 0.46$ Hz, while the 55R45 gauge does not indicate any attenuation until a distinctly higher frequency, where $f_D = 0.86$ Hz. This observation, coupled with similar behaviour for the two gauges positioned at r_s and r_l, strongly suggests that the 55R45 gauge responds *relatively* better than the 55R46 gauge.

For purposes of further comparison, results for the dynamic response frequency of the three gauges are summarized and plotted in Fig.(1.13), where f_D is plotted against τ_D. The respective loci are traced through the data points corresponding to each gauge to indicate the trend of f_D with varying τ_D. The locus pertaining to the 55R45 gauge is always above that for the 55R46 gauge within the common range of τ shared by the 2 gauges, where the ratio of f_D for the 55R46 gauge to the 55R45 gauge averages out to be approximately 0.55. This implies that at the *same* τ, f_D for the 55R45 gauge is clearly superior to the 55R46 gauge. It may also be noted that for the same τ, the flow conditions above the two said gauges are identical. Because the 55R45 gauge has a thinner quartz substrate coating of only 0.5 μm, as compared to the 55R46 gauge which has a 2.0 μm quartz coating over the hot element of similar size, it can be construed that there is a correspondingly larger heat loss through the quartz coating to the flow for the 55R45 gauge, which resulted in a better response as characterized by f_D. This can be further explained in terms of the thermal resistance; the lower the thermal resistance of the wall substrate as for the case of the 55R45 gauge which has a thinner quartz coating, the better is the resultant response characteristic. This deduction about a more responsive flush-mounted hot film as a wall shear stress gauge resulting from larger heat loss from the active element is very similar to the conclusion arrived at in Section 1.3.1 for the marginally-elevated hot-wire as a probe for velocity measurements (where the response increases with increasing heat transfer irrespective of the origin).

If one is allowed to extrapolate the results for the flush-mounted hot-wire into

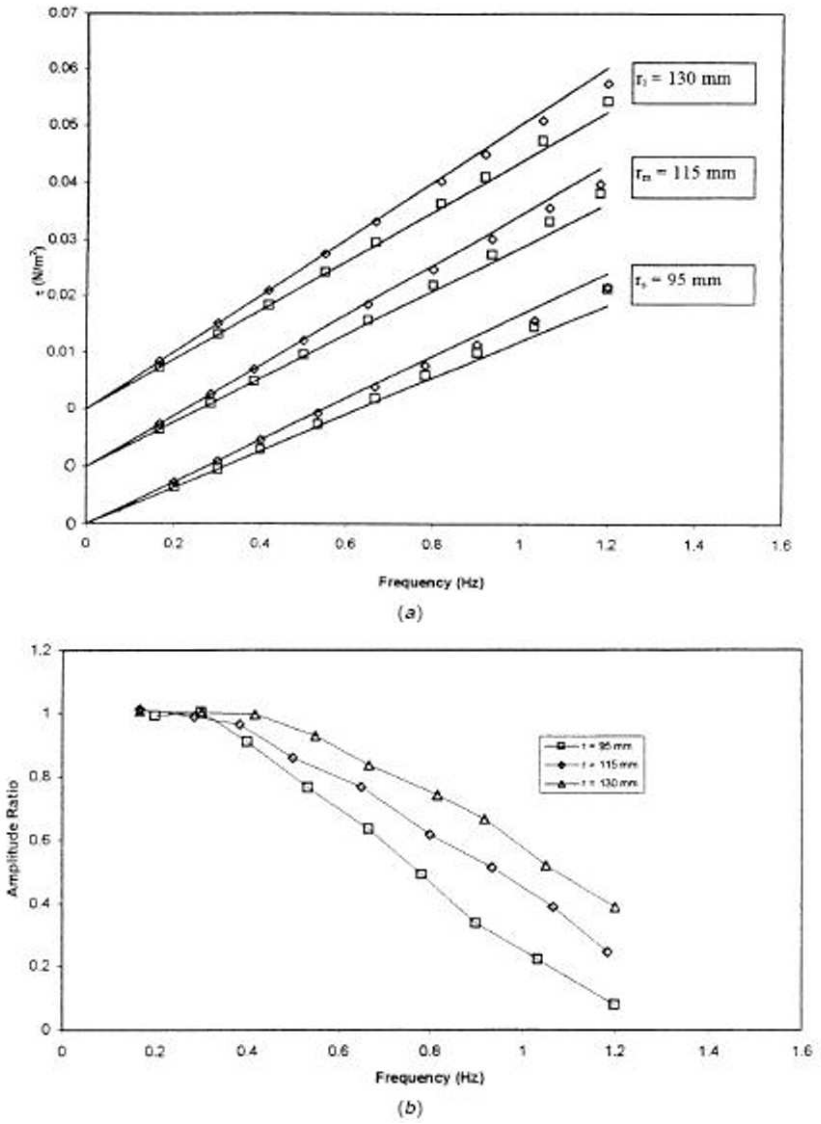

Figure 1.11: Comparison between calculated and measured wall shear stress obtained for the DANTEC 55R46 gauge mounted at $r_s = 95$ mm, $r_m = 115$ mm and $r_l = 130$ mm for different rotation rates and $\delta = 300$ μm. Calculations are represented as full lines according to equation (4**XXX**) with effective gaps given as δ and $(\delta + \delta_r)$. Experimental data: ($\Diamond$), ($\Box$) represent the maximum and minimum of wall shear stress fluctuations respectively. *(b)* Amplitude ratio, defined as a_{mea}/a_{imp}, for the DANTEC 55R46 gauge at $r_s = 95$ mm, $r_m = 115$ mm and $r_l = 130$ mm for different imposed frequencies.

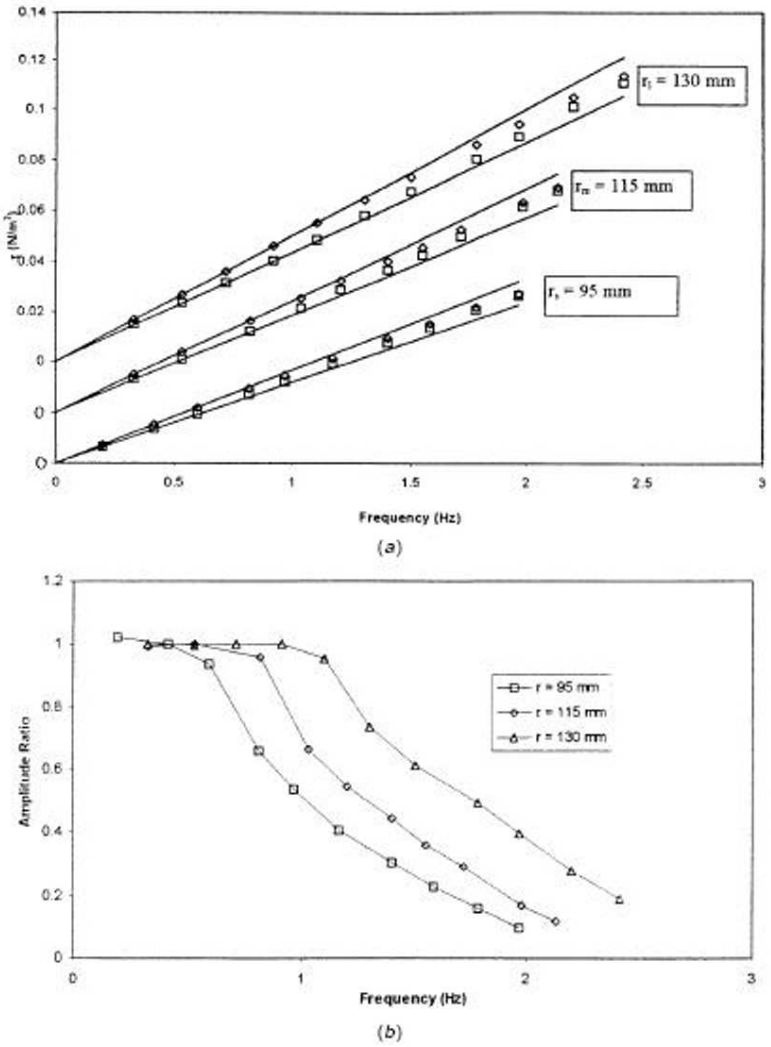

Figure 1.12: Comparison between calculated and measured wall shear stress obtained for the DANTEC 55R45 gauge mounted at r_s = 95 mm, r_m = 115 mm and r_l = 130 mm for different rotation rates and δ = 300 μm. Calculations are represented as full lines according to equation (4**XXX**) with effective gaps given as δ and $(\delta + \delta_r)$. Experimental data: ($\Diamond$), ($\Box$) represent the maximum and minimum of wall shear stress fluctuations respectively. *(b)* Amplitude ratio, defined as a_{mea}/a_{imp}, for the DANTEC 55R45 gauge at r_s = 95 mm, r_m = 115 mm and r_l = 130 mm for different imposed frequencies.

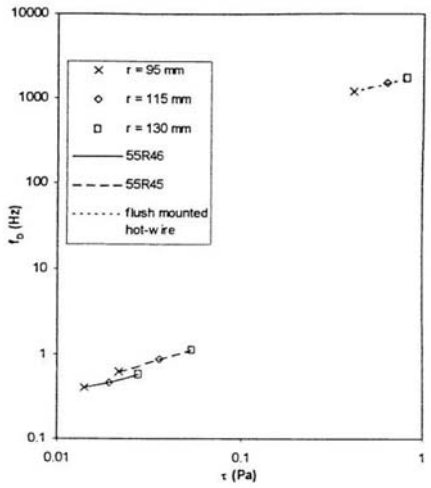

Figure 1.13: Dynamic response frequencies versus wall shear stress at onset of amplitude attenuation for the flush-mounted hot-wire wall shear stress gauge and the DANTEC 55R45 and 55R46 wall shear stress probes mounted at $r_s = 95$ mm, $r_m = 115$ mm and $r_l = 130$ mm.

the lower range of τ, common to the 55R45/55R46 gauges, it may be suggested that the performance of the former is still about two orders better than the latter two gauges at the same τ. Intuitively, it is conceivable that since the flush-mounted hot-wire is positioned almost in full contact with the convecting fluid, any changes in the flow velocity or velocity gradient at the wall will be felt almost instantaneously by the wire, with appropriate response from the CTA unit. For a flush-mounted hot film (like the 55R45 and 55R46 gauges) "buried" within the wall substrate, or even a hot-wire "buried" beneath the wall substrate, any variation in the flow conditions would probably be manifested only as a change in the boundary conditions on the top surface of the wall substrate for unsteady heat conduction to occur from the hot element linked to the CTA unit. For the latter, the thermal inertia of the wall substrate surrounding (and in full contact) with the active element would probably be featured prominently in the response characteristics of the flush-mounted hot film.

With conduction heat loss as the primary mode of heat transfer, the thermal conductivity of the surrounding substrate would also exact an influence on the response as observed for the 55R45 gauge vis-à-vis the 55R46 gauge which is diagnosed above. It can thus be postulated that the response of the said hot-film gauges would not be as fast as the flush-mounted hot-wire, where the dominant mode of heat loss is via direct (forced) convection. Indirect evidence is provided in the work of Cook *et al.* (1988) where they found both the "buried" flush-wire and

hot-film gauges exhibiting responses which lagged behind the imposed oscillating wall shear stress variations even at relatively low frequencies between 3 and 20 Hz. In fact, Cook *et al.* commented that the "buried" flush wire tended to yield a marginally larger magnitude of phase lag than the platinum film gauges. We may suggest that as the hot-wire is "buried" within the substrate, the dominant mode of heat loss becomes conduction, thus resulting in a behaviour which is very similar to that of a flush-mounted hot film. A full discourse of this subject can only be satisfactorily resolved with further work like a direct numerical simulation of an unsteady flow to examine the heat transfer from a hot element placed separately above and beneath the wall substrate and its relation to the ensuing response characteristics.

1.3.2(d) Further comparison of the responsiveness of the flush-mounted hot-wire wall shear stress gauge and DANTEC 55R45 and 55R46 wall shear stress gauges

Because of the inordinately vast difference in the dynamic response of the hot-wire and the hot-film (55R45 and 55R46) wall shear stress gauges, a further series of experiments were carried out to confirm qualitatively the difference in the response characteristics. The hot-wire was mounted at $r_m = 115$ mm on the bottom disk and diametrically opposite, the 55R46 was mounted at the same radial position. The top flat disk was placed at $\delta = 300\mu$m and made to rotate at 100 rpm for a period of time until the voltage outputs from both gauges indicated steady state condition (V_{ss}). The top disk was made to stop by turning off the power supply to the DC motor; due to the back emf induced in the motor, the disk stopped within about O(1) second. The respective non-dimensional voltage-time traces evaluated as

$$\bar{V}(t) = \frac{V(t) - V_o}{V_{ss} - V_o} \tag{1.10}$$

(where V_o is the voltage corresponding to the null state) from the Yokogawa-made (DL1540) digital oscilloscope are plotted in Fig.(1.14). Noting that the viscous action of the fluid medium (i.e. air) would require about $\delta^2/\nu \sim$ O(0.01 sec) for the flow within the gap to come to a halt, therefore the time lag of the flow field following the rotating disk motion is effectively immediate. From Fig.(1.14), the time required for $\bar{V}(t)$ to reach null state for the hot-wire wall shear stress gauge is about 1 second, hence implying a very fast response characteristic. More importantly, the comparison with the 55R46 gauge requiring up to about 160 seconds to reach the null state strongly suggests a qualitative time ratio of about two orders of magnitude, which is in broad agreement to that obtained by comparing the dynamic response frequencies.

Further tests were carried out under the same conditions but with the 55R46 gauge replaced by the 55R45 gauge. Since the voltage-time trace of the hot wire output is fairly repeatable, the later result is plotted staggered with the former result on Fig.(7**XXX**) for comparison. It is apparent that the 55R45 gauge takes a shorter time of about 90 seconds to reach the null state after the rotating top disk comes to a halt, as compared to the 55R46 gauge. The ratio of the time interval

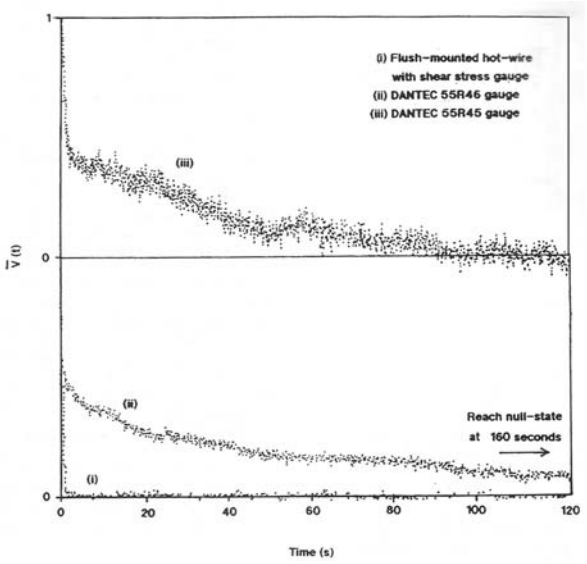

Figure 1.14: Dimensionless voltage-time trace for the flush-mounted hot-wire wall shear stress gauge and DANTEC 55R46 and DANTEC 55R45 gauges subjected to a sudden stoppage of the flat top disk rotating at 100 rpm.

required to reach null state for the 55R45 gauge, compared to the 55R46 gauge works out to be 0.56, which is in fair agreement with the ratio of the respective dynamic response frequencies of about 0.55. This test seeks to provide a qualitative yet independent check on the results obtained in the earlier sections on the dynamic response frequencies of the various wall shear stress gauges.

1.3.2(e) Concluding remarks for Section 1.3.2

Experiments were performed using a modified top rotating disk above a stationary bottom disk where different flush-mounted hot-element wall shear stress gauges were mounted, with the objective of determining the respective dynamic response frequency (f_D). It is found that the flush-mounted hot wire in contact with the wall substrate has a much higher frequency response of up to two orders of magnitude compared to the DANTEC-made 55R45 and 55R46 flush-mounted hot-film gauges. Despite its better performance, the f_D of the flush-mounted hot-wire is still discernibly lower than the marginally-elevated hot-wire used in near-wall velocity measurements as reported in Section 1.3.1. The perceived deterioration in the f_D for the flush-mounted hot-element wall shear stress gauge may have accounted for the relatively lower values of turbulence intensity and other higher order moments of wall shear stress fluctuations as observed by Cook (1994) for his three gauges compared to the equivalent near-wall velocity turbulence statistics

extrapolated to the wall, as reported in Alfredsson *et al.* (1988).

Further discourse on this Section 1.3.2 can be found in Chew *et al.* (1998b).

1.4 The dynamic response (f_D) vis-à-vis electronic perturbation test

The square-wave voltage perturbation test has been and may continue to be the preferred means from which the response of a hot-wire system can be determined in terms of the cut-off frequency. This can be partly attributed to the ease by which such a test can be carried out with any commercial CTA unit and abetted in no small way by the experimental difficulties encountered in carrying out a dynamic test. The latter invariably requires the imposition of a fluctuating velocity of sufficiently high known frequency and amplitude *directly* on the hot-wire so as to obtain the frequency response of the system.

One of the practical direct means incorporates the use of a high-frequency vibrating table with controllable frequency to which the hot-wire was attached. The latter, however, suffers from response problems associated with the vibration of the hot-wire relative to the prongs and the technique was quickly abandoned (Bellhouse & Rasmussen, 1968). Comte-Bellot (1977) employed radiative heating of the hot-wire or hot-film sensor using a sinusoidally amplitude- modulated laser beam from an Argon laser to quantify the frequency response of the sensor. Although the use of laser enables heating frequencies as high as 100 kHz, quantification of the amount of heating based on the output voltage of the anemometer is not so straightforward. The quantification of the amount of heating required is deemed necessary in determining whether the sensor has suffered from any (heat) amplitude attenuation. Another factor which has to be considered is that perturbations in the heating of the sensor may not be strictly synonymous to perturbations in the flow velocity, and it is the latter which is of relevance in quantifying the dynamic response of a velocity-measuring probe.

It is the intention of this Section 1.4 to compare systematically the dynamic response of a near-wall hot-wire system as obtained from direct velocity perturbation with that shown by the usual voltage perturbation test, and to ascertain experimentally if these are similar in magnitude and trend. There are two main types of voltage perturbation tests, namely the square wave perturbation and the sine-wave perturbation; these will be studied in Sections 1.4.1 and 1.4.2, respectively.

1.4.1 Square wave perturbation test (f_S)

1.4.1(a) Square wave perturbation test (f_S) for the hot-wire and hot film: Some preliminaries

Initial trials were performed to determine if the placement of the marginally elevated hot-wire probe above the wall in various geometrical configurations, whether in the vertical, horizontal or upside down positions, will affect the frequency response as deduced from the square-wave test (f_S). It was found that there was no noticeable difference in the value of f_S which suggests that the effects of buoyancy and natural convection surrounding the active element are fairly negligible. In this respect, all subsequent tests were carried out with the hot element mounted above a horizontal wall.

The test configuration to study the effects of different wall temperature and imposed overheat ratio on f_S incorporates the use of the Aluminium plug. The plug was inserted into a through-hole previously drilled on a copper plate with two thermocouple junctions soldered to the inner radius of the copper annulus. The construction is illustrated in Fig.(1.15). Here the overheat ratio is defined conventionally as T_W/T_A, where T_W and T_A are the temperatures of the hot-wire and the surrounding ambient air, respectively. A heater with pre-adjusted temperature was brought into contact with the copper annulus and the steady state temperature registered by the thermocouple was taken to be the temperature of the Aluminium wall substrate to which the hot-wire was exposed. In the same way, by changing the wire temperature, different overheat ratios can be imposed to determine its influence on f_S for a given wall substrate temperature.

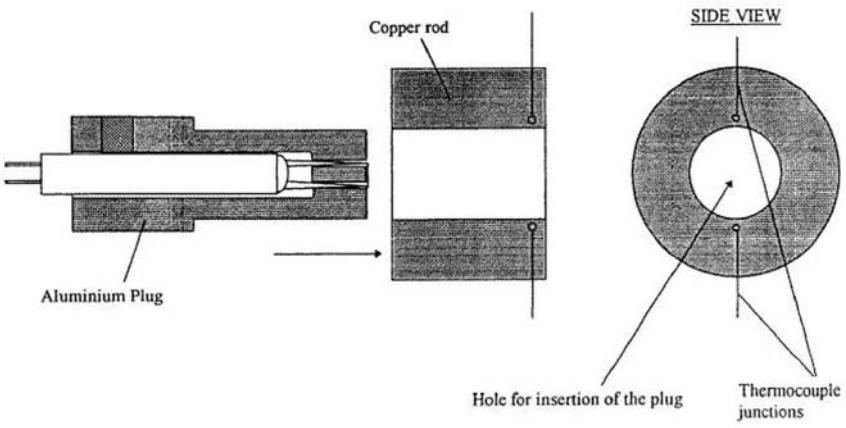

Figure 1.15: A schematic diagram of the plug and the copper sheath used in the square-wave test.

For measurements under mean flow conditions, the hot-wire was placed in the gap formed between a flat bottom stationary disk and a flat top disk rotating at an angular velocity ω. According to the analysis by Stewartson (1953), the flow

field in the gap is previously given in Section 1.2.1 and is repeated here as

$$\frac{v_\theta}{\omega r} = \left[\varepsilon - \left(\frac{Re_\delta^2}{6300}\right)\left(8\varepsilon + 35\varepsilon^4 - 63\varepsilon^5 + 20\varepsilon^7\right) + O\left(Re_\delta^4\right)\right] \quad (1.11)$$

$$\frac{v_r}{\omega r} = -\left[\left(\frac{Re_\delta}{60}\right)\left(4\varepsilon + 9\varepsilon^2 + 5\varepsilon^4\right) + O\left(Re_\delta^3\right)\right] \quad (1.12)$$

$$\frac{v_z}{\omega r} = 2\frac{\delta}{r}\left[\left(\frac{Re_\delta}{60}\right)\left(2\varepsilon^2 - 3\varepsilon^3 + \varepsilon^5\right) + O\left(Re_\delta^3\right)\right] \quad (1.13)$$

where (v_r, v_θ, v_z) are the velocities in the cylindrical (r, θ, z) coordinate system, ε ($\equiv z/\delta$) is the non-dimensional vertical coordinate normalised using the gap spacing (δ) between the two disks and measured from the stationary bottom disk, and Re_δ ($\equiv \omega\delta^2/\nu$) is the flow Reynolds number. By keeping Re_δ small ($Re_\delta << 1$), the flow approaches a Couette-like flow in the azimuthal direction. This feature was further substantiated by Khoo *et al.* (1998b) using DNS (direct numerical simulation) and used in the previous experimental works of Khoo *et al.* (1995), Chew *et al.* (1994) and Brown & Davey (1971) for purpose of near-wall hot-wire calibration. In our application, the hot-wire is subjected to different imposed mean velocities by rotating the top disk at different angular velocities. For all the runs, the hot-wire was connected to a DANTEC 56C01 CTA unit. The output from the latter was fed into a YOKOGAWA model DL1540 digital oscilloscope for monitoring and recording the response of the hot-wire subjected to a square-wave voltage perturbation input. The same CTA unit was used in Section 1.3.1. Adjustment was made to the CTA unit until a "marginally flat low-frequency response as well as the highest cut-off frequency" (Freymuth, 1977) as depicted in Fig.(1.16) was obtained. Here, τ_S is the optimum (minimum) time interval for the pulse (with some 13-15% undershoot w.r.t. the maximum) to decay to 3% of the maximum value as advocated by Freymuth (1977). Freymuth suggested that the frequency response (f_S) of the optimised hot-wire system (-3 dB point) is given by

$$f_S = \frac{1}{1.3\tau_S}. \quad (1.14)$$

The expression was used by Freymuth & Fingerson (1977) in their evaluation of the overall hot-wire response subjected to different free-stream convective velocities for eventual comparison to cylindrical hot-film probes. It may also be noted that DANTEC suggested a rather similar procedure for tuning and optimising the CTA unit w.r.t. the hot-wire probe although no mention was made about the evaluation of the associated frequency response.

For operation of the flush-mounted hot-film used as wall shear stress probe, (specifically the DANTEC-made 55R45 and 55R46), the manufacturer recommended a lower overheat ratio compared to the hot-wire. In this case it was set at 1.4, similar to that used in the velocity/flow perturbation experiments of Section 1.3.2. The hot- film probe was mounted in the rotating disk apparatus where the presence of a Couette flow in the azimuthal direction necessarily prescribed the associated velocity gradient and hence the imposed wall shear stress. The hot-film

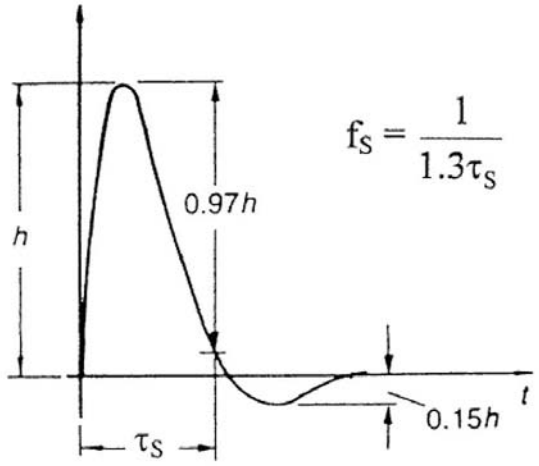

Figure 1.16: The square-wave-test frequency-response estimate for hot-wire sensors; from Brunn (1995).

probe was then connected to the same 56C01 CTA unit used in Section 1.3.2 and subjected to a square-wave voltage perturbation test. The output from the CTA was viewed using the YOKOGAWA made digital oscilloscope. When properly adjusted for optimum operation, the typical voltage-time trace is shown in Fig.(1.17) where f_S (the response frequency using the -3 dB point criteria) is nominally given as

$$f_S \approx \frac{1}{\tau_S}, \tag{1.15}$$

which is obtained empirically by Freymuth & Fingerson and subsequently substantiated by Freymuth (1981) (see also Bruun, 1995). Here, τ_S corresponds to the time interval at the voltage level "midway between the minimum and maximum of the resonance" after the initial peak as reckoned by Freymuth (1981); in Moen & Schneider (1993, 1994), τ_S is evaluated as the time interval from the voltage rise till the first minimum and the difference is not expected to be very significant and limited to about 10% variation. Huang *et al.* (1995) used the same definition for τ_S as Moen & Schneider, but instead modified the expression for the cut-off frequency to $f_S = 1/(1.5\tau_S)$.

One feature worth noting is the presence of the "tail" in the voltage-time trace after the resonance which is effectively absent in the typical optimised hot-wire response. This has been attributed to unsteady conduction heat loss to the wall substrate (e.g. see Davis, 1970) although, as seen above in Moen & Schneider and Huang *et al.* and many others like Kreplin & Eckelmann (1979), its effect is routinely disregarded by researchers in the evaluation of f_S without any explanation. Cook & Giddings (1988) have also commented that "indeed, time-

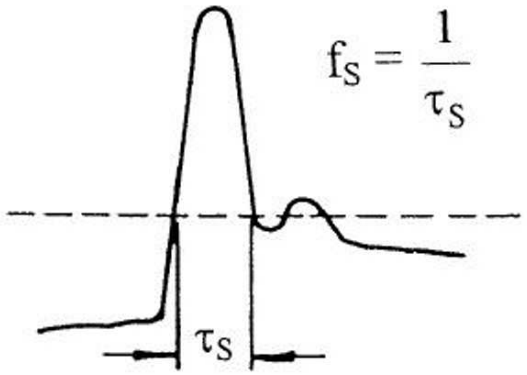

Figure 1.17: The square-wave-test frequency-response estimate for hot-film sensors; from Brunn (1995). See also Freymuth and Fingerson (1977).

dependent heat conduction in the substrate appears to be an important factor in gauge response" in their study of the response of hot-element wall shear stress gauges in laminar oscillating flow. In this Section 1.4.1, we shall primarily adopt this widely accepted practice of evaluating f_S (i.e. Fig.(1.17) and Eq.(1.15)) since it also provides an avenue for comparison to published works. However, for purpose of further qualitative comparison, we shall also evaluate $(f_S)_{withtail}$ taking into account the tail end response of the hot film. Because of the large experimental uncertainty incurred in determining the exact time taken for the output voltage to reach the null state due to the nature of the asymptotic decay, it is suggested that the time interval $(\tau_S)_{withtail}$ corresponding to the state when the output voltage has decreased to 10% of the maximum value be used for evaluation of $(f_S)_{withtail}$ in conjunction with Eq.(1.15). It may be noted in Moen & Schneider (1994) where the square-wave tests were carried out for their flush-mounted hot-film sensors, it was mentioned that the characteristic "tail" in the output voltage is due to "high-order behaviour observed in the system; the voltage did return before the beginning of the next square-wave however".

1.4.1(b) f_S for the near-wall hot-wire at different heights

Under conditions of forced convection where a known mean velocity (V) is imposed on the marginally-elevated hot-wire, the frequency response to a square-wave perturbation is obtained for different V and wire elevations. (The overheat ratio was set at 1.8 throughout, similar to the velocity perturbation experiments of Section 1.3.1.) The results are shown in Figure 1.18(a) with the wire height expressed non-dimensionally in wall units (h^+) for the abscissa.

For any given wire's physical height above the Perspex wall substrate, it is apparent that as V increases, f_S increases monotonically. This implies that as

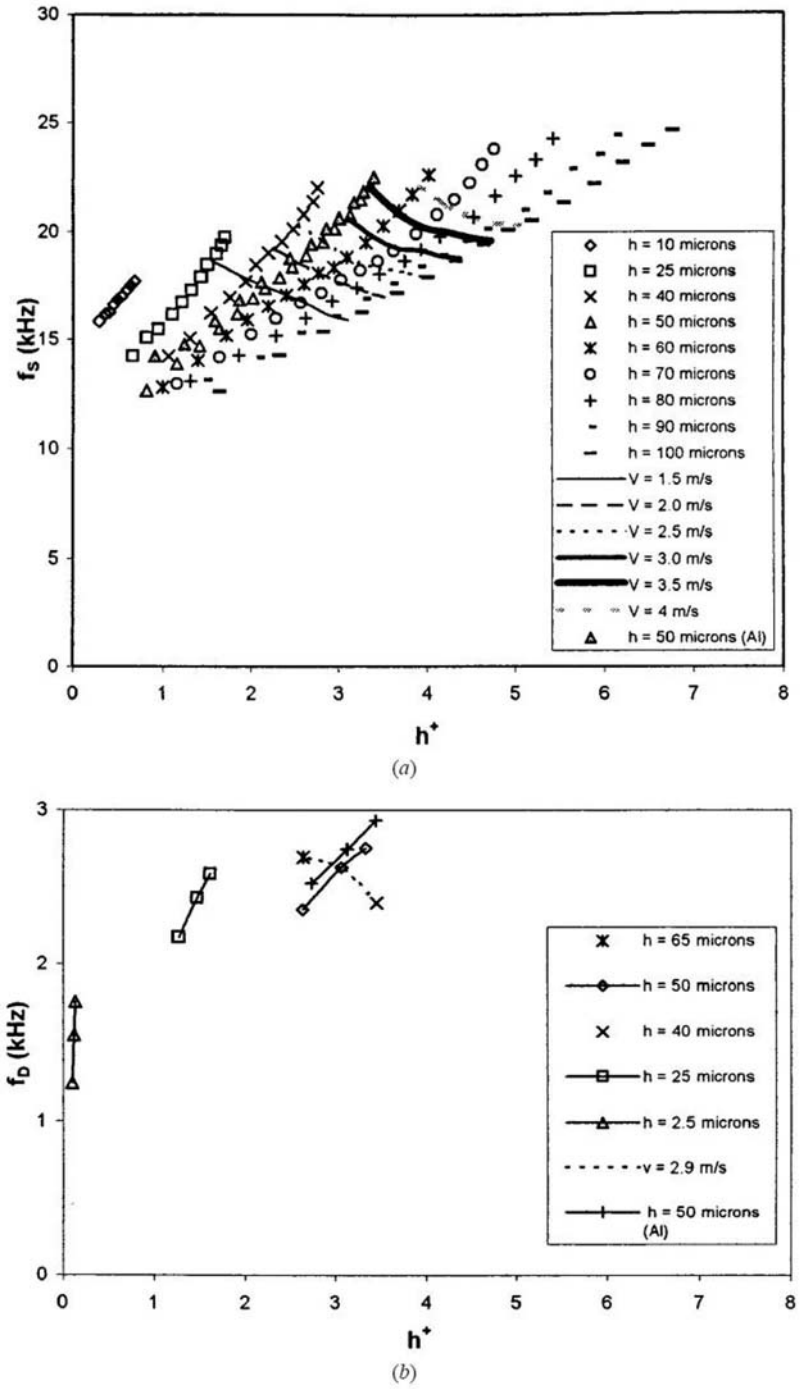

Figure 1.18: The square-wave frequency response f_S of a hot-wire mounted at various heights h above Perspex and aluminium wall substrates subjected to a tangetial convective velocity V plotted against dimensionless wall units h^+. The overheating ratio of the hot-wire is 1.8 and the nominal wall temperature is 24°C. *(b)* A semi-dimensionless plot of the dynamic frequency response f_D for various values of h^+ for marginally elevated hot-wires placed above Perspex and aluminium wall substrates.

the (forced) convective heat transfer from the wire becomes larger, the response characteristics in terms of f_S becomes better. This trend is consistent with the results provided by Freymuth and Fingerson (1977) for their hot-wire placed under free stream conditions where an increase in velocity from 0 to 9.1 m/s (30 ft/s) to 91.4 m/s (300 ft/s) is accompanied by a continuous improvement in f_S. Although Moen & Schneider (1994) only obtained f_S for their hot-film sensors in stagnant air, their final remark that "the steady flow that exists prior to the perturbation is likely to offset the results in a significant manner" attest to the importance of forced convection. Conventionally, the effect of wall influence on hot-wire operation is indicated by the dimensionless variable h^+ as can be deduced from works on wall proximity correction for hot-wire measurements (see Bhatia *et al.*, 1982; Hebbar, 1980 and Khoo *et al.*, 1996). These works show that the wall influence on near-wall hot-wire operation increases with smaller h^+, hence requiring a large correction factor. By keeping h^+ fixed, (i.e. similar wall effect on the wires), the increase in f_S with increasing V in Figure 1.18(a) necessarily implies that an enhanced forced convection leads to an improvement in f_S, all other factors being equal.

When some of the results in Figure 1.18(a) are presented in Table 1.1 for a given typical mean flow velocity of 3.0 m/s with wire's height decreasing from 100 μm to 50 μm (equivalent to a change of h^+ from 4.37 to 3.09), f_S shows a discernible and continuous increase from 18.76 kHz to 20.63 kHz. Using the argument that the nominal heat transfer from the hot wire due to forced convection is directly related to the mean convective velocity which is kept constant, it is reasonable to suggest that the increase in f_S with decreasing h^+ can be attributed directly to the increase in wall effect with accompanying greater heat loss from the wire to its surroundings (see also Chew *et al.*, 1995, for a discourse on the effect of wall influence on h^+ behaviour and its relation to additional heat loss to the flow and nearby wall substrate.) Shown correspondingly in Figure 1.18(a) is the locus of constant convective velocity at 3.0 m/s. Other loci of constant velocity ranging from 1.5 m/s to 4 m/s are also provided which clearly indicate the distinctive trend of increasing f_S with decreasing h^+ hence further attesting to the above suggestion. In Figure 1.18(a), the results for a hot-wire mounted at $h = 50$ μm above an Aluminium wall substrate are provided for further comparison to its counterpart mounted above a Perspex wall substrate at the same wire height. At the same h^+, the effect of wall influence pertaining to the Aluminium substrate on hot-wire operation is greater than the thermally less conducting Perspex substrate. This has effectively resulted in a higher f_S for the former in full accord with the above suggestion.

It is equally interesting to note from Figure 1.18(a) that an increase in V for a wire of fixed height, which translates directly into increasing h^+, has a trend of increasing f_S as noted earlier. This characteristic is irrespective of the adjacent wall substrate material. It can therefore be further argued that the effect of an increase in V with larger convective heat transfer must be sufficiently overwhelming to shadow the effect of decreasing wall effect (or increasing h^+) with the consequential result of increasing f_S. As noted earlier, decreasing wall effect or heat loss to the wall leads to a decrease in f_S. A discussion of the results displayed in Figure

Physical height of the hot-wire from wall substrate h (μm)	Height of hot-wire in terms of dimensionless wall units h^+	Square-wave frequency response (kHz) $f_S = 1/(1.3\tau_S)$
50	3.09	20.63
60	3.39	19.76
70	3.66	19.24
80	3.91	19.14
90	4.15	18.87
100	4.37	18.76

Table 1.1: A comparison of the square-wave-test frequency-response f_S for hot-wires mounted at various heights from a Perspex wall substrate with the same imposed mean flow velocity of 3 m s^{-1}.

1.18(b) will be deferred till Section 1.4.1(d).

The main conclusion drawn is that f_S increases with greater heat transfer from the hot-wire, and this is irrespective of whether it is due to forced/natural convection or effects of wall influence. It may be mentioned that in a given flow, the placement of a hot-wire closer to the wall will necessarily see its response (f_S) decrease due to a decrease in the convective velocity in the near-wall region. This effect will be mitigated to some extent by the increase in heat transfer from the wire due to increasing wall effect.

1.4.1(c) f_D for flush-mounted hot-wire and hot-film wall shear stress probes

The typical response of a hot-wire after optimization is shown in Fig.(1.16). As the hot-wire is lowered until contact is made with the Perspex wall substrate, the optimized response output as depicted in Fig.(1.19) still bears close resemblance to Fig.(1.16) and hence f_S is still evaluated according to Eq.(1.14).

The response characteristics of the "flush-mounted" hot-wire subjected to different flow conditions as indicated by the variation in the imposed wall shear stress (τ) at the wall is shown in Figure 1.20(a). (Whereas for an elevated hot-wire, the amount of forced convection and its influence on f_S is measured by the convecting velocity, in this case an equivalent indicator is the wall shear stress.) Again, the overheat ratio was maintained at 1.8, similar to the direct flow perturbation experiments in Section 1.3.2. Figure 1.20(a) shows explicitly that as τ increases, f_S increases monotonically. This is perhaps not surprising in view that a larger f_S associated with increasing convective heat loss from the flush-mounted hot-wire as τ increases is consistent with our results for the elevated hot-wire. The range of f_S experienced by our flush-mounted hot-wire is in the same order of magnitude as that estimated by Shah & Antonia (1987), who reported a frequency response of 25 kHz for their 5 μm Wollaston wire mounted in contact with a Perspex wall. It was not reported, however, whether Shah & Antonia had used the factor of

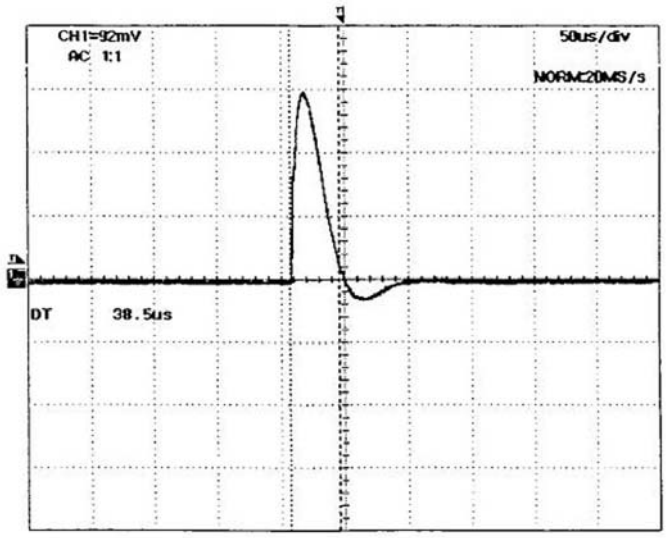

Figure 1.19: The output waveform for a flush-mounted hot-wire wall shear-stress probe subjected to a square-wave voltage-pertubation test at an imposed wall shear stress of 1.34 N m^{-2}.

1.3 in the evaluation of f_S nor was it mentioned whether the test was carried out with the hot wire subjected to a mean flow. The observed differences can also be attributed directly to the instrumentation employed, i.e. the use of different types of hot-wire and CTA units.

Unlike the output waveform for an optimised hot-wire where the decay to null state is fairly rapid, the typical response for an optimised hot-film wall shear stress probe (DANTEC 55R45 and 55R46) is shown in Fig.(1.21) for stagnant air.

Evaluating τ_S according to the definition depicted in Fig.(1.17) and Equation (1.15) gives f_S = 595 kHz and 538 kHz for 55R45 and 55R46, respectively. If one, however, measures the time constant associated with the "tail" of the output voltage (see Section 1.4.1(a)), the 55R45 probe takes a relatively longer time of about 0.14 ms ($\pm$10%) while the 55R46 probe requires an even larger period of about 0.26 ms ($\pm$5%). These are equivalent to $(f_S)_{withtail} \approx$ 7.1 kHz and 3.8 kHz, respectively, assuming the validity of Eq.(1.15). The latter calculations should only be viewed as a broad indicator incorporating the "tail" of the output voltage-time trace which has often been associated with continual heat loss to the surrounding wall substrate (see Davis, 1970) or other "higher order behaviour observed in the system" (Moen & Schneider, 1994). Shown in Figure 1.20(a) is the variation of f_S (with and without "tail") against the imposed wall shear stress (τ) for the wall shear stress probes. Within the range of τ investigated, it is apparent that both f_S and $(f_S)_{withtail}$ are rather independent of the prevailing wall shear stress. A similar

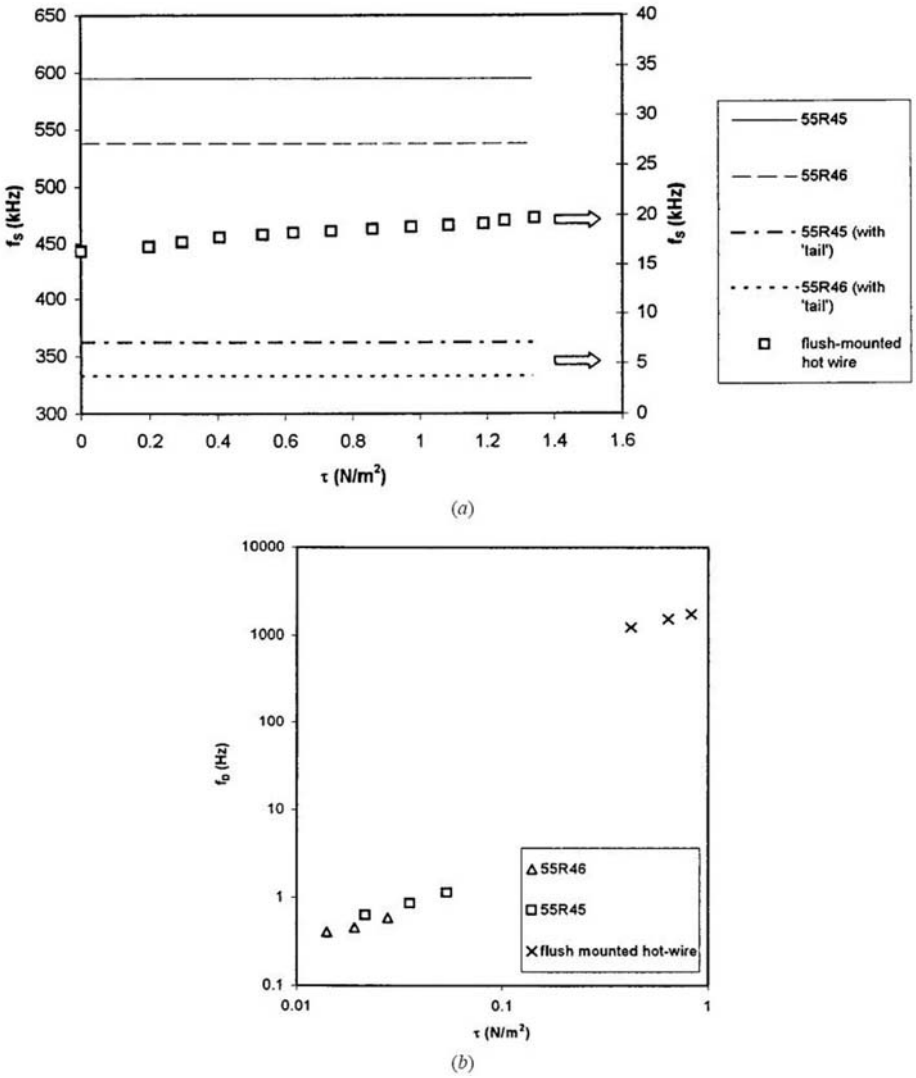

Figure 1.20: The square-wave frequency response f_S for a flush-mounted hot-wire wall shear-stress gauge and for commercially available DANTEC 55R45 and 55R46 hot-film wall shear-stress gauges subjected to various values of the wall shear stress τ. *(b)* The dynamic frequency response f_D for a flush-mounted hot-wire wall shear-stress gauge and for DANTEC 55R45 and 55R46 wall shear-stress probes subjected to various values of the wall shear stress τ.

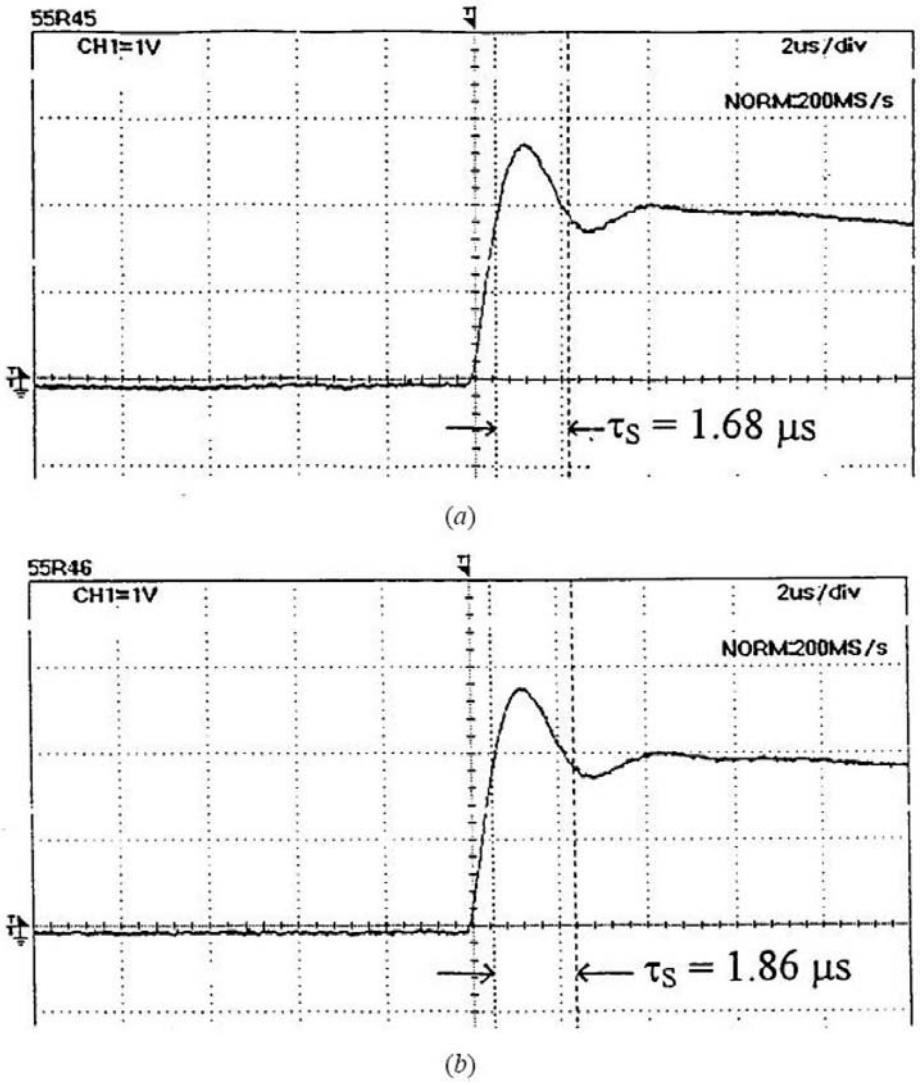

Figure 1.21: The output waveform of the DANTEC 55R45 hot-film wall shear-stress probe subjected to a square-wave voltage-pertubation test in stagnant air. *(b)* The output waveform of the Dantec 55R46 hot-film wall shear-stress probe subjected to a square-wave voltage-pertubation test in stagnant air.

observation was reported by Kreplin & Eckelmann (1979), who noted that their quartz-coated DISA 55A93 flush-mounted hot-film wall shear stress gauge (predecessor to the 55R45 probe) exhibited a square-wave frequency response which remained constant with or without a flow. Regardless of the criterion used to establish f_S, the 55R45 model indicates a better response than the 55R46 counterpart. Since the 55R45 gauge has a thinner top surface quartz coating compared to the 55R46 gauge, it can be construed that the former whose active element is in the midst of a thermally more conducting surroundings, hence experiencing a relatively larger overall heat transfer has given rise to the observed behaviour. This trend is consistent with the findings reported by Huang *et al.* (1995) and Moen & Schneider (1993) that the respective hot-film element mounted on a thermally more conducting substrate material has exhibited better response characteristics in terms of f_S.

1.4.1(d) Comparison of f_S and f_D

(i) Marginally elevated hot-wire velocity probe

Results of the velocity perturbation tests in Section 1.3.1 are reproduced in Figure 1.18(b) as f_D versus h^+. For purpose of completeness, some of the salient features are discussed below. At the same wire height of h = 25 μm or 50 μm above the Perspex wall substrate, an increase in the convective velocity (with an accompanying increase in h^+) results in a continual rise in f_D. This trend bears close resemblance to that observed for the square-wave voltage perturbation test. In Section 1.3.1, it was suggested that the increase in convective heat transfer for the elevated hot-wire has given rise to an improvement in f_D which is identical to the suggestion put forth for the behaviour in f_S (see Section 1.4.1(b)). From Figure 1.18(b), it can be further observed that for the hot-wire set at different heights above the wall substrate, but exposed to the same convective velocity of V = 2.9 m/s (thereby implying similar nominal convective heat loss), the wire mounted at 40 μm exhibits a higher f_D compared to that at 50 μm, followed by the lowest value of f_D registered at h = 65 μm. The wire's height in terms of wall units indicates that f_D increases with decreasing h^+. This suggests that an increase in wall effect with greater heat transfer from the wire due to localised aerodynamic interference of the flow around the wire w.r.t. the nearby wall has resulted in better response characteristics of the hot-wire expressed in terms of f_D.

The results of square-wave voltage perturbation test have also indicated a remarkably similar behaviour for f_S (see Table 1.1 and Section 1.4.1(b)). At the same $h^+ = 2.6$ (Figure 1.18(b)), which can be constructed as having similar level of wall influence for the wires mounted at h = 40 μm and 50 μm above the Perspex wall substrate, the wire at the lower height with higher prevailing convective velocity has seen an improvement in f_D. The said f_D increases from 2345 Hz to about 2750 Hz. Similar behaviour for f_S is apparent from Figure 1.18(a). The increase in convective heat transfer from the wire at the same h^+ (with similar

wall effect) has therefore enabled an improvement in the response characteristics of the hot-wire whether evaluated in terms of f_S or f_D.

Generally, the results from the velocity perturbation test which gives rise to f_D have indicated very similar behaviour to f_S in terms of trends. An increase in heat transfer from the wire, whether due to convective heat loss or to increasing wall influence, results in an improvement in both f_S and f_D. The effect of wall influence is further exemplified from the results of the hot-wire placed at h = 50 μm above the Aluminium wall substrate for comparison to its counterpart above the Perspex wall substrate. Both the trends of f_S and f_D indicate better performance at the same h^+ for which the wall effect pertaining to the Aluminium wall substrate is obviously higher.

The finding of similar trend in the behaviour of f_S and f_D may lull us into the possible belief that the square-wave voltage perturbation and velocity perturbation tests are equivalent. Therefore, it is timely and important to make a quantitative comparison too. Presented in Tables 1.2 and 1.3 are the respective values of f_S and f_D obtained under identical parametric conditions. Because the hot-wire used in conjunction with the CTA unit is the same, possible contributory factors such as equipment employed which may account for the differences in the results of f_S and f_D can be effectively ruled out.

Table 1.2 shows the comparison for the cases of a hot-wire mounted at different heights of h = 25 μm and 50 μm above both the Perspex and the Aluminium wall substrates with varying convective velocities, and Table 1.3 presents the results for different values of h with the convective velocity kept fixed at 2.9 m/s. Although Tables 1.2 and 1.3 depict similar trends for f_S and f_D, there is a great difference in the absolute magnitude for the corresponding cases. The ratio of f_S to f_D for the respective cases is generally in the region of an order of magnitude. There must be some fundamental differences between the square-wave voltage perturbation and the velocity perturbation tests. Further discussion on the possible causes is deferred to Section 1.4.1(e).

(ii) Flush-mounted hot-wire as wall shear stress probe

By lowering the height of the hot-wire until contact was made with the Perspex wall substrate, the flush-mounted hot-wire was used as a wall shear stress probe. The modified rotating disk apparatus of Section 1.3.1 was employed to generate two known quantities of fluctuating wall shear stress for the purpose of obtaining the associated dynamic response frequency (f_D) in Section 1.3.2. The results are reproduced in Figure 1.20(b). With the imposed wall shear stress increasing from 0.42 N/m^2 to 0.82 N/m^2, f_D assumes a continuous and perceptible improvement from 1.2 kHz to 1.8 kHz. This behaviour has the same trend as that discerned for f_S (see Figure 1.20(a)).

Despite the similarities between the observed trend for f_D and f_S, it is equally important to compare the absolute magnitude of frequency. Results of the frequency are tabulated in Table 1.4 for similar parametric conditions of imposed τ. It is clear that f_S is much larger than f_D with a ratio of at least an order of mag-

Material	Physical height of the hot-wire above wall substrate h (μm)	Dimensionless height h^+	Dynamic frequency response f_D (kHz)	Square-wave frequency response (kHz) $f_S = 1/(1.3\tau_S)$	Velocity (m s^{-1})
Perspex	25	1.26	2.17	15.66	1.00
	25	1.47	2.42	17.45	1.36
	25	1.61	2.58	19.14	1.63
	50	2.63	2.35	18.92	2.17
	50	3.06	2.63	20.52	2.94
	50	3.33	2.75	21.97	3.48
Aluminium	50	2.73	2.52	18.4	2.33
	50	3.13	2.74	20.89	3.07
	50	3.44	2.93	24.25	3.71

Table 1.2: A comparison of the dynamic frequency-response (f_D) and the square-wave frequency response (f_S) for hot-wires mounted at the same height above the wall substrate.

Physical height of the hot-wire above wall substrate h (μm)	Dimensionless height h^+	Dynamic frequency response f_D (kHz)	Square-wave frequency response $f_S = 1/(1.3\tau_S)$ (kHz)
40	2.72	2.69	21.57
50	3.04	2.63	20.45
65	3.47	2.39	19.91

Table 1.3: A comparison of the dynamic frequency response (f_D) and the square-wave frequency response (f_S) for hot-wires mounted at various heights above the Perspex wall substrate subjected to the same convective velocity of 2.9 m s^{-1}.

nitude for the corresponding cases. The large difference in magnitude observed justifiably raises the issue of the equivalence between f_S and f_D, of which further discussion on the subject is deferred to Section 1.4.1e).

(iii) Hot-film wall shear stress probes: DANTEC 55R45 and 55R46

Results of the dynamic response frequency (f_D) as in Section 1.3.2 for DANTEC 55R45 and 55R46 are shown in Figure 1.20(b). The feature of better frequency response for the 55R45 gauge as compared to the 55R46 gauge when measured in terms of f_S is replicated for the f_D characteristic. Upon comparing the magnitudes of f_S and f_D, Table 1.4 shows that f_S is at least up to 5 orders of magnitude greater than f_D. (The ratio of $(f_S)_{withtail}$ to f_D is still 3 orders of magnitude or more.) It is thus timely to examine carefully the implications of the frequency responses f_S and f_D, which constitutes the subject of discussion in the following section.

1.4.1(e) Plausible inherent differences between f_S and f_D

Freymuth (1977) carried out an analysis of the constant temperature hot-wire anemometer in an effort to study the frequency response and associated electronic testing. After linearizing the governing equations, and assuming that there are only small deviations of u (output voltage), r (resistance of hot-wire) and v (forced convection velocity at the wire's location) from the steady state operating conditions of U, R and V, respectively, the dynamic (response) equation becomes

$$\frac{MM"}{G}\frac{d^3u}{dt^3} + M_y\frac{d^2u}{dt^2} + M_x\frac{du}{dt} + u = Sv + M_z\left(\frac{\gamma U_t}{c/H} + \frac{dU_t}{dt}\right). \tag{1.16}$$

Here M"is a constant pertaining to the amplifier, G is the amplifier gain, γ is a function of the resistance in the bridge, c is the thermal inertia of the wire, H(V) is a heat transfer function dependent on the flow velocity which accounts for convective heat loss from the wire to the surroundings, and (M, M_x, M_y, and M_z) are further functions of the electrical resistances, G, M"and H(V). S is the sensitivity of the anemometer and simplifies to

$$S \approx \frac{U_0}{2}\frac{1}{H}\frac{dH(V)}{dV} \tag{1.17}$$

where U_0 is dependent on the resistances in the anemometer, the temperature coefficient of resistance of the wire α and the heat transfer function H(V). The first source term on the RHS of Eq.(1.16) represents the (small) velocity v perturbation effect while the second term accounts for the input electronic test signal U_t. It is interesting to note from Eq.(1.16) that for purely electronic testing utilising square-wave voltage perturbations as input (i.e. setting v = 0), the cut-off frequency (f_S) is as much a function of the prevailing convective velocity as verified by the results in Section 1.4.1(b). In the present application of the hot-wire mounted close to the wall, H(V) is also likely to be dependent on the nearby wall substrate thermal

Probe	Dynamic frequency response f_D (kHz)	Square-wave frequency response f_S (kHz)	Shear stress (N m^{-2})
Flush-mounted hot-wire	1.24	17.78	0.42
	1.545	18.28	0.64
	1.760	18.56	0.82
55R45	0.000 63	595	0.022
	0.000 83	595	0.036
	0.001 15	595	0.054
55R46	0,000 41	538	0.014
	0,000 46	538	0.019
	0,000 59	538	0.028

Table 1.4: A comparison of the dynamic frequency-response (f_D) and the square-wave frequency response (f_S) for the flush-mounted hot-wire wall shear-stress probe and the DANTEC 55R45 and 55R46 hot-film wall shear-stress probes.

conductivity. It is thus not surprising that the findings in Section 1.4.1(b) show that f_S is indeed influenced by the wall substrate material. (In this analysis, we have assumed Eq.(6**XXX**) as derived by Freymuth for a wall remote hot-wire in a freestream to be equally valid for near-wall applications by interpreting H(V) as the overall heat transfer function responsible for heat loss from the wire to the surroundings. In this respect, the said equation may still be used to elucidate the main physics for a flush-mounted hot-wire.) Therefore, it is important to realise that f_S does not just measure the response of the electronic system per se without consideration of the actual hot-wire operation.

A careful examination of Eq.(1.16) reveals that both the velocity and electronic perturbation tests routinely introduced to determine the response characteristic of the system, can be considered as separate source terms which appear on the RHS of the equation. The respective source terms are quite different in form and composition with S encompassing the derivative of H(V) w.r.t. V and which governs the velocity perturbation test unique to the first term. In the different perturbation tests, one can be considered to be solving for u to obtain the overall time characteristic with the appropriate source term. If Eq.(1.16) is assumed to be linear with the coefficients on the LHS independent of u and the coefficients of v and U_t on the RHS independent of time, classical control theory (e.g. Ogata, 1990) reveals that the frequency response of the system depends only on the coefficients on the LHS This in turn affects the location of the poles in the transfer functions relating u to v and U_t. Freymuth (1977) considered the two source terms on the RHS of Eq.(1.16) separately, and obtained two dimensionless equations governing the anemometer's response to velocity and electronic testing, respectively. As the coefficients on the LHS are exactly the same, it is thus not surprising that the cut-off frequency deduced from both perturbation tests are identical, although Freymuth did not explicitly state the equivalence of the two tests. If, on the other hand, the coefficients of v (i.e. S) and U_t, which are functions of H(V) are somehow dependent on the imposed frequency of velocity perturbations (see also Guo & Hyung 1997), then the respective source terms on the RHS of Eq.(1.16) must be solved separately together with the LHS to obtain the associated response of the overall system. Furthermore, since S is uniquely dependent on dH/dV, it is very unlikely that the introduction of additional poles and zeros into the transfer function relating u and v will be identical to the overall transfer function relating u and U_t. As a consequence, both perturbation tests will yield entirely different cut-off frequencies.

Freymuth (1978) carried out a similar analysis of the cylindrical hot-film sensor for use under free stream conditions. The equivalent response equation is given as

$$u\left[1+M_x\omega_c\left(\frac{p}{\omega_c}\right)^{1/2}+M_y\omega_c^2\left(\frac{p}{\omega_c}\right)^{3/2}+\frac{MM"}{G}\omega_c^3\left(\frac{p}{\omega_c}\right)^{5/2}\right] = Sv+M_zU_t\left[\frac{\gamma}{c/H}+\omega_c\left(\frac{p}{\omega_c}\right)^{1/2}\right] \qquad (1.18)$$

which is a $2\frac{1}{2}$ order system. Here all the shared symbols are identical to that

pertaining to Eq.(1.16), ω_c is the critical frequency introduced by Weidman & Browand (1975), and $u = \hat{u}e^{pt}$, with p characterising the frequency of input variables v or U_t. H(V) is still taken to be the heat transfer function of the film exposed to the effective (convective) velocity in a free stream. The output voltage waveform subjected to an electrical step input for the cylindrical hot-film sensor (see Fig.(1.17) or Freymuth & Fingerson, 1977) and flush-mounted hot-film sensor (Section 1.4.1(c) and Fig.(1.19)) take on a similar form. This suggests that the primary feature and characteristic of the latter are essentially captured by Eq.(1.18). Previous studies by Moen & Schneider (1994) and Huang *et al.* (1995) have also reported similar output waveforms for their respective flush-mounted hot-film wall shear stress sensors. It is also conceivable that for an electronic step input, the $2\frac{1}{2}$-order system of Eq.(1.18) which gives rise to the transient response reflected in Fig.(1.17) for a hot-film sensor is different from Fig.(1.16) for a hot-wire sensor with a 3rd-order system equation as put forth by Freymuth (1981). Following the same argument as for the hot-wire sensor, due to the possible dependence of H(V) on frequency, and the uniqueness of the term dH/dV in S, the introduction of additional poles and zeros into the transfer function linking u to v is unlikely to be similar to the poles and zeros of the overall transfer function relating u to U_t. To a hot-film user, the direct test which yields f_D is a far better indicator and more direct reflection of the probe's responsiveness to imposed wall shear stress fluctuations.

1.4.1(f) Concluding remarks for Section 1.4.1

Experiments using the electronic square-wave voltage perturbation test were systematically performed for the first time to evaluate the response frequency (f_S) of near-wall hot wires. In addition, two commercially available flush-mounted wall shear stress gauges were tested. A fixed wire height above the wall substrate, an increase in the convective velocity leads to an increase in f_S. For a hot-wire exposed to a constant convective velocity, f_S increases with decreasing heights from the wall substrate. This is also equivalent to a decreasing h^+ with increasing effect of wall influence, hence suggesting that f_S improves with greater wall effects. A hot-wire mounted at the same height h = 50 μm above a thermally more conducting Aluminium wall substrate exhibits a higher value of f_S compared to its counterpart above a Perspex wall substrate under similar operating conditions. These findings strongly suggest that f_S increases with increasing heat transfer from the wire, regardless of whether it is due to forced/natural convection or effects of wall influence. For a flush-mounted hot-wire, an increase in the imposed wall shear stress yields a corresponding increase in f_S. The value of f_S (with and without "tail") for the DANTEC 55R45 wall shear stress gauge is consistently higher than that for the 55R46 gauge, hence indicating the better frequency response of the 55R45 gauge.

Results of the frequency response according to square-wave voltage perturbation tests (f_S) were then compared to those obtained using velocity perturbation tests (f_D) in Section 1.3.1 and Section 1.3.2. Although f_S and f_D show similar

trends for the near-wall hot-wire and hot-film probes, f_S is consistently greater than f_D. The magnitudes of f_S and $f_D$are vastly different, being an order of magnitude for the marginally-elevated and flush-mounted hot wires. For the hot-film wall shear stress probes, this (ratio) difference is up to five orders of magnitude (without "tail") and three orders of magnitude (with "tail"). From a user's point of view, however, the dynamic frequency response (f_D) should serve as a more accurate indicator of the overall frequency response of the hot-wire/film system, since f_D signifies the onset of amplitude attenuation when the hot-wire/film is subjected to *direct* velocity or shear stress perturbations.

The large differences in magnitude between f_S and f_D show that the square-wave voltage perturbation test may not be all-sufficient in establishing the response frequency of a near-wall hot-wire or flush-mounted hot-film shear stress probes. Plausible inherent differences between f_S and f_D may be explained using the response equation for a hot-wire anemometer (Freymuth, 1977) and a hot-film anemometer (Freymuth, 1978). The sensitivity of the anemometer S depends on the heat transfer function (H) and the derivative of H with respect to the velocity V (dH/dV), which are likely to be frequency dependent. As a result, S may introduce additional poles and zeros into the transfer function which relates the output voltage to the perturbation velocity, thus rendering this transfer function to be different from that which relates the output voltage to the perturbation voltage. This is physically manifested as a difference in cut-off frequencies deduced from both types of perturbation tests.

Further discourse on this Section 1.4.1 can be found in Khoo *et al.* (1999).

1.4.2 Sine-wave perturbation test (f_{sine})

Although the square-wave test serves as a convenient means of quantifying some frequency response of a wall-remote hot-element system, one must exercise extreme caution in interpreting and associating it with the dynamic response especially in near-wall application. Freymuth (1979) noted that a constant temperature hot-wire anemometer has essentially *two* or *two* groups of attenuation frequencies when subjected to velocity, voltage or temperature perturbations. The first attenuation which occurs at low frequencies is due to end conduction heat loss for hot wires of low aspect ratios, which results in an attenuation in heat transfer fluctuations. One of the first thorough investigations on this issue was performed by Bremhorst & Gilmore (1978). A similar low-frequency attenuation has also been observed by Bellhouse & Schultz (1967), Bellhouse & Rasmussen (1968) and Comte-Bellot (1977) for non-cylindrical hot-film probes and have been termed as "side loss" effects.

The heat transfer from a hot-element sensor essentially consists of two main components. The first and desirable component is the heat flux that is convected *directly* from the heated sensor into the surrounding fluid. The second component is the heat flux that is first conducted to the prongs or wire-supports for the case of

hot wires and to the surrounding wall substrate for the case of hot film sensors, and this heat flux is subsequently convected into the surrounding fluid. Alternatively, one may generally view the second component as the additional heat loss to the wall substrate or due to the presence of the wall such that the occurrence would be absent for wall-remote applications. As the frequency increases from steady-state, the conduction fluctuations are first attenuated due to the attenuation of heat waves along the wire or substrate. This continues until a sufficiently high frequency when only the first desirable component of the heat flux associated with convective heat transfer remains. This first attenuation due to the so-called "end/side loss" occurs at low frequencies, after which the attenuated response extends to high frequencies before the second and final attenuation. The latter is attributed to the finite frequency response of the electronic feedback control components in the anemometer. It is imperative to note that the second attenuation bears no reference or relevance to the first attenuation and they are completely separate effects (Freymuth & Fingerson 1977 and Freymuth 1979).

From the above discussion, it is perhaps reasonable to suggest some possible association between the *lower* magnitude dynamic response frequency (f_D) obtained in Sections 1.3.1 and 1.3.2 and the range of frequencies at which the first attenuation occurs. On the other hand, the frequency corresponding to the second attenuation is reflected by the square-wave test results (f_S) which yield the much higher magnitude cutoff frequency of the anemometer. For the marginally-elevated or flush-mounted hot-wire probes used in Sections 1.3.1 and 1.3.2, the wire length to diameter ratio was consistently greater than the conventionally accepted value of 200 so as to reduce end conduction losses through the prongs (Ligrani & Bradshaw 1987 and Chew *et al.*, 1998a). It is thus suggested that the amplitude attenuation corresponding to f_D is attributed to the effect of additional heat loss to or due to the presence of the wall.

In this Section, an extensive series of sine-wave tests will be carried out systematically for the marginally-elevated hot-wire and wall shear stress sensors investigated previously. The sine-wave test results are analyzed over the entire frequency range of interest to detect/seek the (causality) presence of any attenuation occurring below the high cutoff frequency which may correspond to f_D in the dynamic velocity or wall shear stress perturbation tests. The high cutoff frequency which is obtained from the sine-wave test (f_{sine}) can also be compared to that obtained using the conventional square-wave test (f_S) to investigate the equivalence or consistency of the two electronic perturbation tests for near-wall hot-element probes.

1.4.2(a) Sine wave perturbation test (f_{sine}) for the hot-wire and hot film: Some preliminaries

In the square-wave voltage perturbation test, the output response of the anemometer subjected to an *instantaneous* rise (or fall) in the input test signal is used to determine a characteristic time which quantifies the frequency response of the hot-element system. However, it is not possible to merely employ a *single* characteristic time (or frequency) to study or assess the relative response of

a system over a *range* of frequencies. In contrast, for the sine-wave voltage perturbation test, an entire range of frequencies of sine-wave voltage perturbation is used to investigate the response or flatness of the system over the whole frequency range. This is similar to dynamic perturbation testing, where varying frequencies of dynamic perturbations are employed to obtain the dynamic frequency response of the system.

In order to perform a sine-wave test, a sinusoidal test signal output E_t from a Kenwood model FG-273 function generator was fed into the bridge, as shown in Fig.(1.22). The frequency of the sinusoidal test signal E_t was varied over a wide range of frequencies, while its amplitude was kept constant. Corresponding to each input frequency, the sinusoidal output response E of the anemometer was displayed on the digital oscilloscope and the amplitude (e) of the output was noted. The amplitude of the sinusoidal output e was subsequently plotted against the corresponding frequency f in logarithmic scales to obtain the test response of the hot-wire or hot-film system (see Figure 1.23(a)).

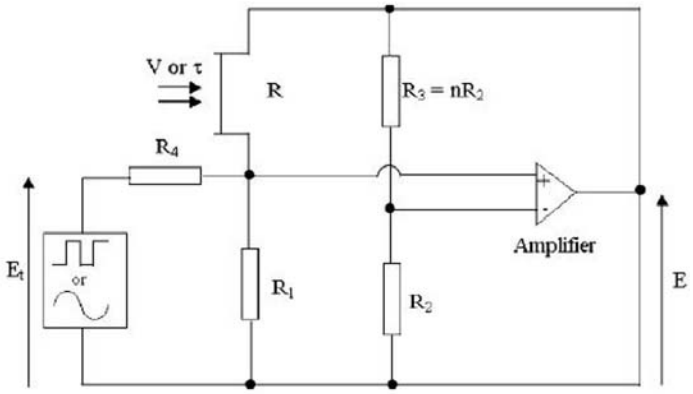

Figure 1.22: The circuit of the constant temperature anemometer.

For a wall-remote hot-wire sensor, the upward positive sloping region of the sine-wave response curve should have a slope of unity. This upward sloping line should extend to infinity ideally if the gain of the amplifier is infinite and there are no reactances in the amplifier or bridge. However, the reactances which are present limit the response to a finite frequency and the actual sine-wave response curve exhibits a decaying trend at high frequencies. The cutoff frequency of the anemometer can then be determined from the value of the frequency at which the actual sine-wave response curve drops 3 dB below the ideal response curve, as depicted in Figure 1.23(a). This cutoff frequency obtained from the sine-wave test (f_{sine}) should correspond to the square-wave frequency response (f_S), as validated by the wall-remote hot-wire model proposed by Freymuth (1977). (In the present work, it was carried out for near-wall hot-wire and flush-mounted hot-film probes.)

Moreover, Freymuth & Fingerson (1977) commented that a 3 dB drop in the actual sine-wave response curve below the ideal one would correspond to the *same* drop for sinusoidal velocity fluctuations. Figure 1.23(b) illustrates the presence of low-frequency bulging effect obtained by Freymuth & Fingerson from the sine-wave tests conducted on a conical film sensor.

1.4.2(b) Comparison for (high) cutoff frequency obtained from sine-wave (f_{sine}) and (f_S)

(i) DANTEC-made 55R45/55R46 flush-mounted hot-film wall shear stress probes

Figure 1.24 shows the sine-wave test results for the 55R45 and 55R46 flush-mounted hot-film wall shear stress probes obtained in the absence of a flow. For the 55R45 probe, overheat ratios between 1.2 and 1.6 were used, whereas for the 55R46 probe, the overheat ratio had to be kept below an upper limit of 1.4 according to the manufacturer. For each probe, when the overheat ratio was held constant, the sine-wave test response was relatively independent of the magnitude of the prevailing wall shear stress over the entire range of frequencies investigated (not shown). The imposed wall shear stress (τ) ranged from 0 to 1.0 Pa in the tests. This implies that the cutoff frequency (f_{sine}) does not have a strong dependence on τ. When the square-wave test was performed at a fixed overheat ratio, the output waveform and hence the square-wave frequency response (f_S) was also found to be invariant when τ was varied. The independence of f_S with τ has also been noted by Kreplin & Eckelmann (1979), who reported that their quartz-coated DISA 55A95 gauge (a precursor of the 55R45 probe) operating at an overheat ratio of 1.02 displayed a square-wave frequency response which remained constant with or without a mean flow.

Presented in Table 1.5 are the values of the cutoff frequencies evaluated using the sine-wave and square-wave tests subjected to different overheat ratios. For each probe, both f_{sine} and f_S increase monotonically with the overheat ratio. Moen & Schneider (1994) have reported a similar trend of f_S increasing with the overheat ratio for their flush-mounted hot-film sensors operated in stagnant air. Table 1.5 also shows that the 55R45 gauge possesses a higher cutoff frequency than the 55R46 gauge, regardless of the type of voltage perturbation test used. The 55R45 gauge, which possesses a thinner top surface quartz coating than the 55R46 gauge, has its active element in the midst of surroundings with lower thermal resistance. It can thus be construed that the higher cutoff frequency of the 55R45 gauge is due to the enhanced overall heat transfer to the surroundings. This is also supported by the earlier observation that the cutoff frequency increases with increasing overheat ratio resulting in enhanced overall heat transfer to the surroundings.

It is evident that for each overheat ratio, f_{sine} and f_S bear the same order of magnitude, with f_S assuming a consistently higher value than f_{sine} by 10 to 20%. This difference might be due to the current CTA unit employing an in-built

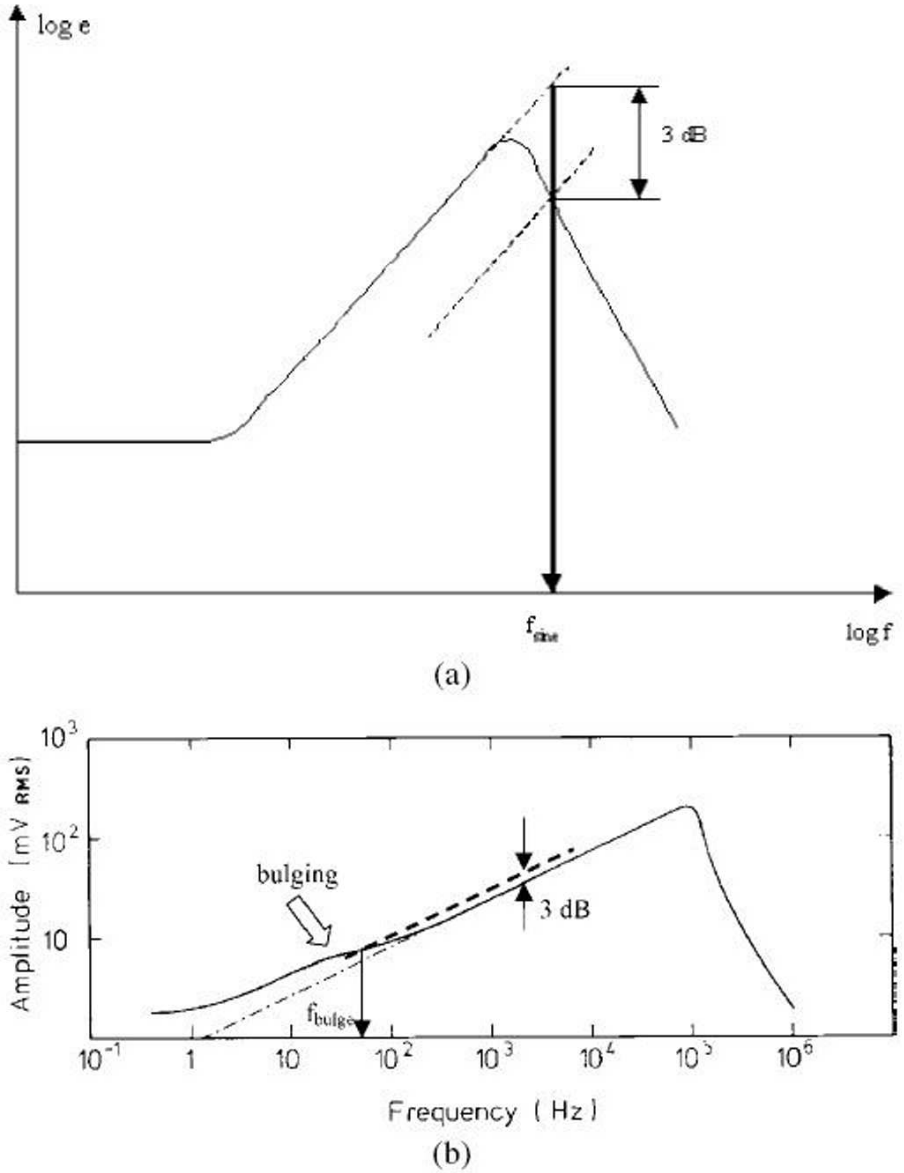

Figure 1.23: The cut-off frequency (f_{sine}) obtained from the sine-wave test response of a hot-wire anemometer. *(b)* The bulging effect observed with sine-wave testing for non-cylindrical hot-film sensors (the experimental results were obtained from Freymuth (1980) with a cone sensor.

Probe	Sine-wave test response f_{sine} (kHz)	Square-wave test response f_S evaluated using equation (1.14) (kHz)	Square-wave test response f_S evaluated using equation (1.19) (kHz)	Overheating ratio
55R45	29.5	35.0	30.3	1.2
	34.5	40.9	35.4	1.4
	40.0	44.2	38.3	1.6
55R46	21.0	25.0	21.7	1.2
	28.0	33.7	29.2	1.4

Table 1.5: A comparison of cutoff frequencies obtained using the sine-wave test (f_{sine}) and the square-wave (f_S) for the DANTEC 55R45 and 55R46 hot-film wall shear-stress probes.

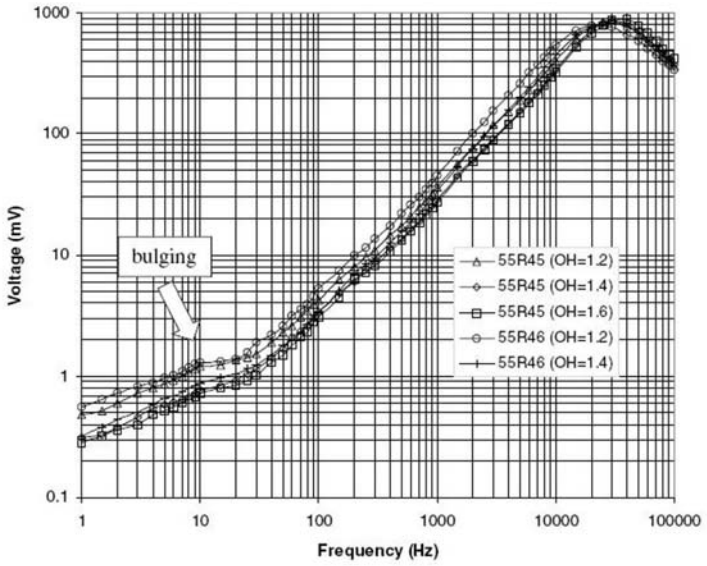

Figure 1.24: Sine-wave test responses of DANTEC 55R45 and 55R46 flush-mounted hot-film wall shear stress probes subjected to various overheating ratios.

amplifier with a shaped gain which renders the square-wave test output for the hot-film gauges to resemble that of a wall-remote hot-wire probe. It should be noted that Freymuth's (1977) derivation of Eq.(1.14) for evaluation of f_S has not taken into account the variation of the amplifier gain with frequency, thus the factor of 1.3 may not be strictly applicable in this case. From Table 1.5, it is apparent that the difference between the cutoff frequencies yielded by both types of voltage perturbation tests reduces dramatically if a factor of 1.5 is used, and f_S is evaluated as

$$f_S = \frac{1}{1.5\tau_S}. \tag{1.19}$$

A similar factor of 1.5 has been just used by Huang *et al.* (1996) in evaluating the square-wave frequency response (f_S) of their micro-electro-mechanical system (MEMS) based thermal shear stress sensors without any explanation. (It may be noted in Berger *et al.* (1963) that if the anemometer system is adjusted to a second order response, the factor of 1.5 applies.)

(II) Flush-mounted hot-wire wall shear stress probe

The sine-wave test response of a flush-mounted hot-wire with and without an imposed τ is shown in Fig.(1.25). The presence of τ at 0.56 Pa compared to null value results in a rightward and downward shift of the output response curve.

The cutoff frequency (f_{sine}) increases correspondingly from 42.5 kHz to 44 kHz. In contrast to the commercial hot-film wall shear stress probes, the increased τ has improved the frequency response of the flush-mounted hot-wire probe slightly. Similar to the trends depicted by the sine-wave test, an imposed $\tau = 0.56$ Pa was found to improve the square-wave cutoff frequency f_S (evaluated using (1)) from 47.4 kHz (at $\tau = 0$) to 50.2 kHz. Such a trend is consistent with Freymuth's (1977) model for a *wall-remote* wire where f_S increased monotonically with velocity (i.e. corresponding to an increase in heat transfer H from the wire). For the flush-mounted hot-wire probe, H is interpreted as the overall heat transfer to the surroundings which increases with τ. For the said hot-wire, it is again evident that Eq.(1.14) results in values of f_S which are higher than f_{sine}. Application of Eq.(1.19) culminates in values of f_S which compare more favourably with those of f_{sine}.

(iii) Marginally-elevated hot-wire velocity probe

Presented in Fig.(1.26 are the sine-wave test response curves of a hot-wire placed at an elevation (y) of 50 μm above a Perspex wall substrate and exposed to varying magnitudes of convective velocity (V). The overheat ratio of the wire was held constant at 1.6. Values of f_{sine} obtained are summarized in Table 1.6. For $y = 50$ μm, an increase in V from 0 to 1.5 m/s leads to a corresponding increase in f_{sine} from 33 kHz to 39 kHz. (Although the elevation of the hot-wire is kept constant, the effects of wall influence experienced by the wire, as quantified by the height of the wire in wall units y^+ ($\equiv yu_\tau/\nu$) varies.) To assess the effects of V and y^+ on f_{sine}, the sine-wave test response of a hot-wire mounted at an elevation $y = 100$ μm and exposed to $V = 0.75$ m/s was obtained and plotted on Fig.(1.25), and the value for f_{sine} tabulated in Table 1.6. For the same y^+ (signifying equivalent effects of wall influence), an increase in V results in a corresponding increase in f_{sine}. On the other hand, a decrease in y^+ (which implies more significant wall effects) leads to an increase in f_{sine} when V is kept constant. These observations are consistent with those obtained for f_S, where enhanced heat loss from the wire either brought about by an increase in V or a decrease in y^+ results in higher values for f_S.

Similar to the flush-mounted hot-wire, f_S evaluated using Eq.(1.14) was found to be higher than f_{sine} for each corresponding parametric condition (see Table **??XXX**). Once again, Eq.(1.19) leads to values of f_S which are in better agreement with f_{sine}.

1.4.2(c) The low frequency attenuation from the sine-wave test (f_{bulge})

(i) DANTEC-made 55R45/55R46 flush-mounted hot-film wall shear stress probes

Although the square-wave test can be performed easily, the sine-wave test is

Physical height of hot-wire above wall substrate y (μm)	Dimensionless height y^+	Sine-wave test response f_{sine} (kHz)	Square-wave test response f_S evaluated using equation (1.14) (kHz)	Square-wave test response f_S evaluated using equation (1.19) (kHz)	Velocity (m s^{-1})
50	NA	33.0	36.3	31.5	0
50	1.68	37.5	42.1	36.5	0.75
50	2.37	39.0	43.8	38.0	1.5
100	2.37	34.5	39.0	33.8	0.75

Table 1.6: A comparison of cutoff frequencies obtained using the sine-wave test (f_{sine}) and the square-wave test (f_S) for marginally elevated hot-wires mounted above a Perspex wall substrate. NA = not applicable.

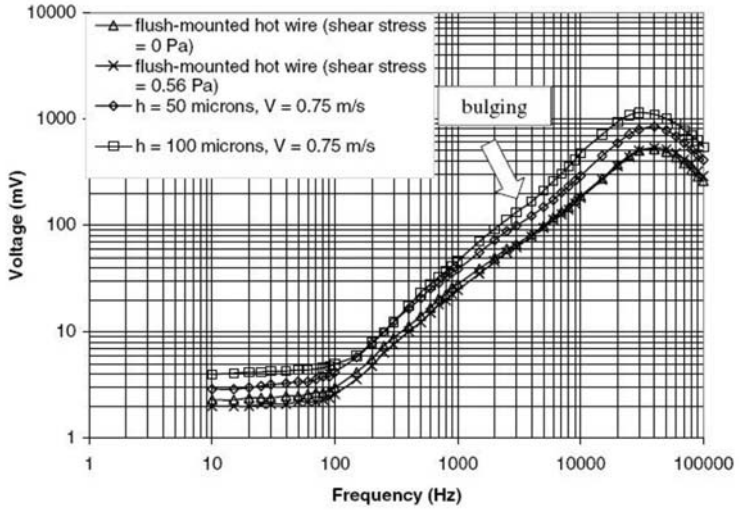

Figure 1.25: Sine-wave responses of flush-mounted and marginally elevated hot-wire.

able to yield more precise information pertaining to the flatness of the frequency response over the entire range of frequencies tested. Figure 1.24 shows the sine-wave frequency response of the DANTEC 55R45 and 55R46 probes subjected to different overheat ratios. At frequencies below approximately 100 Hz, a distinctive bulging effect appears in the test response curve for all overheat ratios investigated. This bulging effect, corresponding to the first amplitude attenuation at low frequencies, was observed by Freymuth & Fingerson (1977) for non-cylindrical cone and wedge-shaped sensors used for velocity measurements.

It would be useful to identify where this low-frequency attenuation of the thermal waves (which appears as a bulge in sine-wave tests) occurs. However, there appears to be some uncertainty in locating the *exact* frequencies at which this attenuation begins and ends. We have thus adopted the following methodology for obtaining a characteristic frequency representing the range over which the flush-mounted hot-film sensor suffers from this low-frequency amplitude attenuation. As shown in Fig.(1.23b), the said frequency (f_{bulge}) at which the amplitude response to sine-wave testing has risen by 3 dB above the straight line rising portion of the amplitude response curve (as the frequency is decreased) is used in the characterization. (In essence, this procedure follows that of Freymuth (1977, 1981a) and other workers in characterizing the (high) cutoff frequency of a hot-wire or hot-film anemometer by utilizing the value of the frequency at which the amplitude response to sine-wave electronic testing has dropped 3 dB *below* the region of flat response which corresponds to the ideal straight line rising portion of the amplitude response curve.) The results of f_{bulge} for the 55R45 and 55R46 probes

Probe	Frequency characterizing bulging effect f_{bulge} (Hz)	Dynamic frequency response f_D (Hz)	Overheating ratio
55R45	20	0.75	1.2
	16	0.8	1.4
	17	0.73	1.6
55R46	17	0.43	1.2
	22	0.45	1.4

Table 1.7: The frequencies (f_{bulge}) characterizing the bulging effect observed in the sine-wave test response curve and the dynamic frequency response (f_D) for the DANTEC 55R45 and 55R46 hot-film wall shear stress probes. NB: the wall shear stress τ was varied between 0 and 1.0 Pa and was found to have no influence on the values of f_{bulge} for the same probe operating at the same overheating ratio.

at different overheat ratios are presented in Table 1.7. It can be seen that f_{bulge} is range-bound between 16 and 22 Hz, with no seemingly clear trend within limits of experimental accuracy. This suggests that the bulging effect is fairly independent of both the overheat ratio and the thickness of the quartz coating above the active heated element. As mentioned in Section 1.4.2(b), corresponding to the same probe operated at the same overheat ratio, the sine-wave response is independent of the magnitude of τ. Therefore it can be concluded that f_{bulge} is not affected by the prevailing flow conditions.

In Section 1.3.2, it was already established that the dynamic frequency response (f_D) of the hot film wall shear stress probes is of the order of 1 Hz. If we further assume an average value of 20 Hz for f_{bulge}, it is possible to relate f_{bulge} and f_D by a causal relationship given by

$$f_{bulge} \sim 20 f_D. \tag{1.20}$$

This broad relationship would be invaluable to users who have no access to dynamic testing facilities, but have the means to perform sine-wave electronic testing. We wish to emphasize that from a user's point of view, it is the dynamic response, i.e. the response of the sensor to *actual* wall shear stress perturbations that is of prime concern when the probe is employed for turbulent wall shear stress measurements. Therefore, in view of the complexities in conducting a separate dynamic perturbation test, the sine-wave electronic test can serve as an invaluable proxy or indicator to estimate f_D by invoking the above causal relationship.

Although f_S and f_{sine} are comparable in magnitude and consistent, both are approximately 5 orders of magnitude greater than f_D. Users of non-cylindrical hot-film thermal sensors who persist, whether knowingly or otherwise, in relying solely on the square-wave test to substantiate the use of such probes for high frequency turbulence measurements are likely to obtain erroneous results. This is exemplified by the work of Alfredsson *et al.* (1988) who employed near-wall

hot-wire/film probes to obtain near-wall turbulence statistics in a turbulent air boundary layer flow at a Reynolds number (based on boundary layer thickness and free stream velocity) of 28,000. The same DANTEC 55R45 probe yielded a value of 0.095 for the intensity of streamwise wall shear stress fluctuations ($\tau'/\bar{\tau}$), whereas a marginally-elevated hot-wire probe gave a value of 0.39. Here $\bar{\tau}$ and τ' denote the mean and RMS value of the wall shear stress fluctuations respectively. Alfredsson *et al.* further reported a f_S quantity of more than 10 kHz for both the 55R45 hot-film and marginally-elevated hot-wire probes, although Section 1.3.2 has shown clearly that f_D is about 2 kHz for the latter compared to the extremely low values of O(1) Hz for the former. Alfredsson *et al.* did not report any sine-wave testing. Instead, they discussed about the frequency response by comparing the streamwise wall shear stress power spectra obtained from the 55R45 probe and their marginally-elevated hot-wire sensor. It was found that the power spectrum yielded by the 55R45 probe grossly underestimated the latter. Corresponding to a frequency of 10 Hz, the power spectrum obtained from the 55R45 probe was up to 90% lower. In contrast to the square-wave test which only emphasizes the high cut-off frequencies, the sine-wave test is further able to reveal the effects of low-frequency thermal wave attenuation effects for non-cylindrical hot-film sensors. From the causality condition proposed above, f_{bulge} is still a closer and better approximation to f_D as compared to f_S or f_{sine}.

It is appropriate to mention a word of caution in the use of the sine-wave test. Huang *et al.* (1996) did evaluate the frequency response of their micro-electro-mechanical system (MEMS) based thermal shear stress sensors using both the sine-wave and square-wave voltage perturbation tests. The cutoff-frequencies (9 kHz for their sensor with a cavity and 130 kHz for their sensor without a cavity) yielded by both tests were found to be consistent, similar to our observation for the near-wall hot-wire/film sensors. However, a close examination of their sine-wave test response revealed that it has been plotted on a linear-log plot rather than a classical log-log plot. Such a procedure is not sufficiently sensitive to reveal the bulging effect due to the attenuation of thermal waves at low frequencies.

(II) Flush-mounted hot-wire wall shear stress probe and marginally-elevated hot-wire velocity probe

Sine-wave tests were first performed on a wall-remote hot-wire subjected in turn to a stationary fluid and a uniform flow at 12 m/s, so that detailed comparisons can be subsequently made w.r.t. the results for a near-wall hot wire at y = 50 μm (see Figure 1.26). In Fig.(1.26), the response of a wall-remote hot-wire bears close resemblance to the corresponding results of Freymuth & Fingerson (1977). In particular, the flatness is vindicated by the positive sloping region of the response curves bearing a gradient close to unity. Although the near-wall hot-wire still exhibits a continuously upward increasing trend for frequencies ranging between 100 Hz and tens of kHz, differences exist between the observed response and its wall-remote counterpart. The response curve of the near-wall hot-wire shows a bulging effect similar to that observed for the flush-mounted hot-film wall shear

stress gauges. However, the observed bulging effect for the near-wall hot wire is very much weaker than that for the flush-mounted hot-film gauges. The location of the bulging effect also occurs over a much higher and wider frequency range of 0.8 to 4 kHz for the near-wall hot-wire, as contrasted to O(20 Hz) for the flush-mounted hot-film gauges.

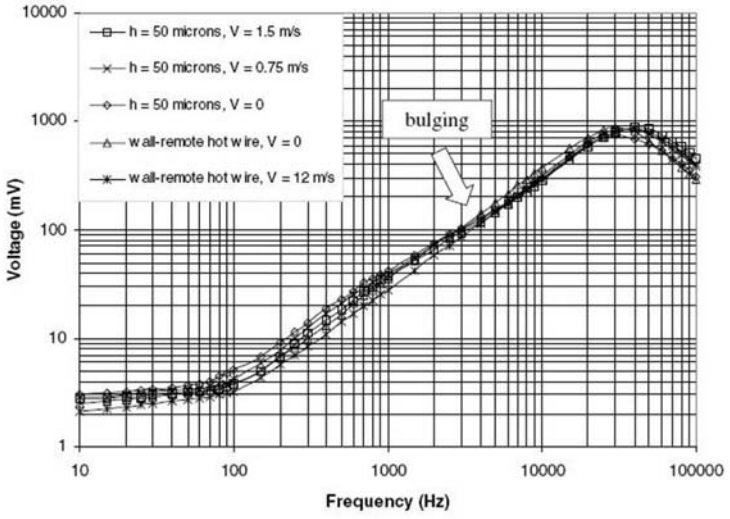

Figure 1.26: Sine-wave responses of marginally elevated and wall-remote hot-wire probes.

Extensive dynamic velocity perturbation tests performed in Section 1.3.1 have indicated that the dynamic frequency response f_D of near-wall hot-wire probes is O(2 kHz). Square-wave tests conducted on the said probes yielded values of f_S which are approximately one order of magnitude higher than f_D (see Table 1.6) or Section 1.4.1).

From the above sine-wave test results, the frequency range where the bulging effect is observed corresponds much more closely to f_D. It may be suggested that the low frequency amplitude attenuation effect observed (f_D) is also due to the attenuation of the heat waves from the heated wire to the surrounding wall substrate. However, in contrast to the flush-mounted hot-film gauges, where the active elements are completely embedded in the surrounding quartz substrate, the near-wall hot-wire is also exposed to the surrounding ambient air. This attenuation of heat waves to the surrounding wall substrate is thus deemed to be less severe for the near-wall hot-wire than the flush-mounted hot-film sensors, which serves to explain the qualitatively weaker bulging effect for the near-wall hot-wire. When the hot-wire is placed at a higher elevation of 100 μm and subjected to V = 0.75 m/s (Figure 1.25), the bulging effect is still barely discernable near the 0.8 to 4

kHz range. Also displayed in Fig.(1.25) are the response curves of a flush-mounted hot-wire wall shear stress probe exposed to varying wall shear stress. The bulging effect occurring in the 0.8 to 4 kHz range seems qualitatively stronger. Overall, for the marginally-elevated and flush-mounted hot-wire probes, it is thus possible to relate f_{bulge} and f_D by a causal relation ship given by

$$f_{bulge} \sim f_D \sim O(2kHz). \tag{1.21}$$

1.4.2(d) Concluding remarks for Section 1.4.2

Experiments using the electronic sine-wave voltage perturbation test were systematically performed for the first time on marginally-elevated and flush-mounted hot-wire probes. Two commercial flush-mounted hot-film wall shear stress gauges were also tested. For both the hot-film and hot-wire sensors, the cutoff frequency of the anemometer yielded by the sine-wave test (f_{sine}) was found to be in fair agreement and to exhibit the same trends as results obtained using the traditional electronic square-wave voltage perturbation test (f_S). For the hot-film gauges, f_{sine} obtained for the DANTEC 55R45 gauge was consistently higher that those for its 55R46 counterpart under identical conditions of overheat ratio and wall shear stress (τ). For both gauges, an increase in overheat ratio resulted in a rise in f_{sine}, whereas variations in τ for the same overheat ratio did not seem to have cast any effect. For the marginally-elevated hot-wire probes, an increase in the convective velocity (V) leads to an increase in f_{sine} when the wire is either kept at a fixed physical distance or at the same y^+ above the wall substrate. When V is held constant, a decrease in y^+ signifying increased wall influence culminates in larger values of f_{sine}. These results suggest that f_{sine} increases with increasing heat transfer from the wire, regardless of whether it is due to forced convection or effects of wall influence. For the flush-mounted hot-wire wall shear stress sensor, an increase in the imposed τ results in a corresponding increase in f_{sine}.

Apart from yielding the cutoff frequency of the anemometer, the sine-wave test is also capable of indicating the flatness of the frequency response over a limited frequency range and detect the presence of any amplitude attenuation which arises as a result of the attenuation of heat waves to the surrounding wall substrate at high frequencies. A significant bulging effect appears in the sine-wave test response curves for the hot-film wall shear stress probes. A causality relationship $f_{bulge} \approx 20 f_D$ was observed for the hot-film gauges, where f_{bulge} and f_D denote the frequency characterizing the bulging effect and the dynamic frequency response respectively. Compared to f_S (and f_{sine}) which is five orders of magnitude greater than f_D, f_{bulge} provides a much better indicator or proxy for predicting f_D. It is to be realized that in the application of the hot-film wall shear stress gauges to measure fluctuating shear stress in a turbulent flow, it is the lower dynamic response frequency f_D which sets an upper limit to the overall responsiveness of the gauge.

For the flush-mounted and marginally-elevated hot-wire sensors, a very slight bulging effect was also observed in the 0.8 to 4 kHz range, which corresponds much

more closely to the values of f_D. This is contrasted to f_S, which is typically one order of magnitude larger than f_D. The frequencies f_{bulge} and f_D can be related by the causality relationship $f_{bulge} \sim f_D$ for the near-wall hot-wire probes. It must be noted that the lower magnitude f_D is the critical frequency ultimately determining the responsiveness of the near-wall hot-wire probe to fluctuating velocities expected in a turbulent flow. Therefore, it is suggested that instead of relying solely on the square-wave test, users of near-wall hot-wire or hot-film anemometers who do not have access to dynamic perturbation testing facilities should perform a sine-wave test to detect the presence of any amplitude attenuation for frequencies (f_{bulge}) below the cutoff frequency.

Further discourse on this Section 1.4.2 can be found in Teo *et al.* (2001).

1.5 A model for the frequency response of a near-wall hot-wire

In Section 1.4.2, we have proposed a causality relationship between the bulging frequency (f_{bulge}) and f_D, both of which occur at the lower frequency range below that indicated by either f_s or f_{sine}. This has one very important implication: simply by employing the sine-wave voltage perturbation test, one may be able to deduce the dynamic response frequency of the near-wall hot-wire system. After all, from the user's point of view, it is the response of the sensor to the actual flow fluctuation /perturbation that is of prime concern when the probe is employed for turbulent flow measurements in near-wall configurations.

In this Section, we seek to present a simplified 1-D model capable of predicting the behavioral trend of a hot-wire operating close to the wall under different parametric/operating conditions. The computed results of f_D and f_{bulge} are compared to the experiments under the conditions of varying wire height (in terms of wall units) and different magnitudes of convection velocity. It is important to note that compared to a full scale 3-D numerical simulation where it is much more time consuming and compute-intensive, the model can accord a very timely discourse on the changes to the response characteristic of the near-wall hot-wire as a velocity probe operating under different conditions.

1.5.1 A simplified 1-D model for the hot-wire probe

In the analysis of the 1-D model for the flushed-mounted hot-film wall shear stress probe, Freymuth (1980) greatly simplified the complicated 3-D heat transfer across the substrate into areas adjacent to the film by 1-D heat transfer from the planar film surface across the substrate to another planar surface below the substrate at temperature T(z=-h). The active planar film at temperature T(z=0), which is exposed to the convection heat loss at the top section, is assumed to be of negligible thickness compared to the thickness h of the substrate. The length and breadth of the film are l and L, respectively (see Figure 1.27). The model hot film is placed on one arm of the Wheatstone bridge and a circuit analysis is carried out

with input sine-wave voltage or imposed fluctuating wall shear stress on the hot film.

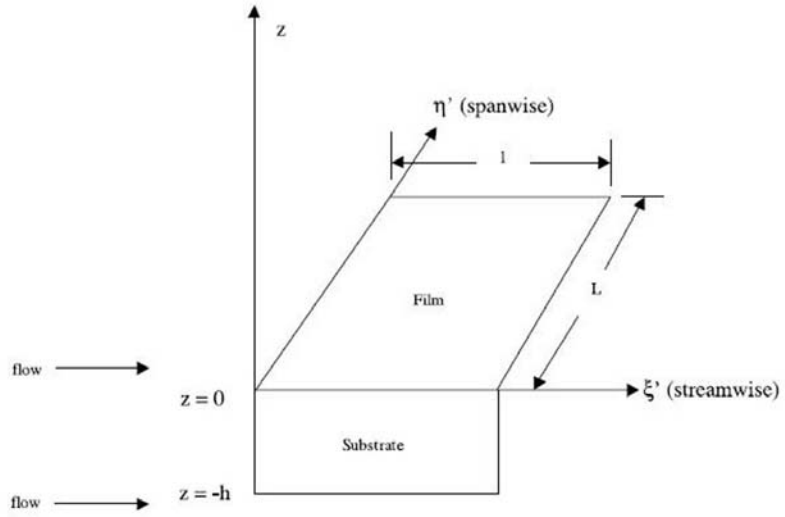

Figure 1.27: Model of a non-cylindrical hot-film according to the Bellhouse-Schultz model.

In a move similar to Freymuth (1980) and Teo *et al.*, applying an energy balance to the near-wall hot-wire which is placed on one arm of the Wheatstone bridge yields

$$\frac{E^2 R}{(R+R_1)^2} - H(V)(T_w - T_0) = lLK \left.\frac{\partial T}{\partial z}\right|_{z=0} + \frac{c}{\beta}\frac{dR}{dt}, \tag{1.22}$$

where c is the thermal inertia of the wire, H(V) represents the heat transfer function from the wire to the flow, K is the thermal conductivity of the substrate, β denotes the temperature coefficient of the wire resistance R, and T_w and T_o are temperature on the hot-wire and ambient, respectively. The electrical circuitry of the Wheatstone bridge of the CTA is provided in Fig.(1.22). Here R_1 is another bridge arm in series with R, whereas R_2 and R_3 (=nR_2), which constitute the remaining 2 arms of the bridge, are resistances connected in parallel to R_1 and R, respectively. The electronic test signal E_t is fed into the bridge via resistance R_4 ($>> R_1$) and E is the voltage over the bridge. R_0 is the wire resistance at ambient reference temperature. A schematic of the near-wall hot-wire is given in Fig.(1.28).

Equation (1.22) is almost identical to the equation by Freymuth (1980) describing the energy balance of the non-cylindrical hot film, except for the additional second term on the RHS of Eq.(1.22) which takes into consideration the hot-wire's change in internal energy with time. It may be noted that the heat transfer to

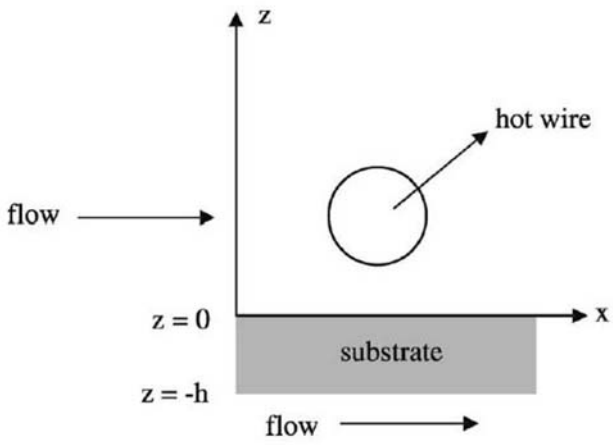

Figure 1.28: Model of a near-wall hot-wire.

the substrate is modelled as one-dimensional and represented by the first term on the RHS of Eq.(1.22). As in Freymuth, the boundary condition at the lower, not electrically heated, surface reads

$$H'(V)\{T(z=-h)-T_0\} = lLK \left.\frac{\partial T}{\partial z}\right|_{(z=-h)} \tag{1.23}$$

Here H'(V) is the heat transfer function from the lower surface of the substrate to the surrounding fluids. Equation (1.22) can be re-written as

$$\frac{E^2R}{(R+R_1)^2} = H(V)(T_w - T_0) + \frac{H'(V)}{x'+1}(T|_{z=0} - T_0) + \frac{c}{\beta}\frac{dR}{dt}, \tag{1.24}$$

where the Biot number $x' = hH'(V)/(lLK)$. Further simplification can be made if we assume since the hot-wire is placed very close to the wall within the viscous sublayer such that $T_{z=0} \sim T_w$ and $H' \sim H$ for a given V. (In similar 1-D analysis as carried out in Bellhouse & Schultz (1967) and Freymuth (1980) for a non-cylindrical hot film probe subjected to convection velocity, we have here largely assumed that the heat transfer of the near-wall hot-wire under convection velocity V has the same order of magnitude as that for a surface subjected to the same V. On the other hand, a general but more complex model of relating H to H' by a factor or even set independent of each other will invariably introduce further unknowns that have to be calibrated against experiments and cannot be used on its own for prediction or comparison.) This is also in line with the intent of a simplified 1-D model able to predict to predict the behavioral trend of the near-wall hot-wire as opposed to convey numerical quantity per se. Equation (1.24)

becomes

$$\frac{E^2R}{(R+R_1)^2} = H(V)(T_w - T_0)\left(\frac{2+x}{1+x}\right) + \frac{c}{\beta}\frac{dR}{dt}, \tag{1.25}$$

where $x = hH(V)/(lLK)$. As such, the first term on the R.H.S. can be interpreted as the sum of the heat loss directly from the hot-wire to the flow (i.e. H(V)$(T_w - T_0)$) and the heat loss from the wire to the wall substrate (i.e. $H(V)(T_w - T_0)\left(\frac{1}{1+x}\right)$). After linearizing the boundary conditions and taking into account the bridge-amplifier combination, we obtain the final governing response equation for the anemometer output e subjected to sinusoidal voltage, velocity and ambient temperature fluctuating perturbations (denoted by E_t, v and $T_0^{'}$, respectively)

$$\begin{aligned} e = \frac{n+1}{2}\frac{R}{R-R_o}\frac{R_1}{R_4}\frac{1+x}{2+x}E_t\left(\gamma' + a'\frac{b'-c'}{b'+c'} + \frac{i\Omega Dc}{h^2H}\right) \\ -\frac{E}{2}\frac{1+x}{2+x}\frac{\alpha}{R-R_o}T_o'\left(1+\frac{2a'}{b'+c'}\right) + \\ \frac{E}{2}\frac{1+x}{2+x}\frac{1}{H}\frac{dH}{dV}v\left(1+\frac{1}{1+x}\frac{2a'}{b'+c'}\right), \end{aligned} \tag{1.26}$$

where

$$\begin{aligned} a' &= (i\Omega)^{1/2}/x\,, \\ b' &= \exp[(i\Omega)^{1/2}]\{[(i\Omega)^{1/2}/x] + 1\}\,, \\ c' &= \exp[(i\Omega)^{1/2}]\{[(i\Omega)^{1/2}/x] - 1\}\,, \\ \gamma' &= 1 + \frac{R-R_1}{R+R_1}\frac{R-R_o}{R}\frac{2+x}{1+x}\,, \end{aligned}$$

and $\Omega = (2\pi f)h^2/D$ is the dimensionless frequency. Here f and D denote the frequency and the thermal diffusivity of the substrate, respectively.

The normalized amplitude response of the anemometer subjected to dynamic velocity perturbations is given by

$$|R_v| = 1 + \frac{(1+x)\frac{2a'}{b'+c'} - 1}{2+2x+x^2}. \tag{1.27}$$

For the near-wall hot-wire probe subjected to electronic sine-wave perturbations (i.e. $T_0' = v = 0$), the fluctuating output is proportional to

$$e' = \frac{\alpha}{1-1/\alpha}\frac{1+x}{2+x}\left(1 - (1-\alpha)\frac{1-n}{1+n}\frac{2+x}{1+x} + a'\frac{b'-c'}{b'+c'} + i\Omega m\right), \tag{1.28}$$

where the overheating ratio $\alpha = R/R_0$ and $m = Dc/(h^2H)$.

1.5.2 Results and discussions on the 1D model

1.5.2(a) Probe subjected to different magnitudes of convection velocity (V)

Previous DNS by Chew *et al.* (1995), Lange *et al.* (1999) and Li *et al.* (2006) simulating the heat loss from a hot-wire operating in close proximity to the wall have revealed that the amount of heat loss by the wire to the wall, when evaluated as a fraction of the total amount of heat loss or dissipated by the wire, remains fairly constant for the same value of y^+, as long as the thermal conductivity of the wall substrate material is unchanged. From Eq.(1.25), since this fraction is only a function of the Biot number x, it can be deduced that for the same value of y^+, x can be assumed to be a constant. To study the effect of V on the frequency response of the near-wall hot-wire while keeping y^+ constant, it is necessary to vary H. It may be noted that, for a given wall substrate, keeping y^+ constant (and x fixed) is equivalent to constant wall influence on the operation of the near-wall hot-wire. However, since x ($\equiv hH/(lLK)$) depends on the heat transfer function H, the value of the substrate thickness h has to be varied in order that x remains unaltered.

We shall first discuss how the model predicts the dynamic response of a near-wall hot-wire subjected to velocity perturbations. The distributions of $|R_v|$ against Ω are depicted in Fig.(1.29) for various values of x ranging between 0.05 and 0.5. Each curve shows the variation of $|R_v|$ with Ω for the same y^+.

Consider two near-wall hot wires with identical effects of wall influence and exposed to V_1 (wire 1) and V_2 (wire 2) such that $V_2 > V_1$. Since H(V) for the second wire is higher than that for the first wire, $h_2 < h_1$ in order to keep x unchanged. For the same x, $\Omega_D$corresponding to the point when $|R_v|$ has decayed or attenuated to 0.9 remains fixed. (In the experiments in Section 1.3.1, the onset of amplitude attenuation was taken to be the frequency of the imposed fluctuation when the ratio of the measured amplitude to the imposed amplitude (a_{mea}/a_{imp}) equals 0.9.) Since for the two wires $(\Omega_D)_1 = (\Omega_D)_2$ and $\Omega_D = (2\pi f_D)h^2/D$, the presence of $h_2 < h_1$ necessarily implies that $(f_D)_2 > (f_D)_1$. That is wire 2 which is exposed to a larger V possesses a higher dynamic frequency response than wire 1. This concurs with the experimental observations in Section 1.3.1, where it was found that an increase in V at the same y^+ has resulted in a concomitant improvement in f_D for the near-wall hot-wire.

In the experiments, a hot-wire mounted at height y = 40 μm above the perspex wall substrate and exposed to V = 2.7 m/s has a dynamic frequency of f_D = 2690 Hz. This value is larger than the corresponding quantity of f_D = 2345 Hz when the same hot-wire was exposed to a smaller V = 2.17 m/s. For the latter, the wire was set at y = 50 μm such that the same $y^+ = 2.6$ prevailed.

From the model it is clear that a higher convection velocity on near-wall hot-wire with similar influence of wall effect exhibits a better dynamic response frequency. Next, it would also be interesting to investigate how the model predicts the frequency response of a near-wall hot-wire subjected to sine-wave voltage per-

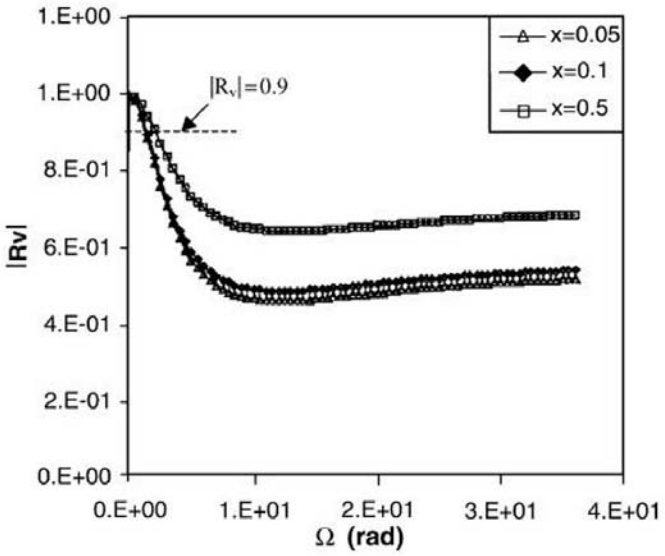

Figure 1.29: Normalized amplitude response of near-wall hot-wire anemometer subjected to dynamic velocity pertubations for various values of Biot numer x.

turbation testing. Again, for a given y^+ (and hence x), the product of h and H remains invariant. The response given by Eq.(1.28) shows that e' is only dependent on the value of m ($\equiv Dc/(h^2H)$). If $H_2 > H_1$ as with $V_2 > V_1$ (i.e. larger convection velocity), a constant value of x implies that $h_2 < h_1$ and hence $m_2 > m_1$. Equation (1.28) is plotted on Fig.(1.30) for various values of m ranging from 0.1 to 10 for x = 0.05, say, and $\alpha = 1.6$ and a resistance ratio n = 1/20.

Smaller values of m are observed to result in a more significant and distinct "bulging" effect. As the value of m increases to 10, the "bulging" effect becomes less distinct. Two interpretation of results can be suggested. At smaller values of m where the "bulging" effect is more distinct, the dimensionless frequency Ω corresponding to the location of the "bulge" (Ω_{bulge}) remains somewhat unchanged. (The bulging effect occurs over a range of frequency; see also Section 1.4.2.) This implies that dimensional $(f_{bulge})_2 > (f_{bulge})_1$, which is similar to that observed for the above-mentioned f_D. The diminishing "bulging" effect as m becomes larger can be construed as the decreasing importance of the lower magnitude dimensional f_{bulge} in deference to the higher magnitude cut-off frequency f_{sine}. Overall, it may be suggested that for a near-wall hot wire subjected to equal effects of wall influence, a larger convection velocity will improve the frequency response and may cause the "bulging" effect to be diminished.

Another salient feature which can be observed from Fig.(1.30) is that the slopes of the predicted sine-wave test response curves asymptote to a limiting value of

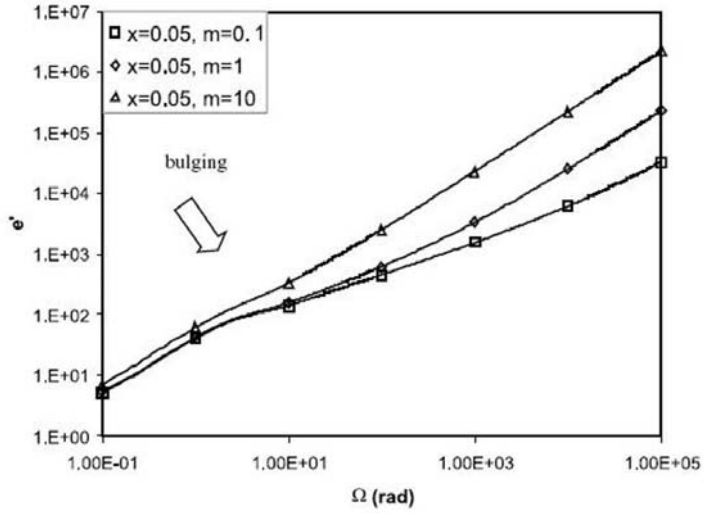

Figure 1.30: Sine-wave test response of a near-wall hot-wire anemometer subjected to different magnitudes of convecting velocity.

unity for large values of the dimensionless frequency Ω. This is comparable to the results obtained for the sine-wave tests (prior to the cutoff frequency) performed on near-wall hot-wire probes, as shown in the experiments discussed in Section 1.4.2. Moreover, the range of values of Ω corresponding to the "bulging" effect predicted by the model in Fig.(1.30) bears the same order of magnitude as Ω_D (Figure 1.29). This is consistent with the experimental observations in Section 1.4.2 where it was found that $f_{bulge} \sim f_D \sim O(2\text{kHz})$ for the 5 μm diameter near-wall hot-wire probe. The experiments in Section 1.4.2 had led to the proposal of the causality relation

$$f_{bulge} \sim f_D \tag{1.29}$$

for ease of obtaining the dynamic response frequency of the hot-wire in near-wall operations.

1.5.2(b) Probe subjected to different values of y^+ (V constant)

In this section, we wish to analyze how the proposed model predicts the effect of y^+ on the frequency response subjected to the *same* V. As mentioned in Section 1.5.2(a), the amount of heat loss from the hot-wire to the wall, evaluated as a fraction of the total amount of heat dissipated by the wire, depends on the value of y^+ for a particular wall substrate material. The numerical works of Chew *et al.* (1995) and Lang *et al.* (1999) indicate that this fraction is weakly dependent on the friction velocity u_τ and it increases as the value of y^+ decreases. From Eq.(1.25),

this fraction works out to be 1/(2+x). A smaller value of y^+ (associated with greater wall influence and a subsequent larger fraction of heat loss to the wall) thus implies a smaller value for x. In other words, x can be broadly construed as an indicator of the wall influence and is inversely proportional to it.

Referring to Fig.(1.29), Ω_D decreases as the value of x decreases. For a probe subjected to the same V, the heat transfer function H should remain approximately constant. Consider two hot wires 1 and 2 having Biot numbers $x_1 = 0.1$ and $x_2 = 0.05$, respectively. Since $x_2 < x_1$, it is obvious that $y_2^+ < y_1^+$. As H remains invariant since V is held constant, $x_2/x_1 = h_2/h_1 = 0.5$. From Fig.(1.29), it can be seen that $(\Omega_D)_2/(\Omega_D)_1 \approx 1$. This implies that $(f_{D2}h_2^2)/(f_{D1}h_1^2) \approx 1$ and hence $f_{D2}/f_{D1} \approx 4$, i.e. $f_{D2} > f_{D1}$. It can thus be inferred that wire 2 which loses a larger fraction of heat to the wall substrate due to its lower value of y^+, has a better dynamic frequency response.

To illustrate further, consider wires 1 and 3 possessing $x_1 = 0.1$ and $x_3 = 0.5$, respectively. For the same V, $x_3/x_1 = h_3/h_1 = 5$. Similarly, from Fig.(1.29), it can be deduced that $(\Omega_D)_3/(\Omega_D)_1 \approx 1.5$ and hence $f_{D3}/f_{D1} \approx 0.06$ (note that although $(\Omega_D)_3 > (\Omega_D)_1$, $f_{D3} < f_{D1}$). An increase in x, corresponding to a smaller fraction of heat loss to the wall and larger values of y^+, has culminated in a poorer f_D. In the experiments of Section 1.3.1, f_D for the near-wall hot-wire was found to increase from 2390 Hz (y = 65 μm, $y^+ = 3.44$) to 2625 Hz (y = 50 μm, $y^+ = 3.05$) to 2690 Hz (y = 40 μm, $y^+ = 2.63$) at the similar convection velocity of V = 2.9 m/s. It should be noted that with V fixed, the convection heat loss remains unchanged. A larger fraction of heat loss to the wall substrate as observed above such that there is an overall greater heat loss from the hot-wire has led to a larger value of f_D. This, together with the results in Section 1.5.2(a), suggests that the dynamic response frequency of a near-wall hot-wire increases with larger heat loss from the wire, which is irrespective of whether the loss is due to forced convection or to the effect of wall influence.

The output response curves of a near-wall hot-wire subjected to sine-wave voltage perturbation testing are presented in Fig.(1.31) for various values of x. With a fixed V, and $\alpha = 1.6$ and n = 1/20, a rise in x corresponds to an increase in h and hence decreasing wall influence (i.e. y^+ increases).

Figure 1.31 shows that the location of the bulge or Ω_{bulge} remains relatively unaffected, and there is a mildly perceptible diminishing bulging effect for the lower magnitude range of m. As in Section 1.5.2(a), we can suggest two interpretations. For the range of higher m which indicates invariant Ω_{bulge}, this corresponds to f_{bulge} decreasing with increasing x which is similar to that observed for f_D above. The diminishing effect of bulging as x becomes even larger (and m becomes much smaller) is associated with ever increasing y^+ such that the wall effect becomes increasingly insignificant. In experiments, a hot-wire operating under increasing free-stream conditions will experience increasingly better f_D, the presence of only the f_{sine} feature in the electronic sine-wave testing, and the absence of f_{bulge}. It can be construed that the "bulging" effect is caused by heat loss to the substrate and is thus related to the first attenuation. As the proportion of heat loss to the wall decreases greatly with large y^+ (towards outside the viscous sublayer),

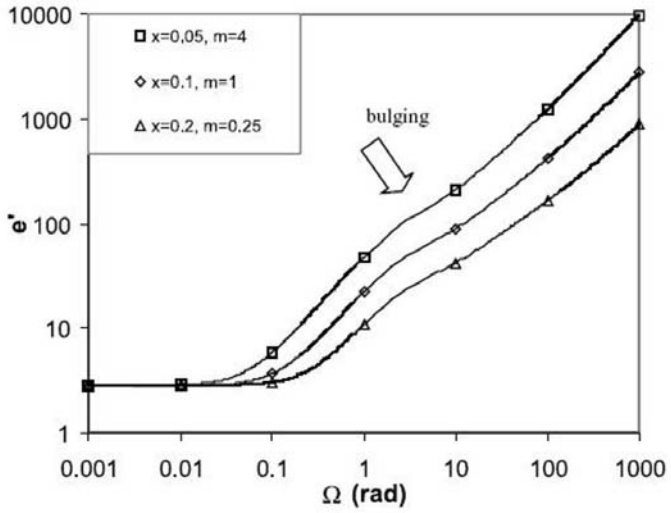

Figure 1.31: Sine-wave test response of near-wall hot-wire subjected to different effects of wall influence (y^+). (For a fixed V, an increasing wall influence of decreasing y^+ is equivalent to decreasing Biot number x with greater proportion of heat loss to the wall substrate.)

we thus observed the bulging effect becoming less conspicuous in the sine-wave response curve. This concurs with the experiments observations of Section 1.4.2.

1.5.2(c) Consideration of other effects

In Section 1.3.1, it was found that f_D for the hot-wire mounted at 50 μm above the aluminum wall substrate is always higher than the corresponding hot-wire at the same height above the perspex wall substrate. The results obtained can be expressed in terms of dimensionless wire height in wall units such that for a given y^+ both wires are exposed to the same convection velocity, and any difference in heat transfer characteristic of the wire is solely attributed to the different additional heat loss to the wall substrate. For the aluminum wall substrate, there is greater heat transfer from the wire (Khoo *et al.*, 1996 and Chew *et al.*, 1998b) which is in accord with the conclusion reached in Section 1.5.2(b) on the link between heat transfer and f_D. It would be interesting to analyze the prediction based on the model.

At the same V, we have

$$x_{perspex}(\equiv hH/lLK_{perspex}) > x_{aluminum}(\equiv hH/lLK_{aluminum})$$

to account for greater effect of the aluminum wall influence on the near-wall hot-

wire operation. From Fig.(1.29), it is clear that

$$(\Omega_D)_{perspex} > (\Omega_D)_{aluminum}$$

which apparently may imply that the model has given the incorrect trend. On closer examination, since $\Omega_D = 2\pi h^2 f_D/D$, even if $(\Omega_D)_{perspex} > (\Omega_D)_{aluminum}$, it is *not* so straightforward that $(f_D)_{perspex} > (f_D)_{aluminum}$ since the thermal diffusivity of aluminum is much greater than perspex by a factor of at least two orders of magnitude. That is $D_{aluminum}/D_{perspex} \sim O(10^2)$. Therefore any change in Ω_D in response to the change in x due to the different thermal conductivity of wall substrate will be mitigated or even overwhelmed by the change in D such that f_D may take on different direction of change from Ω_D. (It may just be noted too from Fig.(1.29) that corresponding to a change of one order of magnitude of x, Ω_D changes by a much smaller factor.) In essence, the model suggests that a change of wall substrate of different thermal conductivity will only give rise to a limited change in f_D. From the experiments in Section 1.3.1 with $K_{aluminum}/K_{perspex} \sim O(10^2)$, we observed that f_D of a hot-wire placed above an aluminum substrate improves by only about 10-15% over the corresponding perspex substrate.

It is worth mentioning that the effect of a change in wire diameter (d) on the dynamic response of a near-wall hot-wire can be deduced from the model. As d is decreased, l will be corresponding smaller. From the heat transfer relationship by McAdams (1954) correlating the Nusselt number (Nu) of a cylinder in a submerged flow,

$$(Hd/\nu)Pr^{-0.3} = 0.35 + 0.56(\rho V d/\mu)^{0.52}, \tag{1.30}$$

we can infer that H is broadly related inversely to d such that H increases with decreasing d while keeping V constant. From the definition of x, the effect of a smaller d which entails smaller l gives rise to larger value of x. Therefore, from Fig.(1.29), the model suggests that we can possibly obtain better f_D simply by reducing the wire diameter.

Although there are no experiments for verification, this is perhaps not very surprising since logically a smaller wire diameter has lower thermal inertia and a possibility exists that it should be more responsive to changing external flow conditions. One word of caution, though, the thermal inertia of the wire is not related explicitly to f_D as seen in Eq.(1.27) for the model.

Applying the idea of a smaller d to the model for sine-wave test while keeping V constant, the effect of a corresponding increase in x can be inferred and interpreted from Fig.(1.31). As d decreases, the thermal inertia of the wire also decreases and together with a larger H lead to a much smaller m. Figure 1.31 therefore suggests a resultant output response curve which has a diminishing bulging effect. As discussed in Section 1.5.2(b), the decrease in bulging effect can be construed as an improvement in the frequency response of system such that the effect of first amplitude attenuation at low frequencies (due primarily to influence of wall effect) becomes unimportant. Only the second and final attenuation due to the finite frequency response of the electronic feedback in the anemometer remains.

Although the results in Sections 1.5.2(a) and 1.5.2(b) have indicated similar trend behavior of f_D and f_{bulge}, and the experimental findings in Section 1.4.2 suggested a functional relationship between them, it should be noted that according to the model there is one marked difference. That is, f_{bulge} is dependent on the additional parameter m which also clearly indicates the explicit dependence on the wire thermal inertia c. There is no such dependence on m for f_D.

It may be added, however, that the material used in the fabrication of the hot-wire has been predisposed towards tungsten or platinum after many years since the beginning of hot-wire anemometry and having taken into consideration many other features like ductility for ease of manufacturing, strength ... etc. The use of different material solely to affect a change in c is not deemed likely to be considered as an alternative by an end user to change the hot-wire response characteristic, and hence may not pose a critical issue in the continual use of f_{bulge} as an effective proxy to obtain f_D via the functional relationship given in Eq.(1.29). However, the model serves as a reminder that the various types of perturbation tests, in particular the sine-wave test which gives rise to the bulging effect for a near-wall hot-wire and the velocity perturbation test, are not exactly equivalent even though they share several important characteristic traits.

1.5.2(d) Concluding remarks for Section 1.5

In this work, a model for the response characteristic of the near-wall hot wire subjected to sine-wave voltage perturbation and velocity perturbation tests is developed. It is found that the computed response frequency f_{bulge} (according to sine-wave perturbation test) and f_D (according to velocity perturbation test), which correspond to the first of the two groups of attenuation frequencies, concur very well with the experiments discussed in Sections 1.3.1 and 1.4.2. The first attenuation which occurs at low frequencies is attributed to the influence of wall effect whereas the second and final attenuation is associated with the finite frequency response of the CTA system. Both f_D and f_{bulge} indicate a similar trend of increasing with the convection velocity and increasing effect of wall influence (i.e. y^+ decreases) or both, and support the causality relationship of $f_D \sim f_{bulge}$ as suggested in Section 1.4.2.

It is further shown from the model that the response frequency of the near-wall hot-wire can be made to increase by decreasing the wire diameter and the effect of different wall substrate material as measured by the property of thermal conductivity is very much limited. In experiments, it was found that a change of the wall substrate from perspex to aluminum has only resulted in about 10-15% improvement for f_D even though the ratio of the respective thermal conductivity is at least two orders of magnitude. The model, however, indicates that there are differences between f_D and f_{bulge}. It is an important and timely reminder that such perturbation tests are not identical in all aspects as f_D measures the response to heat lost from the wire or gauge by velocity perturbation while f_{bulge} measures the frequency response to the total heat lost from the wire or gauge.

Overall, although the model developed is a very simplified one-dimension, it

is able to provide insight into the behavioral trends of the response frequency of the near-wall hot-wire without the complexities of a full 3D numerical simulation with the associated requirement of extensive computing resources. It can also serve as a predictive tool for the end-user who may want to change or ensure sufficient responsiveness of the near-wall hot-wire probe operating under different conditions.

1.6 On near-wall hot-wire velocity measurements

During the past decade, the quest for drag reduction has prompted several researchers to propose various schemes which seek to alter the flow structures and velocity profile very close to the wall, in view of the fact that skin friction drag constitutes the major component of drag for streamlined bodies. Examples of such schemes include the employment of riblets (Walsh 1992), the use of large eddy break-up (LEBU) devices (Savill & Mumford 1988), the application of compliant surface (Lee *et al.* 1993) and the addition of polymers (Koskie & Tiederman 1993). In assessing the merits of these passive drag reduction schemes, it is imperative to attain a thorough comprehension of the flow characteristics very close to the wall, so that detailed comparison can be made with respect to the unmanipulated flow in order that the physics and mechanism responsible for the said reduction in drag can be brought to light.

It is well known that all the commonly available velocity measuring instruments are plagued by problems very close to the wall, although the cause of limitation differs from one instrument to another. The rapid development of PIV and the accessibility of LDV have not culminated in the extinction of the hot-wire anemometer, especially for near-wall measurements. Both the LDV and PIV require seeding of the flow and measurements significantly depend on the passage of the said particles through the respective control volumes, hence yielding a non-continuous output. This issue is accentuated in the near-wall region where the particle count diminishes considerably, resulting in an appreciably lower and variable data rate. Moreover, the relatively large measuring volume of the LDA raises doubts pertaining to the spatial averaging of the particle velocity, especially in the near wall region where the velocity gradient is normally large. For instance, in the LDV measurements of Karlsson & Johansson (1988) made in the viscous sublayer of a low-speed water boundary-layer flow, the extent of the measurement volume in the direction normal to the wall was $O(0.5\nu/u_\tau)$, where ν/u_τ is the viscous length unit. Durst *et al.* (1995) made LDA measurements in the near-wall region of a turbulent pipe flow and their axial velocity component was measured in the vertical plane with a spatial resolution of $0.7\nu/u_\tau$ at the lowest Reynolds number (the spatial resolution must necessarily be larger than $0.7\nu/u_\tau$ for their results at higher Reynolds numbers). In contrast, the hot-wire whose diameter is merely microns enables an extremely fine spatial resolution and yields a continuous signal, hence ensuring a non-biased statistical account of the turbulent flow field characteristics.

The ability of the hot-wire to yield a continuous output does not necessarily imply that it possesses an infinitely high frequency response for accurate time resolution of the flow field. In Section 1.3.1, we found that the dynamic response of a near-wall hot-wire was typically better than 2 kHz, which should be adequate for the accurate time resolution of most commonly encountered wall-bounded turbulent shear flows. Spalart (1988), who performed a direct numerical simulation (DNS) for a turbulent boundary layer on a flat plate with zero pressure gradient, commented that a typical timescale of turbulence near the wall is about 15 wall time units (i.e. $15\nu/u_\tau^2$, where ν and u_τ are the kinematic viscosity and the mean friction velocity, respectively), which further implies that the dynamic frequency response of the hot-wire probe must be greater than $u_\tau^2/15\nu$ in order for the most rapid turbulence generating events to be accurately resolved by the probe.

Having ascertained the sufficiently high frequency response of a hot-wire operating in close proximity to the wall, near-wall hot-wire sensors can next be applied to investigate the physics of the flow in the very near-wall region of various wall bounded turbulent shear flows. Despite a dynamic frequency response of more than O(2 kHz) for a near-wall hot-wire, in the near-wall turbulence measurements of Fernholz & Warnack (1998), the sampling frequency for their near-wall hot wires was limited to a relatively low value of 250 Hz (thus giving an even lower cutoff frequency of 125 Hz), which may not be sufficiently high to elucidate the correct physics that characterize the high frequency components (or the dissipating range) of the turbulent flow field. Fernholtz & Warnack employed the traditional square-wave test to justify the frequency response of their near-wall hot wires. Although they obtained a square-wave frequency response "in excess of 20 kHz", their sampling frequency was limited to 250 Hz without any explanation.

In Section 1.4.1, we have cautioned against the over-reliance on the square-wave test, since it overestimates the dynamic frequency response of a marginally-elevated hot-wire by close to one order of magnitude. In this Section 1.6, higher sampling frequencies will be used for measurement of the wall shear stress and streamwise velocity fluctuations in the viscous sublayer.

The establishment of a viable calibration procedure for near-wall hot-wire probes, coupled with the above-mentioned investigations pertaining to the ability of near-wall hot-wire probes to accurately resolve all the length and time scales of turbulence in the viscous sublayer, have strongly boosted our confidence in the application of the said probes to actual turbulence measurements in the viscous sublayer of different types of flow. As described previously, the motivation of near-wall velocity measurements stems from the importance of measuring the flow field very near the wall accurately in order to elucidate the physics and mechanisms of near-wall turbulence events in both unmanipulated and manipulated wall-bounded flows using passive drag or skin friction reduction schemes.

A further motivation of the present work arises from its application to near-wall turbulence modelling. Statistical descriptions of turbulence based on the Reynolds-averaged Navier-Stokes equations suffer from the problem of closure in that the Reynolds stresses and the extra terms which appear in the scalar transport equations as a consequence of time averaging are unknown and thus require

modelling. The two-equation k-ε model which attempts to model most of the constituent terms in the transport equations for k (turbulence kinetic energy) and ε (dissipation rate of the turbulence kinetic energy), has been and may continue to be a turbulence model extensively used by many computational fluid dynamists. At high Reynolds numbers, the standard k-ε model (Launder & Spalding 1974) avoids the need to integrate the model equations right down to the wall by making use of the universal behaviour of near wall flows. Different modifications to the k-ε model to enable it to cope with low Reynolds number flows are reviewed in Patel *et al.* (1985). At low Reynolds numbers, wall damping functions are invariably applied to ensure that the viscous stresses take over from the Reynolds stresses in the viscous sublayer adjacent to the wall. However, the damping functions introduced to model the different terms in the ε-equation are rather ad-hoc and a critical assessment of the models is by no means possible because the accurate measurement of ε in the near-wall region poses insurmountable difficulties. Our near-wall hot-wire measurements can help in assessing the validity of the wall damping function.

1.6.1 Calibration of near-wall hot-wire probe for spanwise intensity measurement

Calibration of the hot-wire for the streamwise velocity follows that described in Section 1.3.1(a). On the other hand, the use of a single hot-wire probe inclined at different angles to the mean flow direction for time-averaged two-component velocity measurements has been documented in detail by Bruun (1995). During calibration of the inclined hot-wire probe, the output E of the probe is normally determined in terms of the magnitude of the flow velocity V and the yaw angle α (where the yaw angle α is defined as the angle between the direction of the velocity vector and the normal to the axis of the hot-wire), i.e.

$$E = E(V, \alpha), \tag{1.31}$$

with E being correlated with the effective velocity V_e using King's Law; that is

$$E^2 = A + BV_e^n. \tag{1.32}$$

V_e can be expressed as

$$V_e = Vf(\alpha), \tag{1.33}$$

where f(α) is the yaw function. Several expressions have been proposed for f(α), the most popular being

$$f(\alpha) = (cos^2\alpha + k_T^2 \sin^2\alpha)^{1/2}, \tag{1.34}$$

where k_T is the tangential cooling coefficient, which was first proposed by Hinze (1959). Another extensively-used expression for f(α), first introduced by Bradshaw (1971), is

$$f(\alpha) = \cos(\alpha_{eff}), \tag{1.35}$$

where α_{eff} is the effective angle which has to be determined from a yaw calibration. The probe is calibrated by first setting $\bar{\alpha}$ to be 45° or -45° in order to determine the calibration constants A, B and n in (1.32). This is followed by rotating the probe in the x-z plane through small variations $\theta = \alpha - \bar{\alpha}$, in the yaw angle as the flow velocity is kept constant, and noting the output voltage E_α of the CTA for each value of α (or θ). The values of θ used were 0°, ±5°, ±10° and ±15°. Following the procedure recommended by Bradshaw, a graph of (cos θ - E_θ) is plotted against sin θ, where E_θ is defined as

$$E_\theta = \left[\frac{E_\alpha^2 - A}{E_{\bar{\alpha}}^2 - A}\right]^{1/n}. \tag{1.36}$$

The effective angle α_{eff} for a particular velocity can then be determined from the slope of the best-fit line, m, with $m = \tan(\alpha_{eff})$.

For each different height h of the hot-wire above the wall substrate, the near-wall hot-wire probe is first calibrated in the laminar flow calibration rig at α = 0°, 45° and -45° and the effective angles α_{eff} are obtained over a range of flow velocities. In order to determine the spanwise turbulence intensity in the viscous sublayer of the channel and flat-plate boundary layer flows, the plug housing the near-wall hot-wire probe is rotated with the axis of rotation being normal to the wall (i.e. in the x-z plane) and the output voltages E_0, E_1 and E_2, corresponding to α = 0°, 45° and -45° respectively, are sampled digitally. The effective velocities V_{e0}, V_{e1} and V_{e2} can then be deduced from E_0, E_1 and E_2 respectively via equation (3**XXX**). The Reynolds stresses are then evaluated using the following expressions:

$$\overline{w^2} = \frac{\overline{V_{e1}^2} + \overline{V_{e2}^2} - 2\overline{V_{e0}^2}\cos^2\alpha_{eff}}{2\sin^2\alpha_{eff}} \tag{1.37}$$

and

$$\overline{uw} = \frac{\overline{V_{e2}^2} - \overline{V_{e1}^2}}{2\sin 2\alpha_{eff}} \tag{1.38}$$

For the channel and flat-plate boundary layer flows, $\overline{uw}$ was found to be negligibly small within the viscous sublayer.

1.6.2 Mean velocity profile

The mean velocity profile normalized by the centreline velocity for the channel flow at $h^+ = 390$ is presented in Fig.(1.32). The mean wall shear stress $\bar{\tau}$ and hence the mean friction velocity $\overline{u_\tau}$ were determined from streamwise pressure gradient measurements.

Also shown in Fig.(1.32) are the DNS results of Antonia *et al.* (1992) for a channel flow at $h^+ = 395$. It is evident that the experimental results bear close resemblance to the simulation results. Figure 1.32 also shows the mean velocity profiles normalized using the free-stream velocity for the flat plate boundary layer flow at Re_θ (based on the momentum thickness and the free stream velocity) of

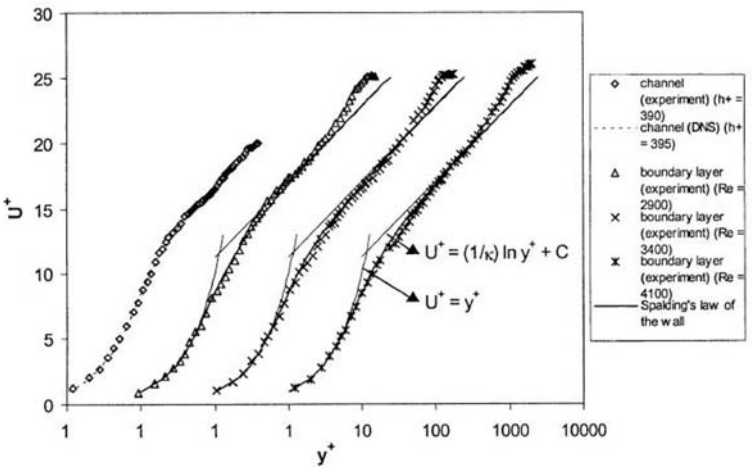

Figure 1.32: Mean streamwise velocity profile normalized using inner variables.

2900, 3400 and 4100. It is apparent that an increase in Re_θ enhances the "bulging" of the boundary layer profile (i.e. the velocity profile becomes fuller). Although not displayed in Fig.(1.32), the near-wall velocity profile of the channel flow at $\mathrm{h}^+ = 180$ compares well to Kim *et al.*'s (1987) DNS results of a channel flow at the same h^+.

Figure 1.33 depicts the mean velocity profiles for the channel and boundary layer flows scaled using inner variables. There is excellent agreement between the experimental and computational results for the channel flow. The wall shear stress values (τ_w) for the boundary layer flow at different values of Re_θ were obtained using the Clauser Chart technique. The evaluated skin friction coefficient C_f ($\equiv \tau_w/(0.5\rho U_\infty^2)$) compares very favourably to those obtained by previous investigators using the Preston tube method, which are compiled in Fernholz & Finley (1996). It can be noted that, away from the wall, starting from $y^+ \approx 30$, the profiles closely follow the logarithmic law of the wall

$$U_{log}^+ = (1/\kappa)\ln y^+ + C, \tag{1.39}$$

with universal constants $\kappa = 0.4$ and $C = 5.5$. At distances further from the wall, Coles (1962) described the development of a low Reynolds number boundary layer using 'the strength of the wake' $\Delta\mathrm{U}^+$, defined as the maximum value of (U^+ - U_{log}^+), which is the largest deviation of the outer layer velocity profile from the log law. This quantity assumes a asymptotically constant value of 2.75 for $\mathrm{Re}_\theta < 6000$ when the defect law is satisfied and drops gradually to zero when $Re_\theta \approx 500$. The values of $\Delta\mathrm{U}^+$ (using the above-mentioned values for the constants in the log law) work out to be 2.35, 2.26 and 2.39 for Re_θ of 2900, 3400 and 4100, respectively. These results are in fair comparison to the experimental results of $\Delta\mathrm{U}^+$ for a wide

range of Re_θ values compiled by Coles (1962) and more recently by Fernholz & Finley (1996).

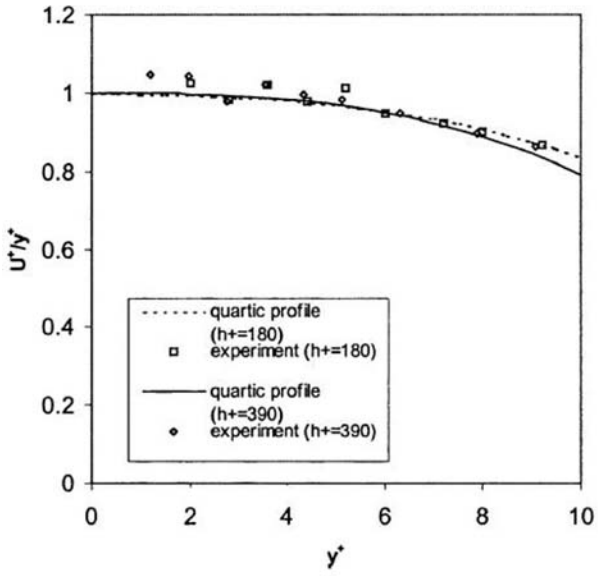

Figure 1.33: Dimensionless streamwise mean velocity U^+ divided by y^+ as a function of y^+ in viscous sublayer of channel flow.

In the immediate vicinity of the wall, the near-wall hot-wire probe accurately predicts the velocity profile

$$U^+ = y^+ \tag{1.40}$$

valid in the viscous sublayer of the channel and boundary layer flows for $y^+ \leqslant 5$, which is the conventionally accepted extent of the viscous sublayer. (See Schlichting, 1979. See also the simulation results of Kim *et al.*, 1987 and Antonia *et al.*, 1992, for a channel flow and Spalart, 1988, for a boundary layer flow.) This clearly demonstrates the viability of the near-wall hot-wire to directly measure the velocity distribution very near the wall accurately (without the need for any wall correction), when the effects of wall influence are calibrated away using the laminar flow calibration rig as described in Section 1.3.1(a).

Spalding (1961), in an attempt to describe fully the mean streamwise velocity distribution next to the wall, proposed the law of the wall given by

$$y^+ = u^+ + e^{-\kappa C}\left[e^{\kappa u^+} - 1 - \kappa u^+ - \frac{(\kappa u^+)^2}{2} - \frac{(\kappa u^+)^3}{6}\right], \tag{1.41}$$

with $\kappa = 0.4$ and $C = 5.5$. In Fig.(1.32), there is reasonable agreement of experimental data with Spalding's (1961) law of the wall for both the channel and

boundary layer flows; for the latter, concurrence is valid up to $y^+ \approx 400$. Very recently, based on theory and analysis of DNS results, Cenedese *et al.* (1998) have suggested the use of a quartic profile to represent the mean velocity in the region $y^+ < 10$. This profile is given as $u^+ = y^+ - (1/2h^+)y^{+2} + ey^{+4}$, where $e \approx -10^{-5}(h^+)^{0.5}$. This quartic profile is evaluated for a channel flow at $h^+ =$ 180 and 390 and the profiles are plotted alongside the experimental results in Fig.(1.33). It can be inferred that the experimental values are fairly well described by the quartic profile for $y^+ < 10$. Attention should also be drawn to Fig.(9) of Cenedese *et al.*, which shows the quartic profile and their very near-wall hot-wire results obtained for $h^+ = 1670$. For $y^+ < 4$, the hot-wire results expressed as U^+/y^+ do not exhibit a fairly constant value tending towards unity as expected. Instead, it displays a clear monotonic increasing trend as the wall is approached, with U^+/y^+ rising to 1.2 when $y^+ \approx 2.5$. This is not surprising in view of the fact that wall effects have not been accounted for nor calibrated away for their near-wall hot-wire results, thus culminating in the spurious rise in value of U^+/y^+ with decreasing y^+. This rise in U^+/y^+ is also a manifestation of increasing wall influence. In contrast, the experimental results in Fig.(1.33) do not bear such a trend as the wall is approached, hence further verifying the validity of our calibration techniques.

1.6.3 Turbulence flow intensities

1.6.3(a) Streamwise velocity component

The root-mean-square (rms) values of the fluctuating streamwise velocities, normalized using the mean friction velocity is presented in Fig.(1.34).

The experimental results for the channel flow at $h^+ = 390$ agree well with the DNS results of Antonia *et al.* (1992) for a channel flow at $h^+ = 395$. The experimental results for the boundary layer suggests a barely discernible trend of increasing u'^+ with Re_θ at a given y^+ valid for $y^+ \geqslant 30$. This trend can also be observed from the extensively compiled boundary layer data in the review article by Fernholz and Finley (1996) and the experimental results for a channel flow at different Reynolds numbers reported in Antonia *et al.* (1992). The DNS results of Spalart (1988) and Antonia *et al.* (1992) confirm the tendency for u'^+ to increase with Reynolds number. Furthermore, it may be noted from Fig.(1.34) that the maximum value of u'^+ is approximately 2.75 and occurs at $y^+ \approx 15$ for both the boundary layer and the channel flows, which compares reasonably well with the values provided by other researchers. For example, Ligrani & Bradshaw (1987b) employed wires of different length to diameter ratios in a turbulent boundary layer at $Re_\theta = 2620$ and found that the results for the value of u'^+ at $y^+ = 17 \pm 0.5$ (where the value of u'^+ reaches a maximum) collapsed onto a single curve when plotted against the wire length in wall units. Their results indicate that the maximum value of u'^+ assumes a value of approximately 2.8 at $y^+ \approx 17$. Kim *et al.* (1987) obtained a maximum value of about 2.7 at $y^+ \approx 12$ for their DNS

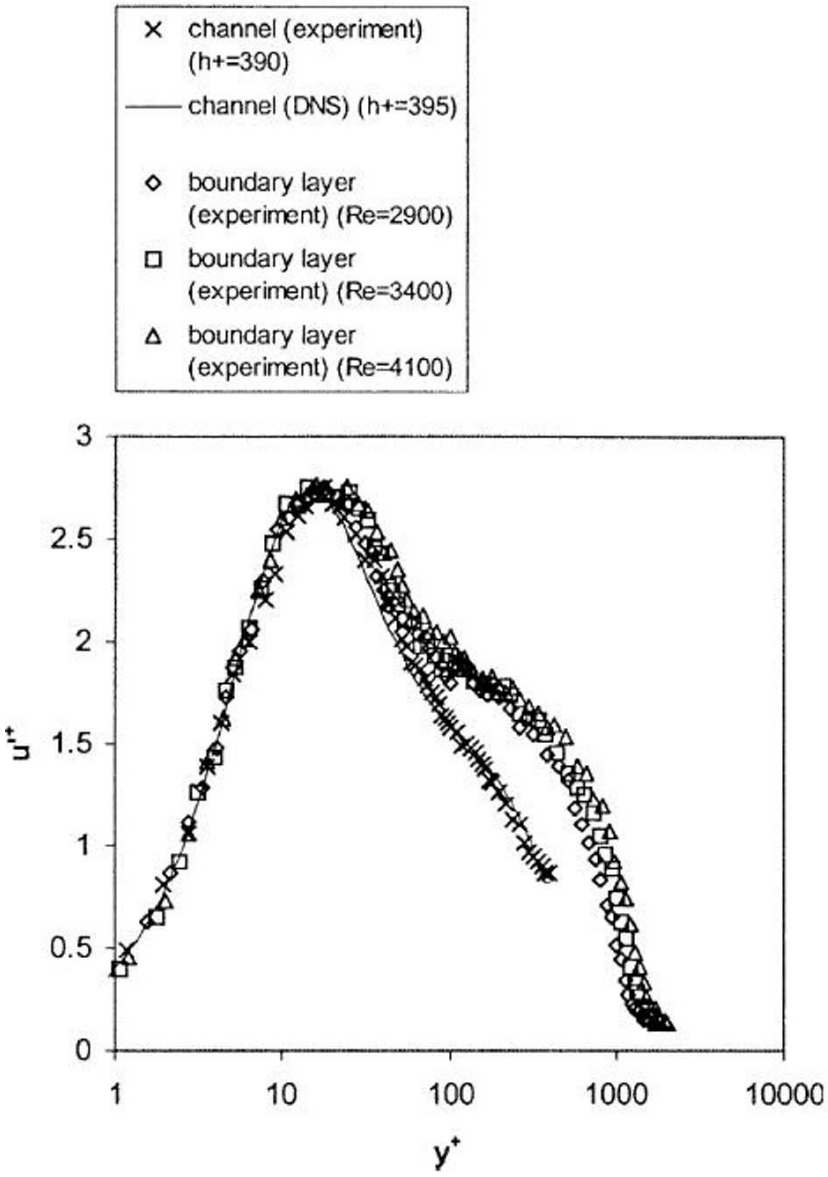

Figure 1.34: Distribution of rms streamwise velocity fluctuations normalized using inner variables.

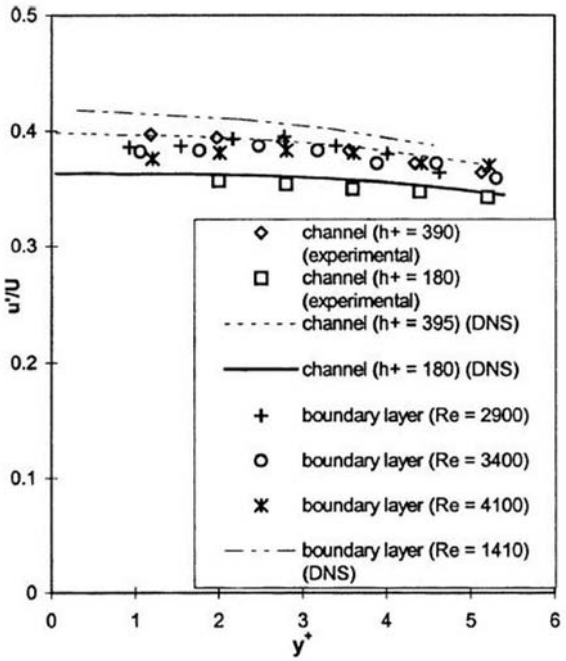

Figure 1.35: Streamwise turbulence intensity distribution in the viscous sublayer.

of a channel flow at $h^+ = 180$. Spalart (1988) found a systematic increase in the maximum value of u'^+ with Re_θ for his DNS of a boundary layer flow, the value increasing from 2.5 to 2.7 corresponding to a Re_θ increase from 300 to 1410. However, within the limits of experimental accuracy, it is not possible to discern any systematic dependence of this maximum value on Re_θ for our boundary layer measurements. On the other hand, Mochizuki & Nieuwstadt (1996) made a survey on 47 independent experimental and numerical studies for zero pressure gradient boundary layer and fully developed internal flows (including pipes and channels) over an extensive range of Reynolds numbers and found the peak value of u'^+ to be independent of the Reynolds number within limits of statistical error. Their survey reveals that this parameter assumes a value of 2.71 ± 0.14 (occurring at an average y^+ of 14.4) and 2.70 ± 0.09 (occurring at an average y^+ of 14.6) for boundary layer and internal flows, respectively. Marusic *et al.* (1997) speculated the peak value of u'^+ occurring at $y^+ \approx 15$ to be associated with "the early formation process of the attached eddies" and further lamented that "very little is understood about this region".

Experimental results in the near-wall viscous sublayer region is shown in Figure 1.35, where the local rms value of the streamwise velocity fluctuations are normalized using the local mean velocity.

The results for the channel flow at $h^+ = 180$ and 390 compare favourably with the simulation results of Kim *et al.* (1987) and Antonia *et al.* (1992) respectively, thus suggesting the calibrated near-wall hot-wire probe's capability in time-resolved velocity measurements and the validity of the calibration technique employed. The general rise in the distribution for the streamwise turbulence intensity corresponding to an increase with h^+ is consistent with the trend revealed by the DNS results. This has been attributed by Spalart (1988) and Antonia *et al.* (1992) and Antonia and Kim (1994) to an "inactive motion", first proposed by Townsend (1961) and Bradshaw (1967), which intensifies as the Reynolds number increases. This inactive motion which consists of the large-scale vorticity field and the pressure fluctuations of the large eddies in the outer layer is nominally irrotational. Such motions have very large wavelengths (of order δ) and time-scales in comparison to the viscous (inner) layer scales. As the wall is approached, the normal (v) component (to the wall) of the inactive motion has to be brought to rest due to the impermeability condition imposed by the wall, thus releasing their normal component of the energy into the other two orthogonal tangential components u and w. This "splat effect" motion's influence on the shear stress is small, thus producing very little effect on the log law of the wall for the mean velocity. As the Reynolds number increases, this inactive motion contributes appreciably to the low wavenumber components of the u and w spectra, thus causing the magnitudes of u'^+ (and hence $u'/\overline{U}$) and w'^+ to increase with Reynolds number.

The turbulence intensity of the streamwise velocity fluctuations at a given y^+ for the boundary layer flow does not reveal any significant variance or increase with increasing Re_θ, which may be attributed to the narrow range of Re_θ investigated in this present study. Furthermore, it can be observed from Fig.(1.35) that the distribution of $u'/\overline{U}$ for the boundary layer flow for the range of Re_θ investigated bears close resemblance to that obtained for the channel flow measurements at $h^+ = 390$. The value of $u'/\overline{U}$ assumes a marginally increasing trend as y^+ decreases towards a constant value of approximately 0.38, which compares favourably with the results of other researchers available in the literature. Alfredsson *et al.* (1988) obtained a slightly higher constant value of $u'/\overline{U} \approx 0.4$ within the viscous sublayer for their marginally-elevated hot-film probes in an oil channel flow at Re_c (based on centerline velocity and channel half-width) of 3800, which concurs well with our findings, within a variation of about 5%.

Unlike (our) near-wall hot-wire operation in air which is strongly affected by wall effects which have to be calibrated away, Alfredsson *et al.*'s hot-film operation in oil is not influenced by such effects as the ratio of the direct heat loss to oil is about one order of magnitude greater than that in air. In fact, when Alfredsson *et al.* utilized a hot-wire probe (whose wall effects have not been calibrated away) in an air boundary layer, they found that $u'/\overline{U}$ attained a maximum of 0.39 at $y^+ = 5$ and decreased considerably towards the wall and attained a value of 0.16 at $y^+ = 0.6$. One important consideration for near-wall hot-wire anemometry is the length of the hot-wire l^+ (in wall units). Ligrani & Bradshaw (1987b) indicated that the streamwise turbulence intensity is independent of l^+ in the buffer region and beyond provided $l^+ < 20-25$. Khoo *et al.* (1997) demonstrated that the

streamwise turbulence intensity at a particular value of y^+ in the viscous sublayer attenuates in magnitude as l^+ increases and would incur an error of at most 5-10% if $l^+ \approx 20$.

Karlsson & Johansson (1988) employed a two-colour counter-based Argon-Ion LDV system to obtain velocity measurements in a turbulent boundary layer of a water channel, with $Re_\theta = 2420$. They also obtained a u'/$\overline{U}$ distribution which displayed an approximately constant value of between 0.37 to 0.39 for $y^+ \leqslant 5$, which serves as a significant and independent comparison, as the measurements are not based on hot-wire anemometry where wall effects influence the convective heat transfer characteristics of the wire. Recently, other near-wall LDV measurements have also been reported. Durst *et al.* (1995) made measurements using a two-component He-Ne LDV system in a pipe flow at Re_B (based on pipe diameter and bulk velocity) of 7442 and obtained an asymptotic value for $u'/\overline{U}$ of 0.37 as the wall was approached. Their results further indicated a slight increase in this asymptotic value as Re_B was increased.

Fontaine & Deutsch (1995) performed three-component, coincident, time resolved LDV measurements in the near-wall region of a pipe flow at a relatively much lower $Re_\theta \approx 720$ and obtained $u'/\overline{U}$ values in the viscous sublayer which compared favourably to those reported by Karlsson & Johansson (1988). However, it may be noted that near-wall LDV users have to contend and account for the drop in data rate as the wall is approached. This can be attributed to a decrease in particles close to the wall. Karlsson & Johansson reported that the substantial drop in data rate very near the wall compelled them to use a lower sampling frequency.

Another problem encountered in the use of LDV for near-wall velocity measurements is the relatively large control volume straddling a region of large velocity gradient. Measurements of near-wall turbulence thus require corrections to be applied to the gradient-broadening effects and the application of such corrections requires caution. As mentioned in Durst *et al.* (1995), "in the literature, no unique correction procedure exists to take this influence into account". If the gradient broadening effects are not accounted for or ad hoc correction methods are applied, the accuracy of near-wall turbulence measurements will greatly suffer. Niederschulte *et al.* (1990) performed two-component LDV measurements in a channel flow at $h^+ = 178.6$ and 158.5 in an attempt to verify the accuracy of the DNS results of Kim *et al.* (1987). Niederschulte *et al.* did not report any attempt to correct for the gradient broadening effects and obtained a streamwise turbulence intensity ($u'/\overline{U}$) of approximately 0.4 for y^+ between 2.5 and 5. This is about 10% larger than the value of 0.36 obtained from the simulation results of Kim et al. For $y^+ < 2.5$, Niederschulte *et al.* found that the value of $u'/\overline{U}$ increases drastically, registering a maximum value of 0.54 at $y^+ = 1$, and attributed this disparity to the lack of accuracy in Kim *et al.*'s computation due to the use of insufficient nodes or an excessively small computational domain.

It is interesting to note that Niederschulte et al's observation of a rising trend in $u'/\overline{U}$ as the wall is approached for $y^+ < 2.5$ is remarkably similar to Durst *et al.*'s (1995) results which have *not* been corrected for gradient broadening effects.

After correcting for the gradient broadening effects, however, Durst *et al.* were able to obtain a $u'/\overline{U}$ distribution for $y^+ < 2.5$ which conformed closely to the simulation results of Kim *et al.*. This is a testament illustrating the importance of implementing appropriate and valid correction techniques for gradient broadening effects encountered in near-wall LDV turbulence measurements.

It should be further mentioned that all the near-wall LDV measurements available in the literature are limited to relatively low Reynolds numbers, as severe spatial resolution problems are imposed by the finite width of the laser beam at high Reynolds number. This is in addition to temporal resolution problems which can and usually arise due to the extremely low particle count very near the wall. On the other hand, it is always possible to extend the use of the near-wall hot-wire probe to high Reynolds numbers, as exemplified by the measurements we have made in the boundary layer flow at $Re_\theta = 4100$, which is already higher than the Reynolds numbers of the flow reported by most of the near-wall LDA researchers available in the literature.

1.6.3(b) Spanwise velocity component

The local rms value of the spanwise velocity fluctuations normalized using the local mean velocity is shown in Fig.(1.36).

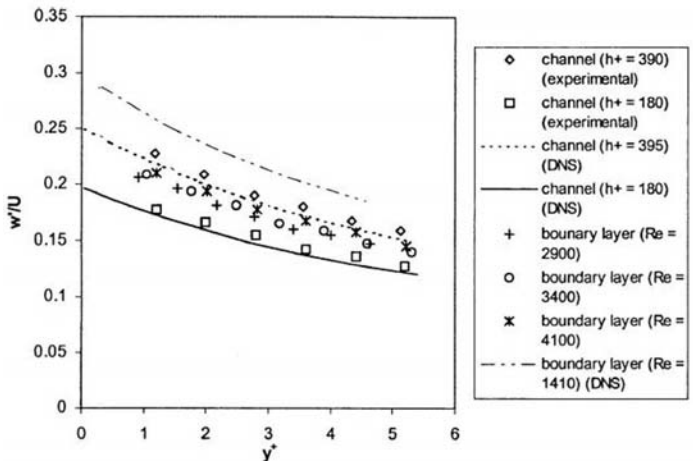

Figure 1.36: Spanwise turbulence intensity in the viscous sublayer.

It is evident that the experimental results for the channel flow at $h^+ = 180$ and 390 lie close to the respective DNS results of Kim *et al.* (1987) and Antonia *et al.* (1992), hence further attesting to the accuracy of the time-resolved velocity measurements by the near-wall hot-wire system. Similar to the streamwise turbulence intensity, the spanwise turbulence intensity distribution also shows an increasing trend for larger values of h^+, which is in line with the trend manifested by the

simulation results. This may be again attributed to an 'inactive motion' which causes both the magnitudes of u'$^+$ and w'$^+$ to increase with Reynolds number, as previously discussed. Moreover, it seems plausible to suggest that an increase in Reynolds number causes an increase in vortex stretching in the inner region, thus resulting in a concomitant increase in the vorticity of the hairpin or quasi-streamwise vortices near the wall, which is subsequently accompanied by an increase in both w'$^+$ and v'$^+$ (not measured). At $h^+ = 180$, $w'/\overline{U}$ assumes a value of 0.18 at $y^+ \approx 1$. This value rises to 0.23 at the same y$^+$ for $h^+ = 390$. On the other hand, the spanwise turbulence intensity at a given y$^+$ for the boundary layer flow only reveals a barely discernibly weak dependence on increasing Re$_\theta$; this may be attributed to the relatively narrow range of Re$_\theta$ investigated in this present study. Overall, the spanwise intensity for the boundary layer flow exhibits a distribution closer to that for the channel flow at $h^+ = 390$. Unlike the streamwise turbulence intensity distribution depicted in Fig.(1.35), which shows that $u'/\overline{U}$ at a particular h$^+$ (or Re$_\theta$) is approximately constant within the viscous sublayer, or at best only increasing very gradually as y$^+$ decreases, the spanwise intensity distribution presented in Fig.(1.36) shows that $w'/\overline{U}$ increases much more rapidly with decreasing y$^+$.

Spanwise turbulence intensity measurements in the viscous sublayer undertaken by other researchers utilizing hot-wire anemometry and LDV have also been reported in the literature, and it would be of interest to compare the present findings with available results. As previously discussed, Kreplin & Eckelmann (1979) made measurements in an oil channel using an in-house V hot-film probe. Their measurements indicated that $w'/\overline{U}$ registered a maximum value of 0.195 at $y^+ \approx 3.5$ and subsequently dropped to 0.065 at the wall. Similar to the trend borne by the streamwise turbulence intensity, the abrupt drop in the spanwise turbulence intensity as the wall was approached can be attributed to wall effects which had not been accounted for nor calibrated away. Our near-wall hot-wire measurements show the correct trend of $w'/\overline{U}$ rising as the wall is approached. Based on the comparison of their $u'/\overline{U}$ results in the viscous sublayer with those of Kreplin & Eckelmann, Alfredsson *et al.* (1988) suggested that the spanwise wall shear stress turbulence intensity (i.e. applicable at y$^+ = 0$) should be approximately equal to the maximum value of $w'/\overline{U}$ in the viscous sublayer obtained by Kreplin & Eckelmann, which was found to be approximately 0.2. Our spanwise turbulence intensity results, which range about 0.2 next to the wall, thus affirms the suggestion put forth by Alfredsson *et al.*. Near-wall spanwise turbulence intensity measurements have also been attempted by several researchers of late.

Karlsson (1993) employed a two-component Argon-Ion LDV system for measurements in a turbulent boundary layer at $Re_\theta = 2400$ and obtained a $w'/\overline{U}$ distribution which increased from approximately 0.12 to 0.18 as y$^+$ decreased from 5 to 1.5. This distribution is of similar trend but lower magnitude compared to the present boundary layer measurements obtained at higher Re$_\theta$. Near-wall turbulence measurements using a two-component He-Ne LDV system were performed by Durst *et al.* (1995) in a pipe flow at Re$_B$ (based on pipe diameter and bulk velocity) of 7442, yielding an asymptotic value for $w'/\overline{U}$ of 0.21 as the

wall was approached. Fontaine & Deutsch (1995) conducted three-component, coincident, time resolved LDV measurements in the near-wall region of a pipe flow at $Re_\theta \approx 720$ and obtained $w'/\overline{U}$ values in the viscous sublayer which compared favourably to the DNS results of Antonia *et al.* (1992) and hence with our experimental results.

1.6.4 Turbulence kinetic energy in the viscous sublayer

Having obtained the streamwise (u') and spanwise (w') components of the velocity fluctuations in the viscous sublayer, it would be interesting to investigate the behavior of the turbulence kinetic energy (k), where

$$k = 0.5(u'^2 + v'^2 + w'^2) \tag{1.42}$$

and v' is the normal (to the wall) component of the fluctuating velocity. Neglecting the v' component in the viscous sublayer has very little effect on the evaluation of the turbulence kinetic energy k, as v' is likely to be negligible compared to u' and w' in the viscous sublayer. For example, Finnicum & Hanratty (1985) deduced the limiting value of v' in the immediate vicinity of the wall to be $v'^+ = 0.005y^{+2}$, while Kim et al (1987) deduced a correlation of $v'^+ = 0.009y^{+2}$ from their DNS results of a channel flow at $h^+ = 180$, with v' being merely 7% of u' at $y^+ \approx 5$, v' decreases very rapidly with decreasing y^+. Gunther *et al.* (1998) obtained a rather similar expression $v'^+ = 0.012y^{+2}$ as $y^+ \to 0$ for their DNS of a channel flow at $h^+ = 300$, with v' being 8% of u' at $y^+ \approx 5$. It may be noted that our use of the very near-wall hot-wire probe to measure the streamwise and spanwise turbulence intensities has inherently assumed that $v' << u'$ and $v' << w'$ in the viscous sublayer. The fact that our near-wall hot-wire results compare favorably to those of other researchers obtained using LDV and DNS provides evidence that this assumption is reasonable and valid in the viscous sublayer.

The distributions of the turbulence kinetic energy normalized using inner variables, k^+ ($\equiv u'^{+2} + v'^{+2} + w'^{+2}$) in the viscous sublayer for the channel and boundary layer flow, neglecting v', are depicted in Fig.(1.37). The experimental results for the channel flow at $h^+ = 180$ and 390 are observed to be reasonably compatible with the simulation results of Kim *et al.* (1987) and Antonia *et al.* (1992). This reaffirms that the neglect of v'^+ has little effect in the evaluation of k^+ in the viscous sublayer, especially for $y^+ \leqslant 4$. Moreover, the rise in k^+ at the same y^+ when h^+ is more than doubled is in line with the trend exhibited by the numerical results. This is not surprising, in view of the rise in u'^+ and w'^+ for the same y^+ when h^+ is increased, which may be attributed to an inactive motion or increased stretching of the vortices in the wall region, as previously discussed. Once again, the k^+ distribution for the boundary layer flow displays greater invariance corresponding to a rise in Re_θ, bearing closer similarity to the results for the channel flow at $h^+ = 390$.

From Fig.(1.37), it is further suggested that, with the exception of the results for the channel flow at $h^+ = 180$, the values of k^+ in the viscous sublayer ($y^+ \leqslant$

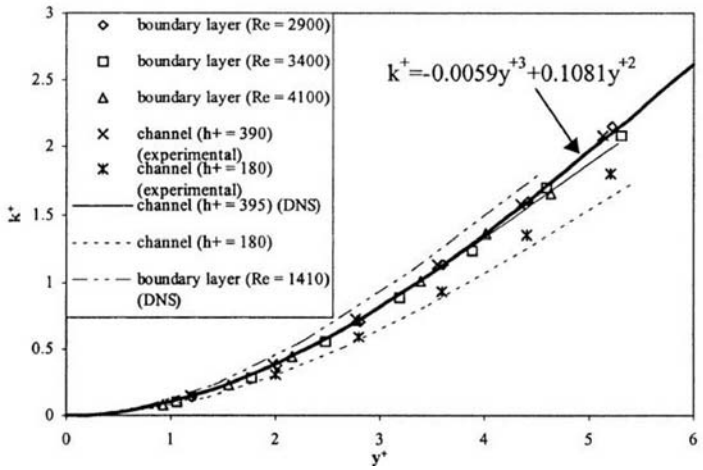

Figure 1.37: Distribution of normalized turbulence kinetic energy k^+ in the viscous sublayer.

5) for the boundary layer flow at $2900 \leqslant \mathrm{Re}_\theta \leqslant 4100$ and $h^+ = 390$ for a channel flow can be correlated well by

$$k^+ = -0.0059y^{+3} + 0.1081y^{+2}. \tag{1.43}$$

This correlation should be invaluable to users of the k-ε model in modeling the behavior of k in the viscous sublayer. Previously, Karlsson (1993) has also provided a correlation equation of the form $k^+ = -0.0064y^{+3} + 0.096y^{+2}$ valid for $y^+ \leqslant 5$ for their near-wall LDV measurements in a turbulent boundary layer based solely on a *single* flow condition of $Re_\theta = 2400$. This relation shows strong resemblance in characteristics to the equation proposed above except for the coefficients. Similarly, Kim *et al.*'s (1987) DNS of a channel flow computed at a single $h^+ = 180$ yields a correlation of $k^+ = -0.0066y^{+3} + 0.0829y^{+2}$ in the viscous sublayer; the difference lying only in the coefficients. At a higher h^+ of 300, Gunther *et al.*'s (1998) DNS results indicate a correlation of $k^+ \approx 0.1076y^{+2}$ in the viscous sublayer, the coefficient of y^{+2} in rather close agreement with ours. Correlations of this form are vital as they provide an avenue for assessing the ability/validity of two-equation and second-order near-wall turbulence closures in predicting near-wall turbulence statistics. Because of the existence of many proposed correlations, based on experiments or otherwise, it is imperative that accurate data be used as a basis of comparison *ab initio*. For example, Patel *et al.* (1985) used the correlation $k^+ = 0.05y^{+2}$ based on experimental data available then (these are near-wall hot-element measurements by Kreplin & Eckelmann, 1979, and others) to assess the behavior of various previously proposed two-equation turbulence closures. However, this correlation clearly yields k^+ values which are substantially

lower than presently available DNS and experimental values (see Alfredsson *et al.*, 1988), and this can lead to incorrect assessment of turbulence models.

1.6.5 The dissipation rate

The full expression for the dissipation rate ε is given by

$$\varepsilon = \nu\overline{u_{i,j}(u_{i,j} + u_{j,i})}, \tag{1.44}$$

where $u_{i,j}$ represents the velocity derivative $\partial u_i/\partial x_j$. However, it should be noted that it is virtually impossible to measure all the 12 terms which appear on the right hand side of Eq.(1.44), especially in the near-wall region where wall influence increasingly dominates generally for all velocity-measuring instruments, including the hot-wire. The physical presence of the wall also causes problems in maneuvering the instrument to obtain a fine distribution across the usually thin viscous sublayer. By assuming the dissipating range of eddy sizes to be statistically isotropic, the dissipation rate ε_{iso} can be substantially simplified to

$$\varepsilon_{iso} = 15\nu\overline{(\frac{\partial u}{\partial x})^2}. \tag{1.45}$$

By further assuming the validity of Taylor's hypothesis, equation (1.45) becomes

$$\varepsilon_{iso} = 15\frac{\nu}{U_c^2}\overline{(\frac{\partial u}{\partial t})^2}, \tag{1.46}$$

where U_c is the local convection velocity, which is usually assumed to be equal to the mean velocity $\overline{U}$ at the point of measurement. Furthermore, if $E_u(k_1)$ is the spectral density of longitudinal velocity fluctuations, where the wavenumber $k_1 = 2\pi f/U_c$,

$$\varepsilon_{iso} = 15\nu \int_0^\infty k_1^2 E_u(k_1) dk_1. \tag{1.47}$$

Equations (1.46) and (1.47) are two commonly used methods for estimating ε.

Azad & Kassab (1989) employed hot wires of different lengths and diameters in a boundary layer flow at $Re_\theta \approx 4200$, $y/\delta = 0.1$ and obtained ε_{iso} using equations (1.46) and (1.47). For wires with the same length and diameter, Azad & Kassab found that the spectra (i.e. Eq.(1.47)) yielded results of ε_{iso} that were consistently higher than those obtained using $\overline{(\partial u/\partial t)^2}$ (i.e. Eq.(1.46)) by about 30%. They attributed the discrepancies to inadequacies in the "calibration of $\partial u/\partial$t, and other deterministic errors owing to the experimental set-up and the experimenter". Their measurements were made in the wall-remote region of $y^+ \geqslant 50$. However, in a separate study conducted by Elsner *et al.* (1993) in a turbulent channel flow, both methods were found to yield almost identical values for ε_{iso}, thus contradicting Azad & Kassab's contention that ε_{iso} yielded by spectra are consistently 30% higher.

To reconcile this apparent controversy of whether the spectra would yield larger values of ε_{iso}, both methods of evaluating ε_{iso} were applied to the present study of boundary layer flow at $Re_\theta = 3400$ for the wall-remote region (as carried out in Azad & Kassab) and the near-wall region. The spectral density $\mathrm{E}_u(\mathrm{k}_1)$ of longitudinal velocity fluctuations was obtained using a Fast Fourier Transform (FFT) algorithm, and the convective velocity U_c was also assumed to be the mean velocity $\overline{U}$ at the point of measurement. The distributions of ε^+_{iso} employing these two methods are plotted on Fig.(1.38). As can be seen from the figure, both methods of evaluating ε_{iso} yield almost identical results throughout the entire channel flow, even in the very near-wall viscous sublayer and buffer region. In particular, in the wall-remote region, the concurrence is almost exact.

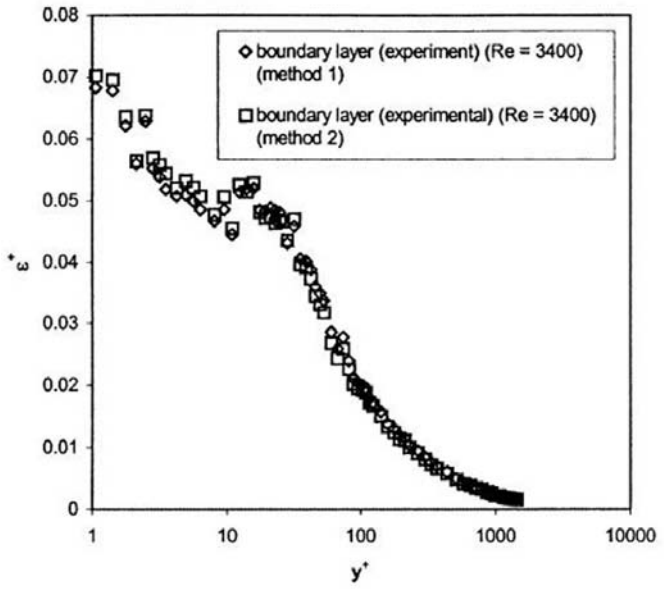

Figure 1.38: Distribution of normalized isotropic dissipation rate ε^+_{iso} dstribution in a boundary layer flow at $Re_\theta = 3400$ using method 1: $\varepsilon_{iso} = 15\nu \int_0^\infty k_1 E_1(k_1) dk_1$ and method 2: $\varepsilon_{iso} = 15\nu\overline{(\partial u/\partial t)^2}/U_c^2$, with $U_c = \overline{U}$.

Similar observations were also obtained for the channel flow at $\mathrm{h}^+ = 180$ and 390 as well as the boundary layer flow at other Re_θ (not shown), thus substantiating Elsner *et al.*'s argument that both methods should yield essentially identical values of ε_{iso}. It is conjectured that the persistently higher values of ε_{iso} obtained by Azad & Kassab using the spectra method might be attributed to an excessively low sampling frequency used and which have inordinate influence on the evaluation, thus rendering $\overline{(\partial u/\partial t)^2}$ to be grossly underestimated. However, this cannot be ascertained, as Azad & Kassab did not explicitly state the sampling frequency

at which they have acquired their hot-wire data.

It would be of further interest to investigate the effects of using different expressions for the convective velocity U_c. Denoting $(\varepsilon_{iso})_1$ as the value of ε_{iso} evaluated by assuming the convective velocity U_c in equation (18) to be the mean velocity at the point of measurement, $\overline{U}$ (an approach widely adopted in the literature), the experimental values of $(\varepsilon^+_{iso})_1$ obtained for the channel flow at $h^+ = 390$ are plotted in Fig.(1.39) together with the true values for ε^+ corresponding to the DNS results of Antonia *et al.* (1992) for $h^+ = 395$. It is evident that the experimental and computational results agree well only when

$$(y^+)_{1,critical} \geqslant 80. \tag{1.48}$$

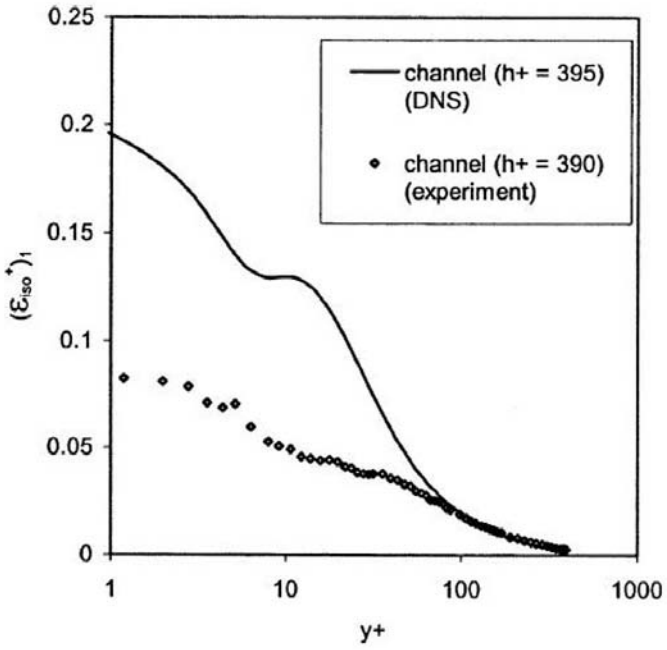

Figure 1.39: Experimental distribution of $(\varepsilon^+_{iso})_2$ and DNS results of ε^+ for a channel flow.

This suggests the validity of assuming U_c to be equal to $\overline{U}$ *and* local isotropy in the evaluation of ε for large values of y^+, which is consistent with the widely accepted notion of local isotropy in a turbulent flow far from the wall (see Hinze, 1975). For low values of y^+, since the assumptions of local isotropy and Taylor's hypothesis are unlikely to be valid due to flow anisotropy in the strong shear flow region (where the strain rate is large), increasing discrepancies are observed between the computational and experimental results.

Strictly, the assumption that the convective velocity U_c is equal to the mean velocity $\overline{U}$ at the point of measurement when Taylor's hypothesis is invoked requires that the streamwise turbulence intensity be less than about 10% (see Saddoughi & Veeravalli, 1994, for example), which is clearly violated in the buffer region and especially in the viscous sublayer, where the streamwise turbulence intensity registers values as high as 40% (see Section 1.6.3(a)). Johansson *et al.* (1991) analyzed the DNS results of Kim *et al.* (1987) for a channel flow at $h^+ = 180$ using a VISA technique (the spatial counterpart of the VITA technique) and deduced that the propagation velocity of the near-wall shear layers was $10.6u_\tau \pm 61.0u_\tau$.

Following the methodology of Kim *et al.*, Xu *et al.* (1996) conducted a DNS of a channel flow at $h^+ = 172$ to analyze the origin of high kurtosis levels of the normal velocity fluctuations in the viscous sublayer. Xu *et al.* observed that the high values of the kurtosis were due to extremely rare spatial and temporal events characterized by spikes in the time series with extremely negative values. These spikes only appeared in the very near-wall region and were propagated at a velocity of $10.6u_\tau \pm 0.8u_\tau$, which is strikingly close to the value deduced by Johansson *et al.*. It is interesting to note that the propagation velocity of shear layers, pressure fluctuations and spikes in the viscous sublayer ($\sim 10.6u_\tau$) is larger than the local mean velocity; this difference increases as the wall is approached. Denoting $(\varepsilon_{iso})_2$ as the value of ε_{iso} evaluated by assuming the convective velocity U_c in Eq.(1.47) to be $10.6u_\tau$, the distributions of $(\varepsilon^+_{iso})_2$ $[\equiv (\varepsilon_{iso})_2\nu/u_\tau^4)]$ for the channel flows at $h^+ = 180$ and 390 are plotted in Fig.(1.40) together with the DNS results of Kim *et al.* (1987) for $h^+ = 180$ and Antonia *et al.* (1992) for $h^+ = 395$; the DNS results for ε_{iso} are obtained without invoking Taylor's hypothesis.

It can be seen that for both values of h^+, within the viscous sublayer and the inner portion of the buffer region, agreement between the experimental values of $(\varepsilon^+_{iso})_2$ and the DNS results is fair. However, the experimental results are consistently greater than the DNS results, this difference increasing as y^+ increases, which is anticipated as the convective velocity is unlikely to remain constant at $10.6u_\tau$ further away from the wall. The experimental distribution for $(\varepsilon^+_{iso})_2$ bears the same trend as the DNS results for

$$(y^+)_{2,critical} \geqslant 15, \tag{1.49}$$

where the local turbulence intensity $u'/\overline{U}$ exceeds 25%. This suggests the reasonable assumption made above that $U_c = 10.6u_\tau$ in the flow region with $u'/\overline{U} > 0.1$ where it is no longer valid to accept the conventionally used relationship of $U_c = \overline{U}$. As h^+ increases from 180 to 390, the experimental value of $(\varepsilon^+_{iso})_2$ at the same y^+ increases, thus reflecting the presence of low Reynolds number effects. It should also be noted that the convective velocity of $10.6u_\tau$ in the very near-wall region deduced from DNS results is strictly valid and obtained for $h^+ \approx 180$, and it is not generally known if this value will change as h^+ increases. Experimental methods of determining the convective velocity have yielded results with marginally greater magnitudes. Johansson *et al.* (1987) used the VITA technique and obtained a value of $13u_\tau$ for the propagation velocity of near-wall shear layers, while Schewe (1983) experimentally obtained the propagation velocity of high-amplitude

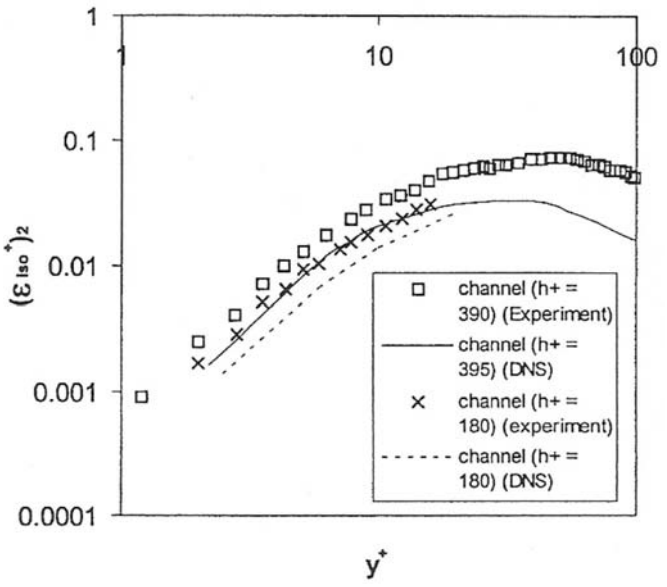

Figure 1.40: Experimental distribution of $(\varepsilon_{iso}^+)_1$ and DNS results for ε_{iso}^+ for a channel flow at different values of h^+.

wall-pressure fluctuations to be approximately $12u_\tau$ in a boundary layer flow at Re_θ of 1400. It may be pointed out that if the convective velocity U_c is assumed to be $13u_\tau$ rather than $10.6u_\tau$, even closer agreement is obtained between the experimental and DNS results (not shown).

It may be of interest to examine how the experimentally obtained $(\varepsilon_{iso}^+)_1$ and $(\varepsilon_{iso}^+)_2$ compare with the true values of ε^+ obtained from DNS results. The ratios of $(\varepsilon_{iso}^+)_1/\varepsilon^+$ and $(\varepsilon_{iso}^+)_2/\varepsilon^+$ for the channel flow at $h^+ = 180$ and 390 are presented in Fig.(1.41). Also depicted in Fig.(1.41) are the DNS results for $(\varepsilon_{iso}^+)/\varepsilon^+$, denoted by $(\varepsilon_{iso}^+)_{DNS}/\varepsilon^+$ which is obtained without invoking Taylor's hypothesis.

It is evident that within the viscous sublayer and lower portion of the buffer region, agreement between $(\varepsilon_{iso}^+)_2/\varepsilon^+$ and $(\varepsilon_{iso}^+)_{DNS}/\varepsilon^+$ is much better than that between $(\varepsilon_{iso}^+)_1/\varepsilon^+$ and $(\varepsilon_{iso}^+)_{DNS}/\varepsilon^+$. This reiterates the finding from Fig.(1.40) that $10.6u_\tau$ is a better representation for the convective velocity U_c in the very near-wall region, as compared to $\overline{U}$. In the viscous sublayer, $(\varepsilon_{iso}^+)_1/\varepsilon^+$ ranges from 0.3 to 0.4, this ratio bearing a slight but discernible increasing trend as h^+ increases for the same value of y^+. However, the ratios $(\varepsilon_{iso}^+)_2/\varepsilon^+$ and $(\varepsilon_{iso}^+)_{DNS}/\varepsilon^+$ are much less than 1 in the very near-wall region. For $h^+ = 395$, the DNS results reveal that $(\varepsilon_{iso}^+)_{DNS}/\varepsilon^+$ decreases very rapidly from approximately 0.1 at $y^+ = 6$ to less than 0.01 at $y^+ = 2$. Similarly, the experimental results for $h^+ = 390$ depict a rapidly declining trend as y^+ decreases, with $(\varepsilon_{iso}^+)_2/\varepsilon^+$ decreasing from 0.09 at $y^+ = 5.1$ to 0.005 at $y^+ = 1.2$. It is thus reasonable to suggest that although

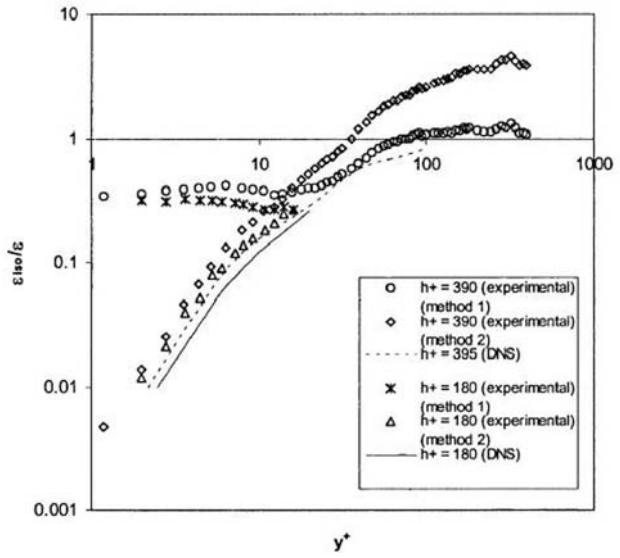

Figure 1.41: Distribution of $\varepsilon_{iso}/\varepsilon$ for a channel flow at different values of h^+, where $(\varepsilon_{iso})_1$, $(\varepsilon_{iso})_2$ and (ε_{iso}) are used to evaluate ε_{iso} for method 1, method 2 and DNS results, respectively.

the assumption of local isotropy per se results in a severe underestimation of the actual value of ε, the additional assumption of Taylor's hypothesis with U_c assumed to be $\overline{U}$ has fortuitously served to reduce significantly the vast difference between the experimentally determined value and the actual value of ε. This is further exemplified by the results of ε obtained by Ligrani & Bradshaw (1987b) in a turbulent boundary layer at $y^+ = 17$. Taking the near-wall DNS results of Antonia *et al.* (1991) at $h^+ = 395$ to be equally applicable to a boundary layer flow, the DNS results reveal that at $y^+ = 17$, the value of $(\varepsilon^+_{iso})_{DNS}/\varepsilon^+$ is approximately 0.3. However, the experimental value of $(\varepsilon^+_{iso})_2/\varepsilon^+$ obtained by Ligrani & Bradshaw was substantially higher at 0.55, thus lending support to the fact that Taylor's hypothesis (with $U_c = \overline{U}$) mitigates, to a certain extent, the underestimation of ε brought about solely by the assumption of local isotropy. Further away from the wall, for $y^+ \geqslant 100$, the value of $(\varepsilon^+_{iso})_{DNS}/\varepsilon^+$ approaches unity, thus substantiating the validity of local isotropy assumption for large values of y^+. Our experimental results show that the distribution for $(\varepsilon^+_{iso})_1/\varepsilon^+$ is close to 1 for $y^+ \geqslant 80$, which also reflects the validity of *both* the assumptions of local isotropy and Taylor's hypothesis with $U_c = \overline{U}$ for large values of y^+.

In addition, it should be noted that the value of the dissipation at the wall ε^+_w can be evaluated from the limiting value of the second derivative of the normalized turbulence kinetic energy k^+ with respect to y^+ as y^+ tends to zero. In fact, the

expression

$$\varepsilon_w = \nu \left.\frac{\partial^2 k}{\partial y^2}\right|_{y=0} \tag{1.50}$$

is often used as a boundary condition for ε in two-equation or second-order turbulence closures. The use of the correlation Eq.(1.43) obtained in Section 1.6.4 thus yields a value of 0.2162 for ε_w^+, which compares favorably to the value of 0.219 obtained by Antonia & Kim (1994) in their DNS of a channel flow at $h^+ = 395$. Based on the same methodology, Karlsson (1993) deduced a lower value of 0.192 for ε_w in a turbulent boundary layer ($Re_\theta = 2400$) using LDV. The second derivative of k^+ yields values of ε_w^+ which are more accurate. This can be attributed to the better accuracy of the measured distribution of k^+ and the fact that no assumptions of local isotropy and Taylor's hypothesis are made in evaluating ε_w^+. Next, one would like to investigate the slope of ε^+ at the wall, since the (usual) boundary condition imposed at the wall for two-equation and second-order turbulence closures can take the form of $\left.\frac{\partial \varepsilon^+}{\partial y^+}\right|_{y^+=0} = 0$ (see Patel *et al.* (1985), for example). The present experimental results can be used to establish the validity of this wall boundary condition. It can further be shown that

$$\left.\frac{\partial \varepsilon^+}{\partial y^+}\right|_{y^+=0} = \frac{2}{3}\left.\frac{\partial^3 (k^+)}{\partial (y^+)^3}\right|_{y^+=0}. \tag{1.51}$$

Based on correlation equation (1.43) , $\left.\frac{\partial \varepsilon^+}{\partial y^+}\right|_{y^+=0} = 4(-0.0059) = -0.0236$. This quantity is in reasonable agreement with the value of –0.0264 obtained by So *et al.* (1991). The latter quantity was estimated from available DNS results. One can observe that the slope of ε^+ at the wall is definitely not sufficiently small and certainly cannot be assumed to be negligible for application as a boundary condition for ε in turbulence studies, particularly for evaluation of turbulence closure models. The negative value of the slope of ε^+ at the wall indicates that ε increases as the wall is approached and possibly registers a maximum at the wall.

1.6.6 The convective velocity U_c

Experiments were performed to determine the convective velocities U_c of the streamwise velocity fluctuations in the boundary layer and channel flows under investigation. This was achieved by employing 2 hot wires separated by a streamwise distance of 9 mm and 10 mm for the boundary layer and channel flows, respectively. The near-wall hot-wire probe, with the active element placed 50 μm (corresponding to 2 wall units approximately) above the perspex wall substrate, is positioned upstream. The downstream wire consists of a DANTEC 55P15 single-wire probe located 0.35 mm above the wall (corresponding to approximately 13 wall units). The output voltages from the 2 wires are sampled simultaneously, and the two-point correlation for the streamwise velocity is determined from

$$R_{u1u2}(T) = \frac{\overline{u_1(t)u_2(t+T)}}{\overline{u_1^2(t)}}, \tag{1.52}$$

where u_1 and u_2 denote the instantaneous fluctuating streamwise velocities at the upstream and downstream locations, respectively. The time delay between the two velocities u_1 and u_2 is denoted by T. Results for the distribution of $R_{u1u2}(T)$ are plotted against T^+ ($\equiv Tu_\tau^2/\nu$) in Fig.(1.42) for the channel and boundary layer flows.

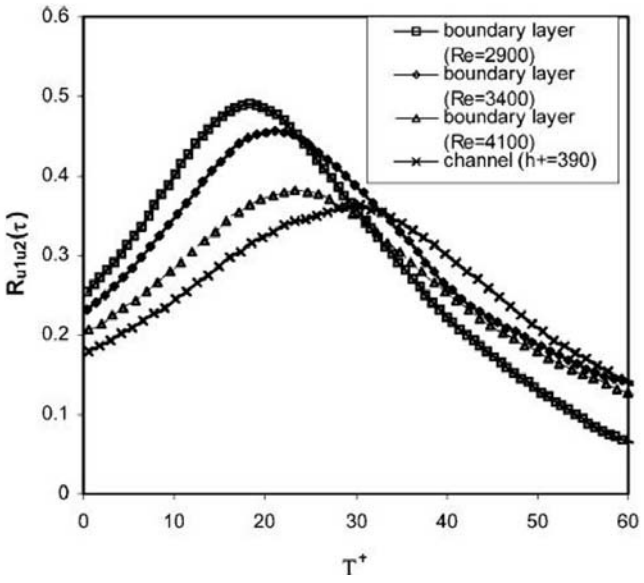

Figure 1.42: Distribution of two-point correlation with $T^+(Tu_\tau^2/\nu)$.

The time interval $(T^+)_{peak} = T_1^+$ corresponding to the peak value of $R_{u1u2}(T)$ signifies the time delay for the downstream instantaneous velocity to achieve a maximum correlation with the upstream instantaneous velocity. This value of T_1 and the streamwise separation of the 2 wires are used to evaluate the average convective velocity U_c of the streamwise velocity fluctuations. This two-point correlation technique was also employed by Krogstad *et al.* (1998) to determine the convective velocities of ejections, sweeps and shear layers in a turbulent boundary layer at $Re_\theta = 1409$. At this point, it is worthy to highlight the relative advantage of hot-wire anemometry over LDV in determining spatial correlations very close to the wall. In addition to the costly requirement that two separate laser sources have to be employed, the extremely low particle count in the very near-wall region culminates in a low and variable data rate. It is thus not feasible to fix the time delay between the two LDV signals and the two point correlation as a function of the time delay $R_{u1u2}(T)$ cannot be determined in a straightforward fashion for the purpose of deducing the value of U_c.

The convective velocity U_c is found to be approximately $13u_\tau$ for the channel flow at $h^+ = 390$. For the boundary layer flow, U_c is observed to remain fairly

constant at $15u_\tau$ for the range of Re_θ investigated. These values of U_c are perceptibly higher than those reported by other researchers in the literature. Johansson *et al.*'s (1991) VISA technique yielded a propagation velocity of $10.6u_\tau \pm 1.0u_\tau$ for near-wall shear layers of a channel flow at $h^+ = 180$, whereas Xu *et al.* (1996) deduced a coincidentally identical value of $10.6u_\tau \pm 0.8u_\tau$ for the propagation velocity of spikes in the very near-wall region based on DNS results of a channel flow at $h^+ = 172$. Using DNS results for a channel flow at $h^+ = 180$, Kim & Hussain (1993) found the propagation velocity for the streamwise velocity perturbations to be virtually constant at $9.6u_\tau$ in the viscous sublayer, which coincides with the convective velocity for the fluctuating streamwise wall shear stress reported by Jeon *et al.* (1999) using the *same* DNS database. The experiments performed in a turbulent boundary layer flow at $Re_\theta = 1409$ by Krogstad *et al.* (1998) revealed a convective velocity ranging between $10.6u_\tau$ and $12.5u_\tau$ for the streamwise velocity fluctuations in the viscous sublayer at $y^+ = 5$. However, it should be noted that these reported values for U_c all pertain to low Reynolds number flows. Romano (1995) conducted two-point measurements of the streamwise velocity using LDV in a turbulent channel flow for values of h^+ ranging between 147 and 300. The convective velocity obtained at $y^+ = 20$ was found to exhibit an increasing trend with increasing Reynolds numbers. Unfortunately, Romano did not present any results for the convective velocity within the viscous sublayer for comparison to our own. Consistent with the findings of Romano, the marginally higher values of U_c we have obtained experimentally may be attributed to the higher Reynolds numbers for the boundary layer and channel flows in which we have performed our experiments.

Further experiments were performed to investigate the effect of the elevation of the upstream near-wall hot-wire on U_c. The elevation of the upstream near-wall hot-wire was varied between 25 and 100 μm (thus maintaining the upstream wire within the viscous sublayer), with the elevation of the downstream wire held fixed at 0.35 mm above the wall. Figure 1.43 shows results for U_c using the two-point correlation technique plotted against the elevation of the upstream near-wall hot-wire (expressed in wall units).

From Fig.(1.43), it can be clearly seen that under the same flow conditions, U_c remains fairly constant within the viscous sublayer and does not show any systematic dependence on y^+. Although the local mean velocity $\overline{U}$ increases linearly with elevation within the viscous sublayer and is zero at the wall, U_c assumes a constant value and bears a larger magnitude than $\overline{U}$ everywhere within the viscous sublayer. This may suggest that streamwise velocity perturbations propagate like waves in the very near-wall viscous sublayer region. A similar conclusion has been made by Kim & Hussain (1993), who obtained the streamwise component of the convective velocity U_c of velocity, vorticity and pressure fluctuations from the DNS results of a turbulent channel flow at $h^+ = 180$. It was found that U_c is approximately equal to the local mean velocity for most of the channel, with the exception of the near-wall region. For $y^+ < 15$, U_c was found to be virtually constant, thus signifying the wave propagating nature for perturbations of all flow variables very close to the wall. Krogstad *et al.* (1998) have also observed that U_c

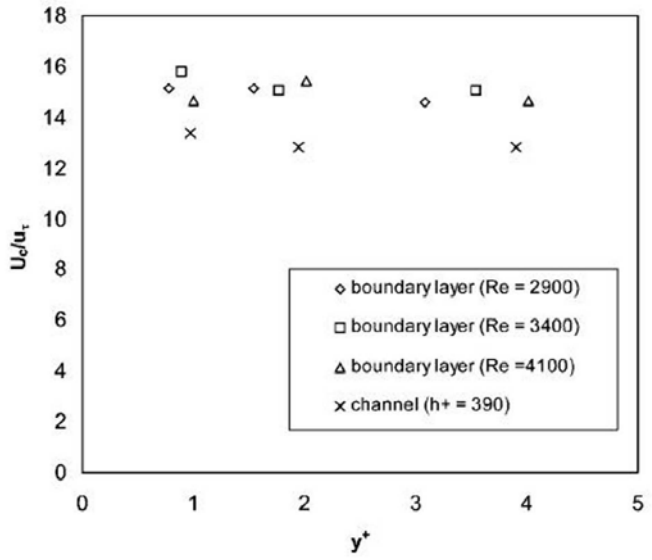

Figure 1.43: Convective velocity U_c for different values of y^+ in the viscous sublayer.

remains almost independent of y^+ for values of y^+ ranging between 5 and 40. As reported by Kim & Hussain, in the very near-wall region, streamwise vortices are temporally very persistent and do not lose their coherence for distances as long as $1000\nu/u_\tau$. The effective vertical mixing due to the presence of these vortices therefore suggests that the fluid particles very close to the wall are well correlated. The variation in U_c is thus expected to be negligible in the very near-wall viscous sublayer region.

It is of further interest to investigate whether the convective velocity U_c deduced using the two-point correlation technique is sensitive to the separation distance between the upstream and downstream probes. The experiments were further repeated for probe separation distances (s) of 6 and 12 mm. The upstream near-wall hot-wire was fixed at a distance of 50 μm from the wall, whilst the downstream hot-wire was placed 0.35 mm from the wall in both cases. The results of U_c for various probe separation distances s^+ (in wall units) are plotted in Fig.(1.44) for the boundary layer and channel flows.

It can be deduced from the figure that for identical flow conditions, U_c does not exhibit any systematic dependence on the probe separation for the range of separation distances investigated. The values of U_c derived for small probe separations are dominated by the small-scale motion and vice versa. The apparent invariance in U_c with probe separation thus suggests that very near the wall, events of different scales are probably convected at an almost constant velocity

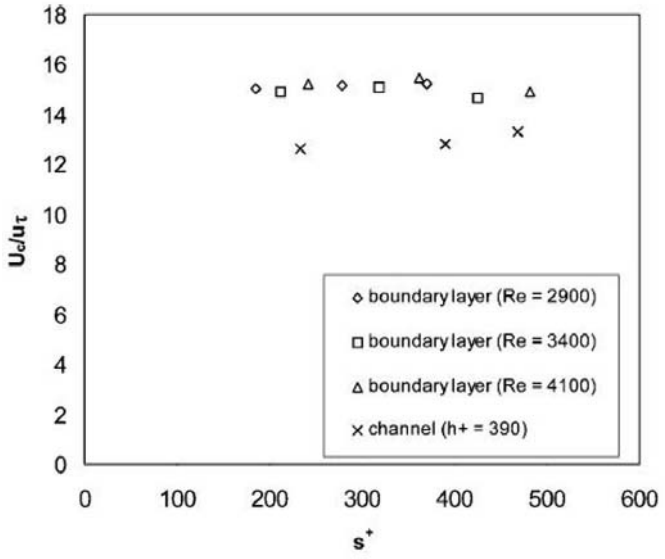

Figure 1.44: Convective velocity U_c for various probe separations s^+ (in wall units).

for the range of separation distances studied. In our experiments, distances larger than 12 mm were not used, as the peak value of two-point correlation $R_{u1u2}(T)$ defined in Eq.(1.52) becomes too small and the peak in the $R_{u1u2}(T)$ versus T^+ distribution becomes too ill-defined for the time delay T_1^+ and hence U_c to be determined accurately. On the other hand, separation distances smaller than 6 mm were not used, as the time delay T_1^+ becomes excessively small, thus culminating in considerable uncertainty in the determination of U_c. Furthermore, placing the two probes excessively close to each other may result in probe interference effects, especially for the downstream wire, which is likely to be influenced by the wake due to the prongs and the sensing element of the upstream probe.

Krogstad (1998) reported that at $y^+ = 5$, U_c exhibits a very gradual increase with increasing probe separation, with U_c increasing by 11.5% when the probe separation distance was increased from 0.08δ to 1.54δ, thus suggesting that large-scale structures move at higher convective velocities than small-scale events. However, as mentioned above, when the two probes are placed excessively far apart (especially for 1.54δ, which corresponds to $930\nu/u_\tau$), it is expected that U_c can only be determined with increasingly large uncertainty, since the peak value of the two-point correlation becomes extremely small and the distribution of $R_{u1u2}(T)$ against T^+ becomes much flatter, with the consequence that the determination of the time delay T_1^+ for which the peak occurs becomes much more ambiguous. The gradual rise in U_c over such large separation distances in the midst of greater experimental uncertainty may have suggested the difference in trend observed for Krogstad

and the present results (obtained for smaller range of separation distance) is not that significant or contradictory. Kim & Hussain (1993) performed bandpass filtering of DNS data for a turbulent channel flow at $h^+ = 180$ to investigate the scale-dependence of U_c.

In contrast to Krogstad, Kim & Hussain found that the large-scale events are convected at lower velocities than the small-scale events, although the variation turns out to be rather insignificant. However, this observation is inconsistent with results of Jeon *et al.* (1999), who obtained the convective velocity of wall shear stress fluctuations for a turbulent channel flow at the same h^+ of 180. Jeon *et al.* concluded that in general, large-scale fluctuations tended to have larger values of U_c as compared to small-scale fluctuations. However, when a overall convective velocity for the streamwise wall shear stress fluctuations was used to convert the one-dimensional frequency power spectrum into the streamwise wave-number power spectrum for the purpose of testing Taylor's hypothesis, there was excellent agreement between the streamwise wave-number spectrum using Taylor's hypothesis and the actual spectrum.

In conclusion, different researchers have reported conflicting trends for the scale dependence of U_c corresponding to the streamwise velocity fluctuations in the very near-wall region. However, the general consensus is that this scale dependence on U_c is probably very marginal in the very near-wall region, which is reiterated from our experimental results, showing no systematic dependence of U_c on the probe separation distance. It is thus logical to assume a single representative or overall convective velocity for all scales in the very near-wall region. In adopting such an approach, substantial simplifications can be made in the practical implementation of Taylor's hypothesis and turbulence modeling.

1.6.7 The integral time scale

The longitudinal (streamwise) autocorrelation between the values of u(t) at times t and $t + \tau_1$ is defined as

$$R_u(\tau_1) = \lim_{T\to\infty} \frac{1}{T} \int_0^T u(t)u(t+\tau_1)dt \tag{1.53}$$

and the autocorrelation coefficient function can be subsequently obtained from the expression

$$\rho_u(\tau_1) = R_u(\tau_1)/\overline{u^2}. \tag{1.54}$$

The longitudinal (streamwise) integral time scale is then evaluated using

$$T_u = \int_0^\infty \rho_u(\tau_1)d\tau_1. \tag{1.55}$$

The dimensionless integral time-scale T_u^+ (normalized using inner variables) for the viscous sublayer of the channel and boundary layer flows is presented in Fig.(1.45).

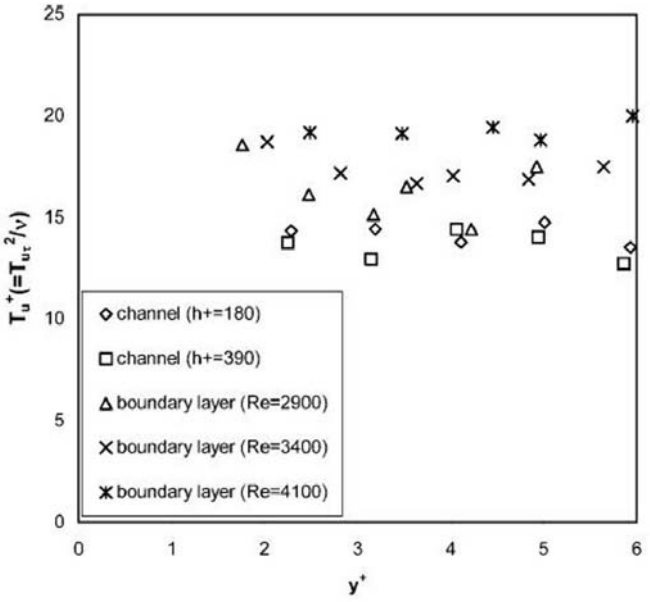

Figure 1.45: Longitudinal integral time scale (in wall units) in the viscous sublayer.

It can be seen that for each h^+ for the channel flow and Re_θ for the boundary layer flow, T_u^+ is almost constant within the viscous sublayer. The channel flow seems to exhibit slightly lower values of T_u^+ than the boundary layer flow in the viscous sublayer. The channel flow yields T_u^+ values close to 15, while perceptibly higher values close to 18 are obtained for the boundary layer flow. Once again, it would be of interest to compare the experimental results to those of DNS and others. However, no such information is available directly in the literature to the best knowledge of the authors. Kim *et al.* (1987) presented two-point spatial correlations in the streamwise direction at $y^+ = 5.39$ for their channel flow DNS at $h^+ = 180$ and the longitudinal integral length scale at that location was estimated to be $190\nu/u_\tau$. According to Taylor's hypothesis, the integral length and time-scales at a particular point are simply related via the convective velocity U_c at that point. However, as discussed in Section 1.6.5, the conventional procedure of assuming the convective velocity U_c to be the mean velocity $\overline{U}$ at the point of measurement in Taylor's hypothesis only applies if the turbulence intensity does not exceed 10%, which is strictly not valid in the viscous sublayer. As mentioned in Section 1.6.6, Kim & Hussain (1993) used Kim *et al.*'s (1987) DNS results for a channel flow at $h^+ = 180$ and found the propagation velocity for the streamwise velocity perturbations to be virtually constant at $9.6u_\tau$ in the viscous sublayer. If an integral length-scale of $190\nu/u_\tau$ and a convective or propagation velocity of $9.6u_\tau$ is assumed in the viscous sublayer, the integral time-scale would work

out to be approximately $20u_\tau^2/\nu$, which compares reasonably with the value of $15u_\tau^2/\nu$ obtained experimentally for the channel flow. Moreover, Spalart (1988) conducted a DNS of a turbulent boundary layer and commented that near the wall, a typical time-scale of turbulence is $15u_\tau^2/\nu$. This is in reasonable accord with our experimental findings of $T_u^+ \approx 18$ for boundary layer flows.

1.6.8 Concluding remarks for Section 1.6

Very near-wall velocity measurements were carried out using a specially constructed hot-wire probe in both a fully developed turbulent channel flow at $h^+ = 180$ and 390 and flat plate boundary layer flow at Re_θ of 2900, 3400 and 4100. The near-wall hot-wire probe, having been calibrated in a specially constructed laminar flow calibration rig, was found to be capable of registering the mean velocity profile and distributions of streamwise and spanwise intensities of turbulence as well as turbulence kinetic energy k in the viscous sublayer; these distributions comparing favorably to available DNS results. Low Reynolds number effects were evident for the channel flow, as manifested by the monotonic increase in the streamwise and spanwise turbulence intensity as well as the turbulence kinetic energy k for the same value of y^+ when h^+ was more than doubled from 180 to 390.

By assuming the validity of Taylor's hypothesis, the dissipation rate ε_{iso} in the very near-wall viscous sublayer region and beyond was determined by assuming the dissipating range of eddy sizes to be statistically isotropic. If the convective velocity U_c in Taylor's hypothesis was assumed to be equal to the mean velocity $\overline{U}$ at the point of measurement, the value of $(\varepsilon_{iso}^+)_1$ thus obtained was found to agree well with that of $(\varepsilon^+)_{DNS}$ for $y^+ \geqslant 80$, hence suggesting the validity of assuming $U_c = \overline{U}$ *and* local isotropy for large values of y^+. However, for $y^+ \leqslant 80$, $(\varepsilon_{iso}^+)_1$ was found to underestimate $(\varepsilon^+)_{DNS}$, this discrepancy increasing as y^+ decreases. However, if U_c was assumed to be $10.6u_\tau$, the value of $(\varepsilon_{iso}^+)_2$ thus obtained was found to compare reasonably well to the distribution of $(\varepsilon_{iso}^+)_{DNS}$ for $y^+ \leqslant 15$, thus suggesting the reasonable assumption that $U_c = 10.6u_\tau$ in the viscous sublayer and inner part of the buffer region, where the local streamwise turbulence intensity grossly exceeds 10% and it is no longer valid to assume $U_c = \overline{U}$.

On the other hand, experiments performed to determine the convective velocity U_c of the streamwise velocity fluctuations in the viscous sublayer yielded values of $13u_\tau$ and $15u_\tau$ respectively for the channel flow at $h^+ = 390$ and the boundary layer flows under investigation. It was also found that the value of U_c remains fairly constant within the viscous sublayer and does not show any systematic dependence on y^+, thus suggesting that streamwise velocity perturbations propagate like waves in the very near-wall viscous sublayer region. U_c was also found to be relatively independent of the separation distance between the two hot-wire probes, thus implying that it is reasonable to assume a single representative or overall convective velocity for all scales in the very near-wall region, which leads to tremendous simplifications in the application of Taylor's hypothesis and turbulence modelling. Finally, the dimensionless integral time scale T_u^+ for the viscous sublayer of the channel and boundary layer flows worked out to be 15 and 18, respectively; these

values are in reasonable agreement with those deduced from DNS.

Further discourse on this Section 1.6 can be found in Khoo *et al.* (2000, 2001).

1.7 Overall concluding summary

Experiments using the electronic square-wave voltage perturbation test (Section 1.4.1) were systematically performed for the first time to evaluate the response frequency (f_S) of near-wall hot wires. In addition, two commercially available flush-mounted wall shear stress gauges were tested. At a fixed wire height above the wall substrate, an increase in the convective velocity leads to an increase in f_S. For a hot-wire exposed to a constant convective velocity, f_S increases with decreasing heights from the wall substrate. This is also equivalent to a decreasing h^+ with increasing effect of wall influence, hence suggesting that f_S improves with greater wall effects. A hot-wire mounted at the same height $h = 50$ μm above a thermally more conducting Aluminium wall substrate exhibits a higher value of f_S compared to its counterpart above a Perspex wall substrate under similar operating conditions. These findings strongly suggest that f_S increases with increasing heat transfer from the wire, regardless of whether it is due to forced/natural convection or effects of wall influence.

For a flush-mounted hot-wire, an increase in the imposed wall shear stress yields a corresponding increase in f_S. The value of f_S (with and without "tail") for the DANTEC 55R45 wall shear stress gauge is consistently higher than that for the 55R46 gauge, hence indicating the better frequency response of the 55R45 gauge.

Results of the frequency response according to square-wave voltage perturbation tests (f_S) were then compared to those obtained using velocity perturbation tests (f_D) in Section 1.3.1 and Section 1.3.2. Although f_S and f_D show similar trends for the near-wall hot- wire and hot-film probes, f_S is consistently greater than f_D. The magnitudes of f_S and $f_D$are vastly different, being an order of magnitude for the marginally-elevated and flush-mounted hot wires. For the hot-film wall shear stress probes, this (ratio) difference is up to five orders of magnitude (without "tail") and three orders of magnitude (with "tail"). From a user's point of view, however, the dynamic frequency response (f_D) should serve as a more accurate indicator of the overall frequency response of the hot-wire/film system, since f_D signifies the onset of amplitude attenuation when the hot-wire/film is subjected to *direct* velocity or shear stress perturbations. The large differences in magnitude between f_S and f_D show that the square-wave voltage perturbation test may not be all-sufficient in establishing the response frequency of a near-wall hot-wire or flush-mounted hot-film shear stress probes.

Separately, the cutoff frequency of the anemometer yielded by the sine-wave test (f_{sine}) in Section 1.4.2 was found to be in fair agreement and to exhibit the same trends as results obtained using the traditional electronic square-wave voltage perturbation test (f_S). For the hot-film gauges, f_{sine} obtained for the DANTEC 55R45 gauge was consistently higher that those for its 55R46 counterpart under

identical conditions of overheat ratio and wall shear stress (τ). For both gauges, an increase in overheat ratio resulted in a rise in f_{sine}, whereas variations in τ for the same overheat ratio did not seem to have cast any effect. For the marginally-elevated hot-wire probes, an increase in the convective velocity (V) leads to an increase in f_{sine} when the wire is either kept at a fixed physical distance or at the same y^+ above the wall substrate. When V is held constant, a decrease in y^+ signifying increased wall influence culminates in larger values of f_{sine}. These results suggest that f_{sine} increases with increasing heat transfer from the wire, regardless of whether it is due to forced convection or effects of wall influence. For the flush-mounted hot-wire wall shear stress sensor, an increase in the imposed τ results in a corresponding increase in f_{sine}.

Apart from yielding the cutoff frequency of the anemometer, the sine-wave test is also capable of indicating the flatness of the frequency response over a limited frequency range and detect the presence of any amplitude attenuation which arises as a result of the attenuation of heat waves to the surrounding wall substrate at high frequencies. A significant bulging effect appears in the sine-wave test response curves for the hot-film wall shear stress probes. A causality relationship $f_{bulge} \approx 20 f_D$ was observed for the hot-film gauges, where f_{bulge} and f_D denote the frequency characterizing the bulging effect and the dynamic frequency response respectively. Compared to f_S (and f_{sine}) which is five orders of magnitude greater than f_D, f_{bulge} provides a much better indicator or proxy for predicting f_D. It is to be realized that in the application of the hot-film wall shear stress gauges to measure fluctuating shear stress in a turbulent flow, it is the lower dynamic response frequency f_D which sets an upper limit to the overall responsiveness of the gauge. For the flush-mounted and marginally-elevated hot-wire sensors, a very slight bulging effect was also observed in the 0.8 to 4 kHz range, which corresponds much more closely to the values of f_D. This is contrasted to f_S, which is typically one order of magnitude larger than f_D. The frequencies f_{bulge} and f_D can be related by the causality relationship $f_{bulge} \sim f_D$ for the near-wall hot-wire probes. It must be noted that the lower magnitude f_D is the critical frequency ultimately determining the responsiveness of the near-wall hot-wire probe to fluctuating velocities expected in a turbulent flow. Therefore, it is suggested that instead of relying solely on the square-wave test, users of near-wall hot-wire or hot-film anemometers who do not have access to dynamic perturbation testing facilities should perform a sine-wave test to detect the presence of any amplitude attenuation for frequencies (f_{bulge}) below the cutoff frequency.

Very near-wall velocity measurements were carried out using a specially constructed hot-wire probe in both a fully developed turbulent channel flow at $h^+ = 180$ and 390 and flat plate boundary layer flow at Re_θ of 2900, 3400 and 4100. Further by assuming the validity of Taylor's hypothesis, the dissipation rate ε_{iso} in the very near-wall viscous sublayer region and beyond was determined by assuming the dissipating range of eddy sizes to be statistically isotropic. If the convective velocity U_c in Taylor's hypothesis was assumed to be equal to the mean velocity $\overline{U}$ at the point of measurement, the value of $(\varepsilon^+_{iso})_1$ thus obtained was found to agree well with that of $(\varepsilon^+)_{DNS}$ for $y^+ \geqslant 80$, hence suggesting the validity of

assuming $U_c = \overline{U}$ *and* local isotropy for large values of y^+. However, for $y^+ \leqslant 80$, $(\varepsilon^+_{iso})_1$ was found to underestimate $(\varepsilon^+)_{DNS}$, this discrepancy increasing as y^+ decreases

Finally, experiments performed to determine the convective velocity U_c of the streamwise velocity fluctuations in the viscous sublayer yielded values of $13u_\tau$ and $15u_\tau$ respectively for the channel flow at $h^+ = 390$ and the boundary layer flows under investigation. It was also found that the value of U_c remains fairly constant within the viscous sublayer and does not show any systematic dependence on y^+, thus suggesting that streamwise velocity perturbations propagate like waves in the very near-wall viscous sublayer region. U_c was also found to be relatively independent of the separation distance between the two hot-wire probes, thus implying that it is reasonable to assume a single representative or overall convective velocity for all scales in the very near-wall region, which leads to tremendous simplifications in the application of Taylor's hypothesis and turbulence modelling. The dimensionless integral time scale T^+_u for the viscous sublayer of the channel and boundary layer flows worked out to be 15 and 18, respectively; these values are in reasonable agreement with those deduced from DNS.

Acknowledgments

The authors would like to put into record the contributions of our collaborators, namely G. L. Li, C. P. Lim and C. J. Teo to this series of works carried out at the National University of Singapore. A special word of thanks to Jeremy Chen who helped to prepare the notes.

One of us (BCK) gratefully acknowledges the financial sponsorship of the Brazilian Association of Mechanical Sciences and Engineering and Brazil's National Research Council to present at the Spring School on Transition and Turbulence 2006.

1.8 References

Alfredsson P., Johansson A., Haritonidis J. and Eckelmann H.; "The fluctuating wall-shear stress and the velocity field in the viscous sublayer," *Phys. Fluids* **31**, 1026-1033 (1988).

Antonia R. A., Teitel M., Kim J. and Browne L. W. B.; "Low-Reynolds-number effects in a fully developed turbulent channel flow," *J. Fluid Mech.* **236**, 579-605 (1992).

Antonia R. A. and Kim J. X.; "Low Reynolds number effects on near-wall turbulence," *J. Fluid Mech.* **276**, 61-80 (1992).

Azad R. S.; "Corrections to measurements by hot-wire anemometer in the proximity of a wall," *Report MET-7* Dept. Mech. Eng. Univ. of Manitoba, Winnipeg, Canada (1983).

Azad R. S. and Kassab S. Z.; "A new method of obtaining dissipation," *Exps. Fluids* **7**, 81-87 (1989).

Bellhouse B. J. and Schultz D. L.; "The determination of fluctuating velocity in air with heated thin film gauges," *J. Fluid Mech.* **29**, 289-295 (1967).

Bellhouse B. J. and Rasmussen, C. G.; "Low-frequency characteristics of hot film anemometers," *DISA Information* **6**, 3-10 (1968).

Berger E., Freymuth P. and Froebel E.; "Theorie and konstruktion von konstant-temperatur-hitzdrahtanemometern," *Konstruktion* **15**, 495-497 (1963).

Bradshaw P.; "'Inactive' motion and pressure fluctuations in turbulent boundary layers," *J. Fluid Mech.* **30**, 241-258 (1967).

Bremhorst K. and Gilmore D. B.; "Influence of end conduction on the sensitivity to stream temperature fluctuations of a hot-wire anemometer," *Int. J. Heat & Mass Transfer* **21**, 145-54 (1978).

Bhatia J. C., Durst F. and Johanovic J.; "Corrections of hot-wire anemometer measurements near walls," *J. Fluid Mech.* **122**, 411-431 (1982).

Brown G. L. and Davey R. F.; "The calibration of hot-films for skin friction measurement," *Rev. Sci. Instrum.* **42**, 1729-1731 (1971).

Bruun H. H.; "Hot-wire anemometry," Oxford University Press (1995).

Cendese A., Romano G. P. and Antonia R. A.; "A comment on the 'linear' law of the wall for fully developed turbulent channel flow" *Exps. Fluids* **25**, 165-170 (1998).

Chew Y. T., Khoo B. C. and Li G. L.; "A time-resolved hot-wire shear stress probe for turbulent flow: use of laminar flow calibration," *Exp. Fluids* **17**, 75-83 (1994).

Chew Y. T., Shi S. X. and Khoo B. C.; "On the numerical near-wall corrections of single hot-wire measurements," *Int. J. Heat & Fluid Flow* **16**, No. 6, 471-476 (1995).

Chew Y. T., Khoo B. C. and Li G. L.; "The investigation of the wall effects on hot-wire measurements using a bent sublayer probe," *Meas. Sci. Tech.* **9**, 67-85 (1998).

Chew Y. T., Khoo B. C. and Li G. L.; "Dynamic response of hot-wire anemometer. Part II: A flush-mounted hot element for wall shear stress measurements," *Meas. Sci. Tech.* **9**, 762-776 (1998).

Coles D. E.; "The turbulent boundary layer in a compressible fluid." Report R-403-PR, The Rand Corporation, Santa Monica, CA (1962).

Comte-Bellot G., Strohl A. and Alcarez E.; "On aerodynamic disturbances caused by a single hot-wire probe," *Trans. ASME J. Appl. Mech.* **93**, 767-774 (1971).

Comte-Bellot G.; "The physical background for hot film anemometry," *Proc. Symp. on Turbulence in Liquids*, University of Missouri, Rolla, 1-13 (1977).

Cook W. J.; "Response of hot-element wall shear stress gauges in unsteady turbulent flows," *A.I.A.A. Journal* **32**, 1464-1471 (1994).

Cook W. J. and Giddings T. A.; "Response of hot-element wall shear-stress gages in laminar oscillating flows," *AIAA J.* **26**, 706-713 (1988).

Davis M. R.; "The dynamic response of constant resistance anemometers," *J. Phys. E: Sci. Instrum.* **3**, 15-20 (1970).

Durst F., Jovanovic J. and Sender J.; "LDA measurements in the near-wall region of a turbulent pipe flow," *J. Fluid Mech.* **295**, 305-335 (1995).

Elsner J. W., Domagala P. and Elsner W.; "Effect of finite spatial resolution of hot-wire anemometry on measurements of turbulence energy dissipation," *Meas. Sci. Tech.* **4**, 517-523 (1993).

Fernholz H. H. and Finley P. J.; "The incompressible zero-pressure-gradient turbulent boundary layer: an assessment of the data," *Prog. Aerospace Sci.* **32**, 245-311 (1996).

Fernholz H. H. and Warnack D.; "The effects of a favourable pressure gradient and of the Reynolds number on an incompressible axisymmetric turbulent boundary layer. Part 1. The turbulent boundary layer," *J. Fluid Mech.* **359**, 329-356 (1998).

Finnicum D. S. and Hanratty T. J.; "Turbulent normal velocity fluctuations close to a wall," *Phys. Fluids* **28**, 1654-1658 (1985).

Fontaine A. A. and Deutsch S.; "Three-component, time-resolved velocity statistics in the wall region of a turbulent pipe flow," *Exps. Fluids* **18**, 168-173 (1995).

Freymuth P.; "Frequency response and electronic testing for constant-temperature hot-wire anemometers," *J. Phys. E: Sci. Instrum.* **10**, 705-710 (1977).

Freymuth P. and Fingerson L. M.; "Electronic testing of frequency response for thermal anemometers. *TSI Quart.* **III**, No. 4, 5-12 (1977).

Freymuth P.; "Theory of frequency optimisation for hot-film anemometers," *J. Phys. E: Sci. Instrum.* **11**, 177-179 (1978).

Freymuth P.; "Sine-wave testing of non-cylindrical hot-film anemometers according to the Bellhouse-Schultz model," *J. Phys. E: Sci. Instrum.* **13**, 98-102 (1980).

Freymuth P.; "Calculation of square-wave test for frequency optimised hot-film anemometers," *J. Phys. E: Sci. Instrum.* **14**, 238-240 (1981).

Gunther A., Papavassiliou D. V., Warholic M. D. and Hanratty T. J.; "Turbulent flow in a channel at a low Reynolds number," *Exps. Fluids* **25**, 503-511 (1998).

Guo Z. X. and Hyung J. S.; "Analysis of the Nusselt number in a pulsating pipe flow," *Int. J. Heat Mass Transfer* **40**, 2486-2489 (1997).

Hebbar K. S.; "Wall proximity corrections for hot-wire readings in turbulent flows," *DISA Information* **25**, 15-16.

Hinze J. O.; "Turbulence. An introduction to its mechanism and theory," McGraw-Hill, New York (1959).

Hinze J. O.; "Turbulence," 2^{nd} Ed., McGraw-Hill, New York, (1975).

Houdeville R., Juillen J. C. and Cousteix J.; "Skin friction measurements with hot-element gauges," *Recherche Aerospatial* **1**, 67-79 (1984).

Huang J. B., Ho C. M., Tung S., Liu C. and Yu C. T.; "Micro thermal shear stress sensor with and without cavity underneath," *IEEE IMTC (Instrumentation Measurement Technology Conf.)* Waltham, Massachusetts, 171-174 (1995).

Huang J. B., Tung S., Ho C. M., Liu C. and Tai Y. C.; "Improved micro thermal shear stress sensor," *IEEE Trans. Instrum. Meas.* **45**, 570-574 (1996).

Isomoto K. and Honami S.; "The effect of inlet turbulence intensity on the reattachment process over a backward-facing step," *Trans. ASME J. Fluids Eng.* **111**, 87-93 (1989).

Jeon S., Choi H., Jung H. H. and Moin P.; "Space-time characteristics of the wall shear-stress fluctuations in a low-Reynolds-number channel flow," *Phys. Fluids* **11**, 3084-3094 (1999).

Johansson A. V., Alfredsson P. H. and Eckelmann H.; "On the evolution of shear-layer structures in near-wall turbulence" in *Advances in turbulence,* Comte-Bellot G., and Mathieu J. (editors). Proc. First European Turbulence Conf., Lyon, July (1986).

Johansson A. V., Alfredsson P. H. and Kim J.; "Evolution and dynamics of shear-layer structures in near-wall turbulence," *J. Fluid Mech.* **224**, 579-599 (1991).

Karlsson R. I. and Johansson T. G.; "LDV measurements of higher order moments of velocity fluctuation in a boundary layer," *Third Int. Symp. on Application of Laser Anemometry to Fluid Mech.* Adrian, R. J. *et al.* (editors), 273-289. Lisbon, Portugal (1988).

Karlsson R. I.; "Near-wall measurements of turbulence structure in boundary layers and wall jets." *Near-Wall Turbulent Flows* So, R. M. C. *et al.* (editors). Amsterdam, Elsevier (1993). 423-432.

Khoo B. C., Chew Y. T. and Li G. L.; "A new method by which to determine the dynamic response of marginally hot-wire anemometer probes for near-wall velocity and wall shear stress measurements," *Meas. Sci. Tech.* **6**, 1399-1406 (1995).

Khoo B. C., Chew Y. T. and Li G. L.; "Time-resolved near-wall hot-wire measurements: use of laminar flow wall correction curve and near-wall calibration technique," *Meas. Sci. Tech.* **7**, 564-575 (1996).

Khoo B. C., Chew Y. T. & Li G. L. 1997: Effects of imperfect spatial resolution on turbulence measurements in the very near-wall viscous sublayer region. *Exp. Fluids* 22, 327-335.

Khoo B. C., Chew Y. T., Lim C. P. and Teo C. J.; "Dynamic response of hot-wire anemometer. Part I: A marginally-elevated hot-wire probe for near-wall velocity measurements," *Meas. Sci. Tech.* **9**, 749-761 (1998).

Khoo B. C., Chew Y. T. and Lim C. P.; "The flow between a rotating and a stationary disk: Application to near-wall hot-wire calibration," *Meas. Sci. Tech.* **9**, 650-658 (1998).

Khoo B. C., Chew Y. T., Teo C. J. and Lim C. P.; "The dynamic response of a hot-wire anemometer. Part III: Voltage perturbation versus velocity-perturbation testing for near-wall hot-wire/film probes," *Meas. Sci. Tech.* **10**, 152-169 (1999).

Khoo B. C., Chew Y. T., and Teo C. J.; "On near-wall hot-wire measurements," *Exp. Fluids* **29**, 448-460 (2000).

Khoo B. C., Chew Y. T., and Teo C. J.; "Near-wall hot-wire measurements. Part II: Turbulence time scale, convective velocity and spectra in the viscous sublayer," *Exp. Fluids* **31**, 494-505 (2001).

Kim J. and Hussain F.; "Propagation velocity of perturbations in turbulent channel flow," *Phys. Fluids.* **5**, 695-706 (1993).

Kim J., Moin P. and Moser R.; "Turbulence statistics in fully developed channel flow at low Reynolds number," *J. Fluid Mech.* **177**, 133-166 (1987).

Koskie J. E. and Tiederman W. G.; "Polymer drag reduction of zero and adverse pressure gradient boundary layers," *Near-Wall Turbulent Flows* So, R. M. C. *et al.* (editors). Elsevier, Amsterdam, 659-668 (1993).

Kreplin H. P. and Eckelmann H.; "Behaviour of the three fluctuating velocity components in the wall region of a turbulent channel flow," *Phys. Fluids* **22**, 1233-1239 (1979).

Krogstad P. A., Kaspersen J. H. and Rimestad S.; "Convection velocities in a turbulent boundary layer," *Phys. Fluids* **10**, 949-957 (1998).

Lange CF, Durst F and Breuer M.; "Wall effects on heat losses from hot wires," *Int. J. Heat & Fluid Flow* **20**, 34-47 (1999).

Launder B. E. and Spalding D. B.; "The numerical computation of turbulent flows," *Comput. Methods Appl. Mech. Engrg.* **3**, 269-289 (1974).

Lee T., Fisher M. and Schwarz W. H.; "Investigation of the stable interaction of a passive compliant surface with a turbulent boundary layer," *J. Fluid Mech.* **257**, 373-401 (1993).

Li W. Z., Khoo B. C. and Xu D.; "The thermal characteristics of a hot-wire in a near-wall flow," *Int. J. Heat Transf.* **49**, 905-918 (2006).

Ligrani P. M. and Bradshaw P.; "Subminiature hot-wire sensors: development and use." *J. Phys. E: Sci. Instrum.* **20**, 323-332 (1987).

Ligrani P. M. and Bradshaw P.; "Spatial resolution and measurement of turbulence in the viscous sublayer using subminiature hot-wire probes," *Exp. Fluids* **5**, 407-417 (1987).

Marusic I., Uddin A. K. M. and Perry A. E.; "Similarity law for the streamwise turbulence intensity in zero-pressure-gradient turbulent boundary layers," *Phys. Fluids* **9**, 3718-3726 (1997).

McAdams W. H., "Heat Transmission," 3^{rd} Edition, McGraw-Hill, New York (1954).

Mochizuki S. and Nieuwstadt F. T. M.; "Reynolds-number-dependence of the maximum in the streamwise velocity fluctuations in wall turbulence," *Exps. Fluids* **21**, 218-226 (1996).

Moen M. J. and Schneider S. P.; "The effect of sensor size and substrate properties on the performance of flush-mounted hot-film sensors," in *Thermal Anemometry*. Proceedings of the Third ASME International Symposium on Thermal Anemometry (1993).

Moen M. J. and Schneider S. P.; "The effect of sensor size on the performance of flush-mounted hot-film sensors," *J. Fluid Eng.* **116**, 273-277 (1994).

Mulhearn P. J.; "A simple device for dynamic testing of X-configuration hot-wire anemometer probes," *J. Phys. E. Sci. Instrum.* **11**, 678-681 (1978).

Niederschulte M. A., Adrian R. J. and Hanratty T. J.; "Measurements of turbulent flow in a channel at low Reynolds numbers," *Exps. Fluids* **9**, 222-230 (1990).

Ogata K.; "Modern Control Engineering," 2nd Ed. Prentice-Hall Inc (1990).

Patel V. C., Rodi W. and Scheuerer G.; "Turbulence models for near-wall and low Reynolds number flows," *AIAA J.* **23**, 1308-1319 (1985).

Perry A. E. and Morrison G. L.; "Static and dynamic calibrations of constant-temperature hot-wire systems," *J. Fluid Mech.* **47**, 765-777 (1971).

Polyakov A. F. and Shindin S. A.; "Peculiarities of hot-wire measurements of mean velocity and temperature in the wall vicinity," Lett. Heat Mass Transfer **5**, 53-58 (1978).

Polyakov A. F. and Shindin S. A.; "Hot-wire anemometer measurement of mean velocity very close to a wall," *Inshenerno-Fizicheskii Zurnal* **36**, 985-990 (1979).

Romano G. P.; "Analysis of two-point velocity measurements in near-wall flows," *Exps. Fluids* **20**, 68-83 (1995).

Saddoughi S. G. and Veeravalli S. S.; "Local isotropy in turbulent boundary layers at high Reynolds number," *J. Fluid Mech.* **268**, 333-372 (1994).

Savill A. M. and Mumford J. C.; "Manipulation of turbulent boundary layers by outer-layer devices skin friction and flow visualization results," *J. Fluid Mech.* **191**, 389-418 (1988).

Schewe G.; "On the structure and resolution of wall-pressure fluctuations associated with turbulent boundary-layer flow," *J. Fluid Mech.* **134**, 311-328 (1983).

Schlichting H.; "Boundary Layer Theory," 7^{th} ed., McGraw-Hill, New York (1979).

Shah D. A. and Antonia R. A., "Scaling of wall shear stress fluctuations in a turbulent duct flow," *AIAA J.* **25**, 22-29 (1987).

So R. M. C., Lai Y. G., Zhang H. S. and Hwang B. C.; "Second-order near-wall turbulence closures: a review," *AIAA J.* **29**, 1819-1835 (1991).

Spalart P. R.; "Direct simulation of a turbulent boundary layer up to $R_\theta = 1410$," *J. Fluid Mech.* **187**, 61-98 (1988).

Spalding D. B.; "A single formula for the law of the wall," *J. Appl. Mech.* **288**, 455-457 (1961).

Stewartson K.; "Flow between two rotating coaxial discs," *Proc. Camb. Phil. Soc.* **49**, 333-341 (1953).

Teo C. J., Khoo B. C. and Chew Y. T.; "The dynamic response of a hot-wire anemometer. IV. Sine-wave voltage testing for near-wall hot-wire/film probes and the presence of low-high frequency response characteristics," *Meas. Sci. Tech.* **12**, 37-51 (2001).

Townsend A. A.; "Equilibrium layers and wall turbulence," *J. Fluid Mech.* **11**, 97-120 (1961).

Walsh M. J.; "Turbulent boundary layer drag reduction using riblets," *AIAA Paper*, 82-0169 (1992).

Weidman P. D. and Browand F. K.; "Analysis of a simple circuit for constant temperature anemometry." *J. Phys. E: Sci. Instrum.* **8**, 553-560 (1975).

Xu C., Zhang Z., den Toonder J. M. J. and Nieuwstadt F. T. M.; "Origin of high kurtosis levels in the viscous sublayer. Direct numerical simulation and experiment," *Phys. Fluids* **8**, 1938-1944 (1996).

Zemskaya A. S., Levitskiy V. N., Repik Y. U. and Sosedko Y. P.; "Effects of the proximity of the wall on hot-wire readings in laminar and turbulent boundary layers," *Fluid Mech. - Soviet Res.* **8**, 133-141, (1979).